Spring 5-20-2021

Theranostic Applications of siRNA Bioconjugates in Cancer Detection and Treatment

Sunil S. Shah
Seton Hall University, sunil.shah@student.shu.edu

Theranostic Applications of siRNA Bioconjugates in Cancer Detection and Treatment

A thesis submitted

to the

Department of Chemistry and Biochemistry, Seton Hall University

in partial fulfillment of the requirements

for the

Degree of Doctor of Philosophy

By

Sunil S. Shah

May 2021

Department of Chemistry and Biochemistry

Seton Hall University

South Orange, New Jersey, USA

Seton Hall University
College of Arts and Science
Department of Chemistry and Biochemistry
DISSERTATION COMMITTEE APPROVALS

We certify that we have read this thesis writer by Sunil Subhashchandra Shah in the Spring 2021 semester and, in our opinion, it is sufficient in scientific scope and quality as a dissertation for the degree of Doctor in Philosophy

APPROVED BY:

David Sabatino, Ph.D.
Advisor
Department of Chemistry and Biochemistry, Seton Hall University

---

Wyatt Murphy, Ph.D.
Reader, Member of Dissertation Committee,
Department of Chemistry and Biochemistry, Seton Hall University

---

Fr. Gerald J Buonopane, Ph.D.
Reader, Member of Dissertation Committee,
Department of Chemistry and Biochemistry, Seton Hall University

---

Stephen Kelty, Ph.D.
Chair, Department of Chemistry and Biochemistry, Seton Hall University

Dedicated to my wife Kinnari Shah, Ph.D. for my motivation, my lovely son Aagam Shah for my inner strength, and my entire family for their inspiration, support, and unconditional love. Professionally, to my enzymatic and cool advisor Dr. David Sabatino and previous advisor Dr. Surekha Devi for their motivations to consistently better myself and accomplish what is possible. They were the driving forces in completing this work and earning my Ph.D. degree.

Abstract

The emerging field of RNA nanotechnology has led to rapid advances in the applications of RNA in chemical biology, medicinal chemistry, and biotechnology. At the forefront of its utility is the ability to self-assemble multiple siRNAs into nanostructure formulations capable of targeting selected oncogenes and potentiating the gene therapy of malignant tumors. Self-assembled siRNA integrates multiple siRNAs within a single molecular platform for silencing multiple oncogenic mRNA targets with high precision and efficacy to potentially induce cancer cell apoptosis through the RNA interference (RNAi) pathway. Furthermore, the conjugation of siRNA self-assemblies with bio-active probes results in multi-functional theranostic (therapy+diagnostic) agents capable of enhancing cancer cell detection and treatment. This includes the introduction of lipids for cell uptake, fluorophores for cell-based detection, and metallic nanoparticle formulations for optimizing siRNA biophysical and biological properties. The latter is a central focus of my thesis research objectives, aimed towards the development of self-assembled siRNA bioconjugates as effective anti-cancer agents.

Glucose-regulated proteins (GRPs) are a class of chaperone proteins of the endoplasmic reticulum that serve as key sensors for misfolded proteins and trigger the unfolded protein response (UPR) under physiological and pathological stress conditions. Moreover, GRPs have been classified as clinically relevant biological markers in cancer detection and treatment and found to be over-expressed and cell surface localized in a wide range of cancer types. In cancer, the GRPs regulate cancer initiation, proliferation, adhesion, and invasion which contributes to metastatic spread and treatment resistance. Over the last decade, our research program has focused on the development of various high-order, self-assembled, multi-functional siRNAs

capable of silencing the oncogenic GRPs, and reversing their protective UPR effects related to proliferative, pro-survival, and anti-apoptotic pathways in selected tumors. Chemical tools have been implemented to improve the poor pharmacological properties of siRNAs to maximize their full therapeutic efficacy against tumorigenic disease conditions, which are highlighted in Chapter 1 of this thesis.

Chapter 2 highlights the development of synthetic strategies to improve siRNA metabolic stability, cellular uptake, and delivery, which are still in widespread demand for effective siRNA therapeutic applications. More specifically, this research aims to incorporate a small set of fatty acids into chemically derived siRNAs to improve their metabolic stability and cancer cell permeability. To achieve this goal, we have generated the higher-order siRNAs based on self-assembled branching structures. The self-assembled branch siRNAs were generated from their corresponding RNA template strands, which incorporated a synthetic ribouridine branchpoint synthon. This monomer was developed by an efficient solution-phase synthesis route and can be effectively incorporated within linear, V, and Y-shaped RNA templates by automated solid-phase RNA synthesis. Furthermore, an optimized coupling procedure has been developed for tagging variable saturated and unsaturated fatty acids onto linear, V- and Y-shape RNA templates. The RNA-fatty acid bioconjugates were analyzed, purified, and characterized by LC/MS. They were then hybridized with complementary RNA single strands to afford the amphiphilic self-assembled branch siRNA bioconjugates. The amphiphilic siRNA bioconjugates were detected by native PAGE, CD spectroscopy, and RP IP HPLC, while characterization of their self-assembled nanostructures was determined by DLS and TEM. Furthermore, the self-transfection capabilities of the siRNA-fatty acid bioconjugates and their biological activities within a model prostate cancer (PC-3) cell line revealed partial cell uptake, which contributed to

modest RNAi activity when compared to the siRNA controls transfected with a commercially available transfection reagent. Nonetheless, this reported solid-phase RNA bioconjugation approach provides an important entry point for the incorporation of various hydrophobic and amphiphilic functional groups. This strategy may enable further development of new generation RNAi molecules for screening important oncogene targets and for improving cancer gene therapy applications.

Chapter 3 describes the synthesis, characterization, and biological evaluation of a new class of bifunctional gold (Au)-RNA nanoparticles to improve cellular uptake and theranostic utility of the multi-functional siRNA nanostructures in prostate cancer cells. In this study, we have developed a simple, bottom-up approach using alkylamino modified RNAs to produce stable and small Au-RNA nanoparticle formulations bearing either a fluorescent reporter (fluorescein) or a fatty acid group (palmitamide) to track cell uptake in PC-3 prostate cancer cells. The resulting Au-functionalized RNA particles were found to be stable under reducing conditions according to UV-Vis spectroscopy. Sample characterization by DLS and TEM confirmed self-assembly into primarily small (~10-40 nm) spherical shaped nanoparticles anticipated to be applicable to cell biology. The application of Au-functionalized siRNA particles in prostate cancer (PC-3) cells resulted in the knockdown of GRP75, which led to detectable levels of cell death in the absence of a transfection vector. Consequently, this novel Au-RNA theranostic formulation may prove to be a valuable bifunctional probe in the early detection and treatment of prostate cancer and related solid tumors.

Chapter 4 of this thesis summarizes our on-going and future work aimed at incorporating cell-targeting ligands within the Au-siRNA nanoparticle formulations for specific cancer

treatment in cell cultures and within tumor-bearing mice models. The study aims to modify the Au-siRNA nanoparticle formulation with cell-targeting peptides (CTPs), which functions to target and bind to a cell surface receptor, in this case, PSMA, found on the surface of select prostate cancer cells. A PSMA-targeting peptide sequence has been selected for targeted delivery of the Au-siRNA formulation directly within $PSMA^{+}$ prostate cancer cells for the application of cancer-targeting gene therapy. Taken together, this thesis will serve to highlight the synthetic strategies towards the development of higher-order self-assembled siRNA bioconjugates with self-transfection capabilities for silencing multiple oncogenic GRPs in cancer.

KEYWORDS: siRNA, Glucose Regulated Proteins (GRPs), Prostate Cancer, siRNA nanostructures, siRNA bioconjugates (Fatty acids, Gold Nanoparticles, Florescent Probes).

ACKNOWLEDGEMENTS

Originally undecided in which direction I wanted to take my life after I came to the United States in December 2012 to support, encourage, and accompany my life-partner for her ambitions to achieve a Ph.D. degree in Engineering. Finally, in the Fall of 2015, following much encouragement and strong will power of my life partner-Kinnari made me look back again to Chemistry. Thereby, I was re-introduced to the world of Chemistry, and since then I never looked back. After completing my education in India in the field of plastics technology, Chemistry and Chemical Engineering, I decided to pursue a Ph.D. degree in Chemistry at Seton Hall University. Five years later, I can confidently state that it has been one of the most challenging and rewarding experiences in my professional life. I have had the privilege of learning lessons that will serve me well in all facets of life.

I would like to express my utmost gratitude to my Ph.D. advisor, Dr. David Sabatino, for accepting me into his research group and helping to mold me into the scientist I am today. Through the rollercoaster of emotions that comes with a graduate degree, he has been there to provide confidence, support, and most importantly, guidance to persevere in the completion of my Ph.D. work to the highest standard. I have been privileged to have Dr. Sabatino as a mentor and a friend. I am grateful to have had the opportunity to complete my thesis work under his guidance.

I would also like to extend my sincerest gratitude to Dr. Jenny Zilberberg for serving as my co-mentor and for taking me under her wing and welcoming me into her research lab. When Dr. Zilberberg formed part of our collaboration, I never imagined it would lead to the relationship we've built and all the work we've been able to accomplish in only two short years.

Dr. Zilberberg instructed me to look at science from a much larger perspective and helped me to grow as an independent scientist. For that, I am thankful and lucky to have had the opportunity to work with her.

I would also like to thank the rest of my thesis committee: Dr. Wyatt Murphy, Dr. Nicholas Snow, Dr. Yuri Kazakevich, and Fr. Gerald Buonopane. A special thank you to Dr. Murphy and Fr. Buonopane for reading and reviewing my dissertation. Your insights and knowledge have helped me complete my thesis work. I am also thankful to Dr. Snow for all the direct and indirect encouragement, support, and motivation. I'd like to extend a thank you to the rest of the faculty in the Department of Chemistry and Biochemistry for all the fruitful interactions over the years. You have constructively challenged me every step of the way and it has helped broaden my horizons. A special thank you to Ms. Maureen Grutt for everything she has done for me. This experience has been all the better because Maureen was a part of it. I would also like to extend my gratitude to the Jimmy-building engineer and Ralf-stock room manager for their timely support. Thanks to the support from the International Office, Registrar's Office, Library, and Career Center.

I thank my friends and colleagues at another home in lab 419 of Seton Hall. To Chris, Steve, Mayur, Mariana, Niki, Gina, Nelson, Akilah, Keith, Claudia, Andreih, Adah, and Vanessa, I extend a warm thank you for making my time here all the better. You've challenged and helped me, and I consider you all as family. I am happy about the relationships we've built, and I hope to keep them moving forward. I would also like to thank my colleagues with whom I interacted during my tenure at Seton Hall University specifically Marko, Hader, Heidi, Neelam, Tiana, Charnette, Christina, Hetal, Usha, Mufeda, Mary, Marius, Santhosh, Ramesh, Jeff, Greg, Erik, Abdul thank you and a very special thanks to 'Kyaw Win (Joe)' and 'Thuan Le Hong' who

is a very kind-hearted, supportive, and very special friend, that formed a special bond with me and my family. I am especially thankful to Merck (Execupharm), Kenilworth, for providing me an opportunity to work as a Senior Scientist before my graduation.

Lastly, and most importantly, I would like to thank my parents and family in India, and my lovely wife -Kinnari, and God-gifted son-Aagam for all their love and support during this time. I cannot express my gratitude for all you've done for me and this has only been possible because of it.

Table of Contents

Chapter 2: Direct Transfection of Fatty Acid Conjugated siRNAs and Knockdown of the Glucose-Regulated Chaperones in Prostate Cancer Cells

Chapter 3: Bifunctional Au-templated RNA Nanoparticles Enable Direct Cell Uptake Detection and GRP75 knockdown in Prostate Cancer

LIST OF FIGURES

LIST OF TABLES

LIST OF SCHEMES

ABBREVIATIONS AND SYMBOLS

P/S	Penicillin/streptomycin
©	Copyright
®	Registered
°C	Degrees Celsius
µg	Microgram
µL	Microliter
µM	Micromolar
µmol	Micromole
™	Trademark
1°mAb	Primary Monoclonal Antibody
2°mAb	Secondary Monoclonal Antibody
A	Adenosine
Annealing buffer	30 µM 10 mM Tris, 50 mM NaCl, 1 mM EDTA, pH 7.5–8.0, 50 µL
A.U.	Absorbance Units
Au	Gold
ASO	Antisense Oligonucleotides
AuNP	Gold Nanoparticles
Ago2	Argonaute 2
AHX	Amino-Hexanoic Acid
AN3CA	endometrial Cell
ASGPR	Asialoglycoprotein receptor
BSA	Bovine Serum Albumin
C	Cytosine
C16	Palmitamide
C. elegans	Caenorhabditis elegans
Ca^{2+}	Calcium
CAS	CRISPR-associated protein
CD	Circular Dichroism
CDC	Complement-dependent cytotoxicity

cDNA	Complimentary DNA
cm-siRNA	Chemically Modified siRNA
CO_2	Carbon Dioxide
CPP	Cell Penetrating Peptide
CRISPR	Clustered Regularly Interspaced Short Palindromic Repeats
CTP	Cell Targeting Peptide
CuAAC	Copper-Catalyzed azide-alkyne cycloaddition
CUNY	City University of New York
DCM	Dichloromethane
DIEA	*N,N*-Diisopropylethylamine
DLS	Dynamic Light Scattering
DMEM	Dulbecco's Modified Eagle Medium
DMF	Dimethylformamide
DNA	Deoxyribonucleic Acid
DOPC	1,2-Dioleoyl-*sn*-Glycero-3-Phosphocholine
DOTAP	1,2-Dioleyl-3-trimethylammonium-propane
dsRNA	Double-Stranded Ribonucleic Acid
DTT	Dithiothreitol
e.g.	For example
EDTA	Ethylenediaminetetraacetic Acid
eGFP	Enhanced Green Fluorescent Protein
EGFR	Epidermal Growth Factor Receptor
EPR	Enhanced Permeability and Retention Factor
ER	Endoplasmic Reticulum
ESI-MS	Electrospray Ionization Mass Spectrometry
ETT	5-ethylthiotetrazole
F	Fluorine
FA	Folate
FACS	Fluorescence Assisted Cell Sorting
FAK	Focal Adhesion Kinase
FA-siRNA	Fatty Acid conjugated siRNA

FBS	Fetal Bovine Serum
FITC	Fluorescein Isothiocyanate
FL	Fluorescence
FL-siRNA	Fluorescently Labeled siRNA
FRET	Fluorescence resonance energy transfer
G	Guanosine
GalNAC	N-acetylgalactosamine
GFP	Green Fluorescent Protein
GAPDH	Glyceraldehyde-3-phosphate Dehydrogenase
GRPs	Glucose Regulated Proteins
GRP75	Glucose Regulated Protein, 75 kilodaltons
GRP78	Glucose Regulated Protein, 78 kilodaltons
GRP94	Glucose Regulated Protein, 94 kilodaltons
H_2O	Water
HCTU	O-(1H-6-Chlorobenzotriazole-1-yl),1,1,3,3-tetramethyluronium hexafluorophosphate
HCS	High Content Screening
HER2	Human Epidermal Growth Factor receptor 2
HeLa	Cervical Celllines
HepG2	Hepatoblastoma Cell
HPLC	High Performance Liquid Chromatography
HSPA5	Heat Shock Protein Family A
Hr	Hour
HRP	Horseradish Peroxidase
IGF-1	Insulin-Like Growth Factor 1
KD	Knockdown
KSP	Kinesin Spindle Protein
LC/MS	Liquid Chromatography/ Mass Spectrometry
LDH	Lactate Dehydrogenase
LDS	Lithium Dodecyl sulfate
LNA	Locked nucleic acid

Lv	Levulinyl
M	Molar
m/z	Mass to Charge Ratio
Me	Methyl
MeCN	Acetonitrile
MEM	Minimum Essential Medium
MeOH	Methanol
mg	Milligram
miRNA	Micro-RNA
mA	Milliamp
mL	Milliliter
mM	Millimolar
mmol	Millimole
MMT	Monomethoxy Trityl
mRNA	Messenger RNA
MS	Mass Spectrometry
n	nucleotide
N	Nucleocapsid
NAb	Neutralizing Antibody
NaCl	Sodium Chloride
NAION	non-arthritic anterior ischemic optic neuropathy
n-BuOH	n-Butanol
N-cad	N-cadherin
ncRNA	Non-coding RNA
ng	nanogram
NIR	Near Infrared
nm	Nanometer
nM	Nanomolar
nmol	nanomole
NP	nanoparticle
NMM	N-methylmorpholine

NMR	Nuclear Magnetic Resonance
MDA-MB-231	Breast Cells
PAGE	Polyacrylamide Gel Electrophoresis
PBS	Phosphate-Buffered Saline
PCa	Prostate Cancer
PEI	Polyethyleneimine
PI	Propidium Iodide
PKN3	Protein Kinase N3
PLGA	Poly Lactic-co-Glycolic Acid
PLL	Poly-L-Lysine
PLK	Polo-like Kinase 1
pM	Picomolar
pmol	Picomole
PNA	Peptide nucleic acid
PSMA	Prostate Specific Membrane Antigen
PVDF	Polyvinylidene Fluoride
qRT-PCR	Quantitative Real-Time Polymerase Chain Reaction
RISC	RNA-Induced Silencing Complex
RNA	Ribonucleic Acid
RNAi	Ribonucleic Acid Interference
RP IP HPLC	Reverse-Phase Ion Pairing High-Performance Liquid Chromatography
RPMI	Roswell Park Memorial Institute Medium
RRM2	Ribonucleotide reductase M2 subunit
RSV	Respiratory syncytial virus
rU	Ribouridine
SDS-PAGE	Sodium Dodecyl Sulfate Polyacrylamide Gel Electrophoresis
saRNA	Small Activating RNA
shRNA	Short-Hairpin RNA
siRNA	Short-Interfering RNA
ssRNA	Single Stranded RNA
T	Thymidine

TAE	Tris/Acetic Acid/EDTA
TBE	Tris/Borate/EDTA
TBST	Tris-Buffered Saline/ Tween-20
TEM	Transmission Electron Microscopy
TES	Triethyl silane
TF	Transferrin
THF	Tetrahydrofuran
TLC	Thin Layer Chromatography
Tris	Tris(hydroxymethyl)aminomethane
U	Uridine
UNA	Unlocked nucleic acid
UPR	Unfolded Protein Response
UV-Vis	Ultraviolet- Visible Spectrophotometry
VEGF	Vascular Endothelial Growth Factor
vs	Versus

Chapter 1: Theranostics Applications of siRNA and their Bioconjugates in RNAi Based Gene Therapy

1.1 Discovery of the RNAi Mechanism

The RNA interference (RNAi) mechanism of mRNA suppression remained enigmatic until the pioneering work of Victor Ambros' group,[1] and by American scientists Andrew Fire and Craig Mello.[2] Their seminal work on the regulation of gene expression with the model organism Caenorhabditis elegans (C. elegans) led to the discovery of small, non-coding RNAs that interfered with gene expression at the mRNA level, leading to suppression of protein synthesis. Their efforts demonstrated that a simultaneous injection of sense and antisense double-stranded RNA (dsRNA) targeting the mRNA transcript of the unc-22 gene exhibited very specific and operative inhibition of the uncoordinated (unc-22 & unc-54) genes. Inhibition of gene expression for the myofilament protein in C. elegans led to articulated twitching which suggested a direct correlation between gene suppression and functional responses within the organism. The proposed mechanism for gene suppression revealed the importance of the antisense RNA strand in targeting and suppressing mRNA expression resulting in the disruption of protein production and observable changes in phenotype characteristics. Subsequent to their findings, Guo and Kemphues[3] worked on the inhibition of the par-1 gene in C. elegans, a major protein involved in the embryonic development of worms. This work led to the discovery of the effects of the sense RNA strand, which seemed to function by a separate mechanism compared to the antisense RNA strand and was found to be rather restricted as a putative passenger strand for a targeted mRNA region. Their mechanistic studies with nematodes revealed that upon treatment with sense and antisense dsRNA targeting the unc-22 gene, nematodes became strong twitchers. This functional response was absent when the organism was treated with either sense or

antisense single-stranded RNA (ssRNA), underscoring the critical importance of dsRNA-mediated suppression of gene expression. The fundamental mechanism of RNAi was later confirmed by Fire and Mello.[4] Based on their previous work on the suppression of unc-22 and unc-54 genes in C. elegans, complementary dsRNA sequences produced a more compelling loss in motor function when compared to the antisense or sense RNA sequences applied independently, even at lower dsRNA doses.[4] Fire and Mellow were subsequently awarded the Nobel Prize in Physiology or Medicine in 2006 for their discovery of the RNAi pathway.[5]

1.2 siRNA Structure and Function in RNAi Pathway

Small interfering RNA (siRNA) is a class of non-coding RNAs composed of a complementary sense and antisense dsRNA containing 18-25 base-pairs.[6-8] The dsRNA is composed of a well-defined structure consisting of a phosphorylated 5'-end and a hydroxylated 3'-end typically containing a two nucleotide (nt) overhang. This small dsRNA also consists of an active guide (antisense) strand and an inactive passenger (sense) RNA strand. Considerable progress has been made to optimize the requisite parameters for stable dsRNA formation while designing siRNAs with enhanced RNAi potency. This includes optimization of thermodynamic properties by the implementation of algorithms used to create thermodynamically stable symmetric and asymmetric siRNAs. Computational analysis has been used to select the sequence compositions for the sense and antisense RNA strands that confers a stable A-type helix dsRNA secondary structure and binding specificity to targeted mRNA. Furthermore, siRNA modifications have been developed for enhancing RNAi activity while minimizing off-target silencing effects, and immunostimulatory activities that are known to cause toxicity. These modifications have also served to improve siRNA stability in biological media while enhancing cell uptake for RNAi activity *in vitro* and *in vivo*. **Figure 1.1** shows the representative sequence

and secondary structure motifs that may be implemented or modified for improved RNAi potency. A comprehensive study on a combinatorial library of chemically synthesized siRNA,[9] revealed four sets of rules based on optimizing the siRNA base composition of the sense strand. These include Rule 1: presence of A/U at position 19, GC at the first position, A/U at position 10, 43 A/Us at position 13–19; Rule 2: presence of A/U at position 19, GC at the first position, GC at position 10, 43 A/Us at position 13–19; Rule 3: presence of G/C at position 19, GC at position 1, GC at position 11, 46 A/Us at position 5–19; and Rule 4: presence of A/U at position 19, A/U at position 1, 43 A/Us at position 13–19. Taken together, these rules provide a general understanding of designing siRNAs of desired structure and sequence compositions for the advancement of more efficient siRNAs in RNAi applications.

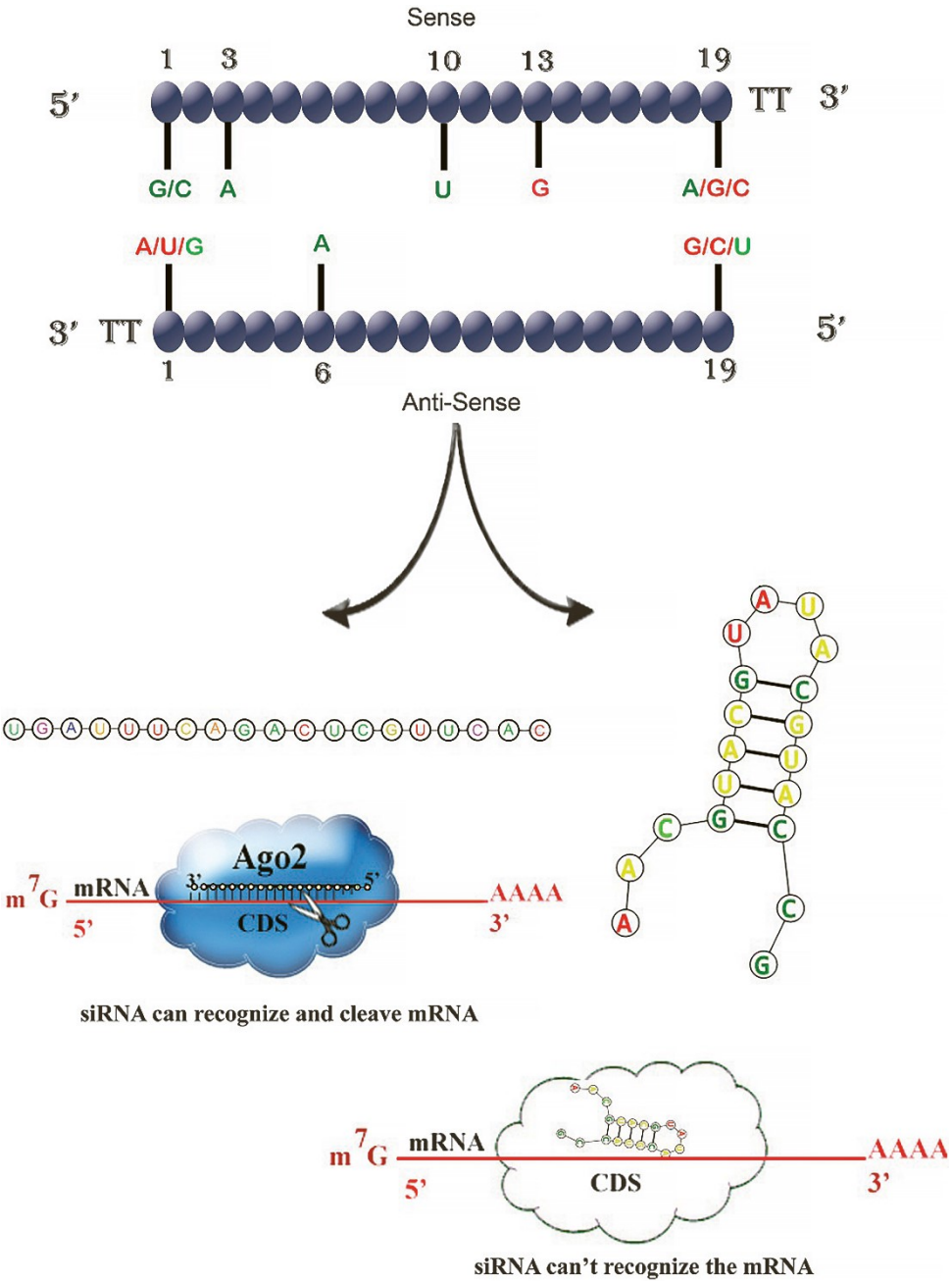

Figure 1.1. Representative characteristics of siRNA sequence and structure compositions; green bases are in favorable positions, whereas bases in red should be avoided. Ago, Argonaute; CDS, coding sequence. Figure reproduced with permission from: Fakhr, E.; Zare, F.; Teimoori-Toolabi, L. *Cancer Gene Ther*. **2016,** 23, 73–82.[7]

The RNAi pathway that occurs in plants, animals, and humans is a natural biological defense mechanism used for the inactivation of exogenous genes and theoretically can be applied to silence any disease-related genes in a sequence-specific manner.[10] Thus RNAi modalities, siRNA, and microRNA (miRNA) provide therapeutic potential, by the knockdown of malignant gene expression in a sequence-specific manner by targeted mRNA translation inhibition and degradation (**Figure 1.2**).[10-12] In this pathway, the active components of the RNAi machinery are identified and assembled to initiate the first step of the RNAi pathway. This involves the processing of long non-coding dsRNA or short hairpin RNA (shRNA) by binding to the cytoplasmic enzyme Dicer, a member of the RNase III family which subsequently cleaves the dsRNA into smaller siRNA fragments, typically 21-23 nucleotides in length.[13] The siRNA is then recruited and bound onto the RNA-activated silencing complex (RISC) complex, which separates the antisense and sense RNA strands. The sense RNA strand dissociates from the RISC complex and eventually undergoes cleavage and degradation by endogenous nucleases, while the antisense RNA strand bound within RISC will target and bind to the corresponding mRNA sequence.[14] The mRNA sequence undergoes inhibition of protein translation and degradation by the catalytic action of the Argonaute II ribonuclease subunit embedded within the active site of the RISC complex.[15] In this manner, the RNAi mechanism is used ubiquitously for the regulation of gene expression in prokaryotes and mammalian cell types as well as in a wide range of organisms resulting in important adaptive and functional changes. It is also important in the defense against various invading pathogens or the elimination of gene expression within malignant cells. The latter holds therapeutic implications, as the design and development of siRNAs targeting malignant mRNA have been applied in the prevention and treatment of a broad

range of human diseases.[16] Thus, the RNAi pathway opens exciting possibilities for use in gene silencing technologies.

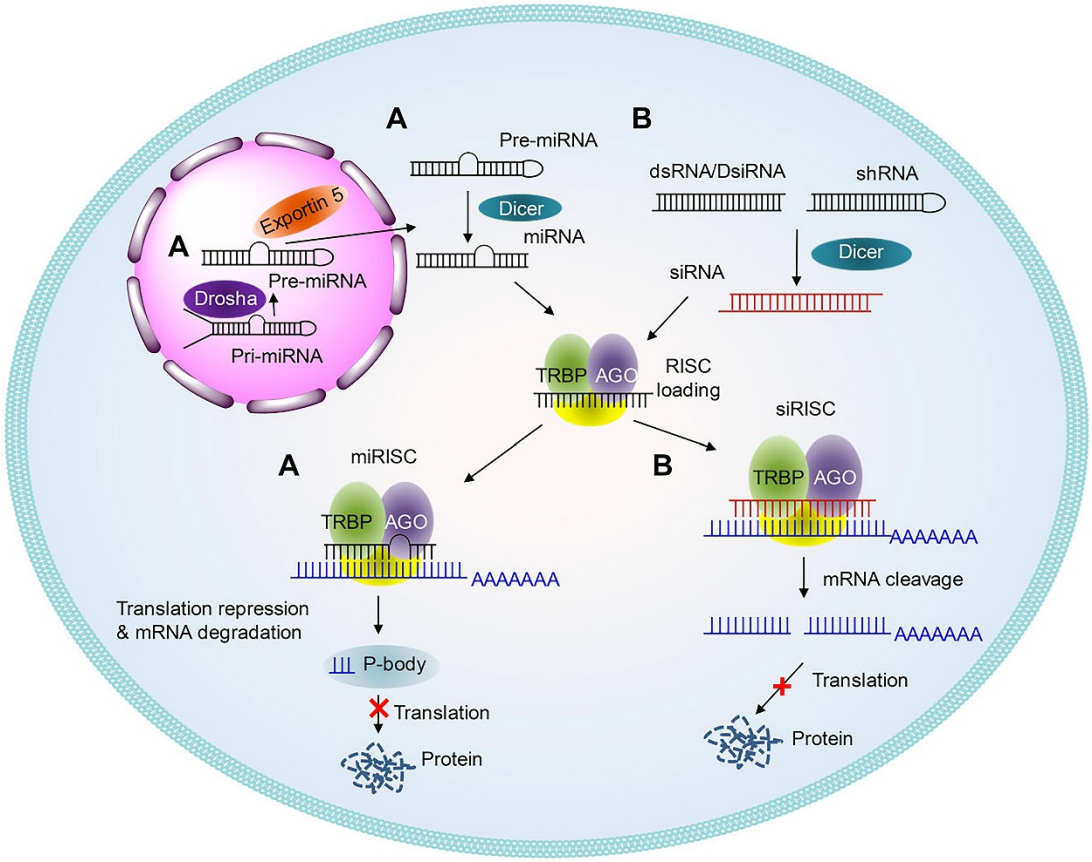

Figure 1.2. Schematic illustrations of the working mechanisms of miRNA (A) and siRNA (B). Figure reproduced with permission from: Hu, B.; Zhong, L.; Weng, Y.; Peng, L.; Huang, Y.; Zhao, Y.; Liang, X.J. *Signal Transduct. Targeted Ther.* **2020,** 5, 101.[12]

1.3. Therapeutic siRNAs

This RNAi method has already become an important research tool in biology and biomedicine. Significantly, after a long journey from its discovery, two clinical approvals of siRNA therapeutics, ONPATTRO® (Patisiran) and GIVLAARI™ (Givosiran) have been recently achieved by Alnylam Pharmaceuticals. These siRNA-based therapeutics are respectively used for the treatment of polyneuropathy in adults with hereditary transthyretin-mediated amyloidosis; or for treatment of acute hepatic porphyria, a genetic disorder resulting in the buildup of toxic porphyrin molecules which are formed during the production of heme.[12] Furthermore, additional RNAi-based treatments are currently in the clinical pipeline for various diseases such as cancer, Huntington's disease, chronic liver diseases, eye diseases such as glaucoma, and retinopathy in diabetes.[17,18]

Among the other clinical siRNA candidates, QPI-1002 (I5NP) and QPI-1007 have been developed by Quark Pharmaceuticals targeting the p53 tumor suppressor for respectively treating acute kidney injury (phase 2 trials) and delayed graft function (phase 3 trials).[19,20] Due to their biochemical nature, the QP-1002 siRNAs accumulated in the kidney at concentrations >40 times compared to other tissues and organs; and resulted in p53 mRNA eradication in proximal tubule cells at a concentration of ~1 nM. Furthermore, bilateral renal-clamp studies confirmed the preservation of kidney function following siRNA treatment. These therapeutic effects were also observed in siRNA-treated animals which showed ischemia with decreased serum creatinine levels from 3.7 mg/dL to 1.9 mg/dL with little toxicity observed at standard dosages. Comparatively, the QPI-1007 siRNAs targeted the pro-apoptotic mediator caspase-2, to treat acute primary angle-closure glaucoma (phase 2 trials) and non-arthritic anterior ischemic optic neuropathy (NAION, phase 3 trials).[23] Preclinical investigations validated potent caspase-2 gene

silencing in HeLa cells and reversed optic nerve damage in injured animal models without any serious side-effects.[21] It was concluded that QPI-1007 significantly protected the optic nerve in pre-clinical and clinical trials, underscoring the therapeutic efficacy of siRNA treatment.[22]

A clinical siRNA candidate, ALN-RSV01 (Asvasiran sodium), has also been developed to thwart the progression of infectious diseases. This unmodified siRNA targets the respiratory syncytial virus (RSV) nucleocapsid (N) gene which consequently inhibits viral replication.[24] Clinical data validated its beneficial effects on long-term allograft function in lung transplant patients infected with RSV,[25-27] while another report showed that ALN-RSV01 aids in the prevention of bronchiolitis obliterans syndrome following lung syncytial virus infection in lung transplant patients.[28] Similarly, other beneficial siRNAs have also been made to target various receptors such as polo-like kinase 1 (PLK1),[29] kinesin spindle protein (KSP),[30] and ribonucleotide reductase M2 subunit (RRM2);[31] which play important roles in cell cycle progression; KRAS(G12D)[32] implicated in cell signaling; protein kinase N3 (PKN3)[33,34], tenascin C[35], and for cell proliferation and angiogenesis vascular endothelial growth factor (VEGF)[36,37] is involved. Thus, therapeutic siRNAs have been used to target a wide range of biological markers implicated in a variety of disease states ranging from infectious to metabolic and genetic disorders.

1.4. Limitations of therapeutic siRNAs and remedial strategies

However, the development of RNAi-based therapeutics is not without challenges.[38,39] Namely, the small RNA molecule may be effectively cleared via the renal system thereby restricting its therapeutic index. Native siRNAs are also widely susceptible to nuclease digestion, limiting their therapeutic efficacy in biological media. Furthermore, siRNAs can exert a toxic

immunological response by binding and activating certain receptors of the innate immune system. For example, Toll-Like Receptors (2), have been activated by siRNAs, igniting a cytokine/chemokine storm which may have detrimental side-effects and widespread toxicity. Among their most significant limitations, siRNAs are negatively charged and lack cell permeability. Delivery of native siRNAs into cells has been a paramount challenge, generally resulting in poor transfection efficiency and ineffective gene therapy. To overcome this challenge, several methods have been implemented—electroporation, calcium phosphate transfection, and microinjection for effective siRNA delivery into target cells.[40] However, these methods are complex and tedious. Moreover, they are not suitable for long-term gene silencing effects and *in vivo* applications.

To overcome these challenges, a thorough evaluation of the sequence and structure compositions, biological potency, and toxicity parameters that may be optimized is critical for enhanced siRNA biological performance. Chemical modifications, self-assembly, and delivery formulations of siRNA have been developed to fulfill the functional requirements of siRNA activity while minimizing toxicity. Advancements in nucleic acid chemistry, bioconjugation approaches, programable and non-programmable self-assembly strategies related to RNA nanotechnology, delivery strategies with viral and non-viral vectors, and functionalized nanocarriers have all been applied for optimizing the efficiency of siRNA activity in target cells. The application of lipids, polymers, nucleic acids, proteins, and organic/inorganic materials have improved the biomedical applications of siRNAs in imaging,[41,42] sensing,[43] targeted drug delivery,[44] electronics, and nanomedicines.[45] Thus, siRNAs may be readily modified or combined with complementary components that may serve to improve their functional utility.

1.5. Chemically modified siRNAs

Chemically modified siRNAs (cm-siRNAs) have also been developed to improve the biophysical and biological properties of the native siRNAs. Typically, the most popular strategies include chemical modifications of the ribose sugar, modification of the phosphodiester backbone, and nucleobase changes which impacts hybrid stability (**Figure 1.3**).[12,46] The ribose sugar chemical modifications include the substitution of the 2'-hydroxyl (2'-OH) group with 2'-fluorine- (2'-F), 2'-O-methyl- (2'-O-Me), and 2'-amino- (2'-NH_2) substitutions which are isosteric and isoelectronic compared to native RNA allowing for dsRNA hybrid formation. Bulkier modifications, including 2'-O-methoxyethyl (2'-O-MOE), have more significantly impacted RNA folding. Similarly, 2'-methylene bridged locked nucleic acids (LNA) and unlocked nucleic acids (UNA), have served to increase RNA chemical and thermal stability while maintaining RNAi activity relative to control siRNA.[12,46-50] Furthermore, modification of the phosphodiester linkage has served to increase siRNA serum stability. The site-selective incorporation and/or replacement of the phosphodiester backbone with a phosphorothioate (substitution of the non-bridging oxygen for a sulfur atom);[51] boranophosphate (substitution of the non-bridging oxygen for a borane)[52] or an amide linkage (peptide nucleic acids, PNA).[53] The latter modification replaces the negatively charged phosphate with the neutrally charged amide bond, which evades nuclease and protease digestion, thereby increasing the chemical stability and gene silencing activity of cm-siRNAs.[54] Interestingly, these modifications have also minimized off-target gene silencing effects which have resulted in diminished toxicity. The single incorporation of 2'-O-Me and LNA within cm-siRNAs has been shown to improve the stability and specificity of the siRNA target gene silencing activity.[55] Modifications to the nucleobases have been explored and resulted in significant changes in base-pairing affinity.[56]

Some of these modifications include 5-bromouracil and 5-iodouracil as uracil derivatives, diamino purine as an adenine analog, 2-thiouracil, 4-thiouracil, pseudo-uracil, 5-methylation of pyrimidines, nonaromatic bases, and dihydrouracil. In most cases, the chemical RNA stability is significantly enhanced, however, the base-pairing function can be altered depending on the location of the modified bases within the sequence. Therefore, nucleobase modifications are less common in cm-siRNA therapeutic applications, although they have contributed to the basic understanding of the molecular requirements for siRNA hybrid formation and thermodynamic stability.[57] Taken together, chemical modifications have served to improve the stability, and biological activity of siRNAs while minimizing toxicity associated with off-target gene silencing or immunostimulatory activities. Thus, cm-siRNAs are preferred analogs that have served to improve the therapeutic efficacy of siRNA drug candidates.

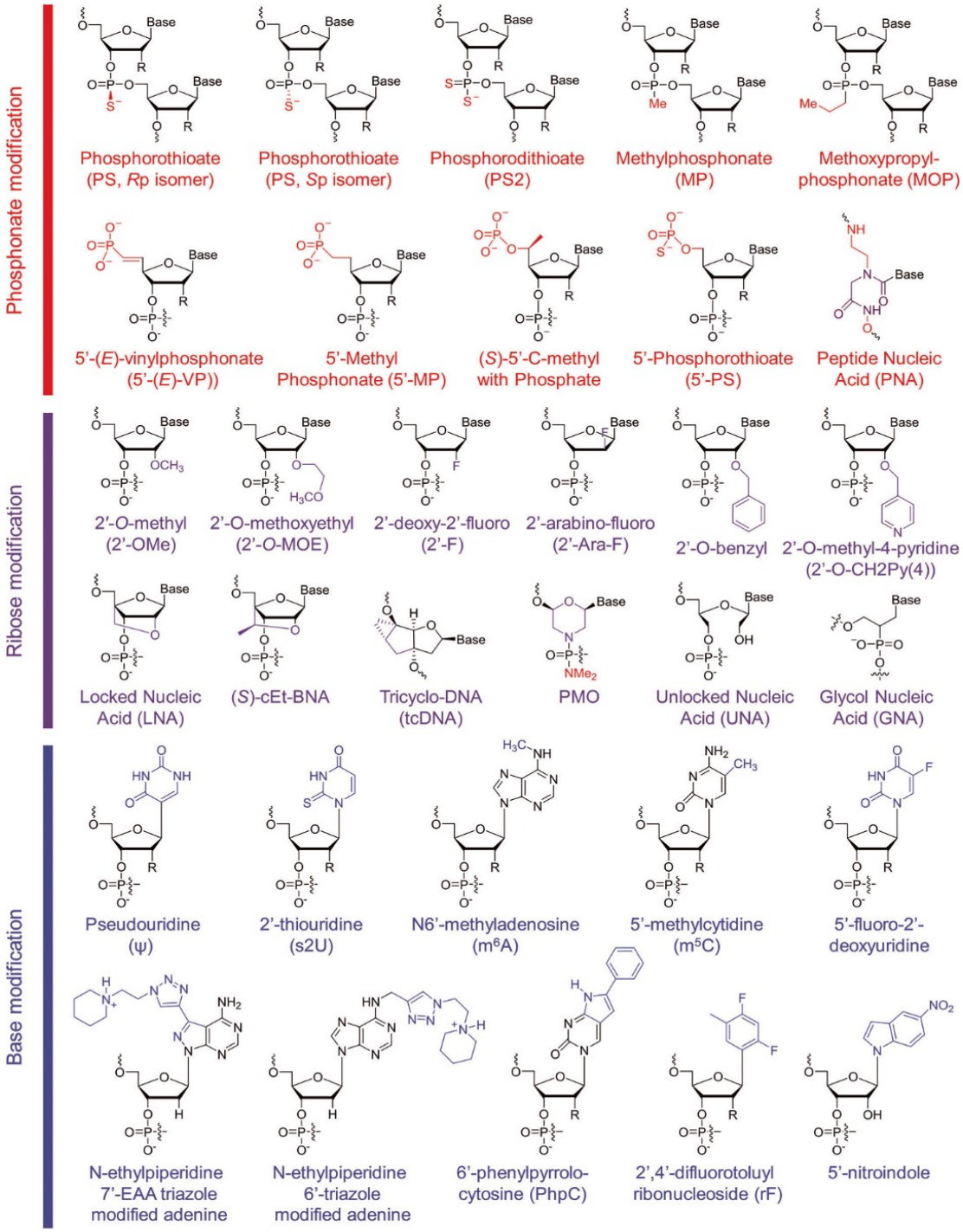

Figure 1.3. Structures of cm-siRNA. These structures can be divided into three classes: phosphodiester backbone, a ribose sugar, and nucleobase modifications, which are marked in red, purple, and blue, respectively. R = H or OH, for RNA or DNA, respectively. (S)-cEt-BNA (S)-constrained ethyl bicyclic nucleic acid, PMO phosphorodiamidate morpholino oligomer. Figure reproduced with permission from: Hu, B.; Zhong, L.; Weng, Y.; Peng, L.; Huang, Y.; Zhao, Y.; Liang, X.J. *Signal Transduct. Targeted Ther.* **2020,** 5, 101.[12]

1.6. siRNA Bioconjugation

Structural and chemical modifications that facilitate the incorporation of functional chemical ligands, such as fluorescent dyes, lipids, chemotherapeutic drugs, or biotin, within RNA by well-established chemical conjugation strategies have served to improve the utility of siRNA bioconjugates (**Figure 1.4**).[58] For example, siRNA bioconjugates have been synthesized by Click chemistry, using the copper-catalyzed azide-alkyne cycloaddition (CuAAC).[59] This conjugation approach produced a series of lipidated siRNA derivatives functionalized with long-chain alkyl, cholesterol, oligoamine, and carbohydrate groups. The siRNA bioconjugates resulted in luciferase knockdown within HeLa cells, thereby validating their potential utility in cancer gene therapy applications. A cancer-targeting approach was realized with folic acid PEG-conjugated siRNAs, prepared by the Cu(I) catalyzed 1,3-dipolar cycloaddition reaction. The functionalized siRNA displayed selective cell line permeability, in Neuro2A cells overexpressing the folate receptor on the cell surface. Cell uptake triggered silencing of the reporter Green Fluorescent Protein (GFP) thereby validating its applicability in receptor-guided gene silencing.[60] It has been shown that targeting ligands may enable binding affinity and cellular uptake via receptor-mediated endocytosis leading to improved RNAi efficacy of the siRNA bioconjugates relative to their native counterparts. For example, the anisamide conjugated siRNA combined with a hepta-guanidino β-cyclodextrin-PEG (G-CD-PEG) copolymer produced a multifunctional formulation which was found to stabilize the nanoparticles in physiological media and extended their circulation time *in vitro*. These desirable pharmacokinetic effects enabled selective binding affinity and effective cell uptake via the targeted s-receptor on the surface of PC-3 human prostate cancer cells, resulting in silencing of the reporter luciferase gene.[61] Conjugation of *N*-acetylgalactosamine (GalNAc) to siRNA via phosphoramidite

chemistry has significantly improved delivery to hepatocytes *in vitro* and *in vivo* by binding to the asialoglycoprotein receptor (ASGPR), followed by receptor-mediated cellular internalization.[62,63] It has been shown that multivalent GalNAc clusters conjugated to siRNAs resulted in potent RNAi-mediated gene knockdown in hepatocytes at therapeutically relevant doses in mice validating their potential to treat liver-associated genetic disorders. Cell-targeting peptides (CTPs) have also been used as homing agents for specific cellular and tissue delivery of siRNA bioconjugates. In a selected application, cRGD peptides targeting the integrin receptors were conjugated to siRNA following Michael addition chemistry of the thiolate functionalized siRNA with the maleimide containing cRGD peptides.[64] The cRGD-siRNAs targeting the luciferase reporter gene in αvβ3 positive $M21^+$ human melanoma cells produced progressive, dose-dependent knockdown, illustrating the synergistic effects of the multi-valent cRGD presentation of the cRGD-siRNA bioconjugates.[65] Selective conjugation approaches have also been developed in between monoclonal antibodies (mAbs) and siRNAs to improve therapeutic efficacy. For example, the Human Epidermal Growth Factor Receptor 2 monoclonal antibody (anti-HER2 mAb) bearing an aminooxy-functionalized cationic block copolymer facilitated condensation of GAPDH-silencing siRNA for delivery within $HER2^+$ tumors.[66] Following treatment, GAPDH levels were significantly reduced underscoring the therapeutic potential of targeted gene delivery approaches. Of relevance to the complementary work reported in this thesis, gold (Au) nanoparticles have been used to track siRNA activity in cells. Bioconjugation of poly-lysine to Au-nanoparticles enabled condensation and controlled release of siRNA silencing the GFP reporter in H1299 cells following exposure to near-infrared light.[67] Thus, multi-functional nanoparticle formulations may be effectively used in siRNA-based gene therapy.

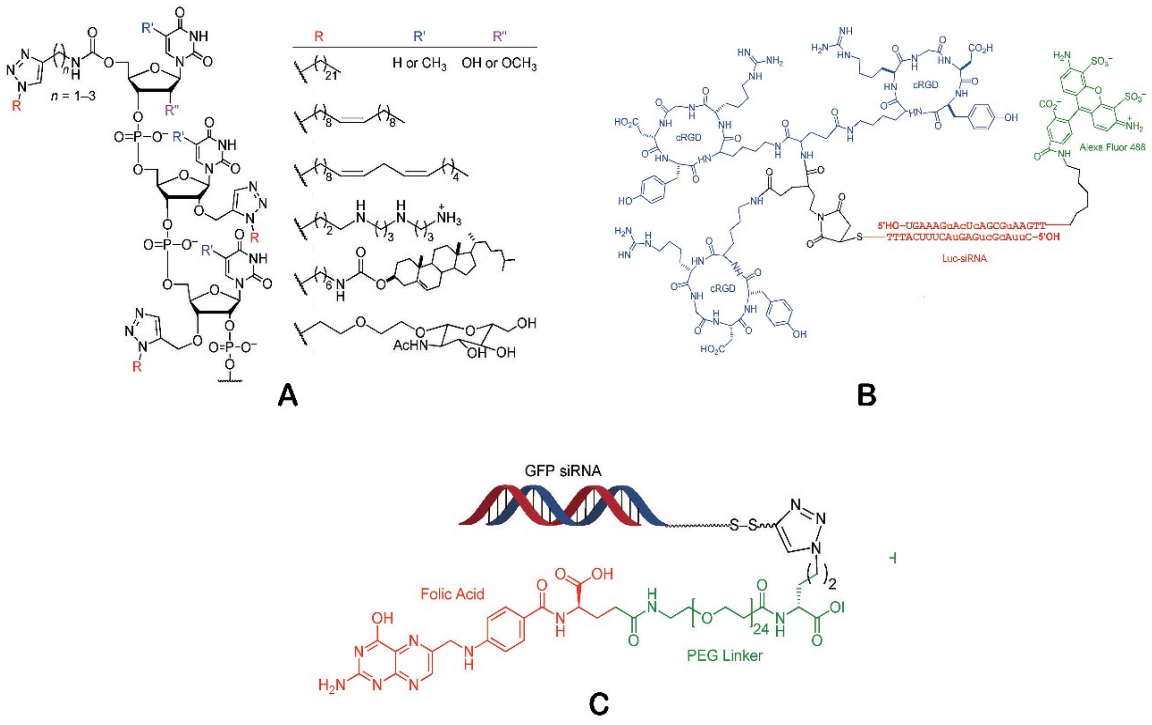

Figure 1.4. Representative examples of siRNA-based bioconjugates. Figure adapted with permission from: Patel PL, Rana NK, Patel MR, Kozuch SD, Sabatino D. *ChemMedChem.* **2016**, *1*(3), 252-269.[58]

1.7. Self-Assembled siRNA Nanotechnology

Advances in RNA structural biology have improved our understanding of the structures and folding properties of naturally occurring self-assembled RNAs.[68] The architectural potential of RNA relies on the ability of a single RNA strand to fold into thermodynamically stable three-dimensional structures. The incorporation of functional and structural RNA elements has been used to template the construction of high-order RNA structures. The presence of secondary structure RNA motifs— bends, stacks, junctions, loops, and chelates with divalent metal cations (Mg^{2+}, Ca^{2+}, Mn^{2+}, Co^{2+}, Pb^{2+}) or high concentrations of monovalent metal cations (Na^{+}) in

buffered pH have improved RNA structural stability and functional utility.[69] Several types of functional RNA or RNA elements have been applied in RNA self-assembly and nanotechnology including the formulation of siRNA nanostructures for multifunctional and synergistic RNAi activities.[70-80]

Some relevant examples of siRNA nanostructures **(Figure 1.5)** include the dumbbell-shaped nanocircular RNAs which triggered Dicer enzyme cleaving activity resulting in the formation of bio-active siRNAs for RNAi activity.[81-83] Trimer or tetramer RNA, containing multiple siRNA motifs embedded within the same higher-order molecular structure resulted in the intracellular release of siRNA for prolonged gene silencing activity as the siRNA nanostructures were found to be stable towards nuclease digestion.[84,85] The nano ring-shaped tectoRNAs also provided unique self-assembled molecular nanostructures which facilitated efficient siRNA cellular delivery for RNAi activity.[86] A spherical RNA nanostructure identified as the siRNA nano-sheet was synthesized by rolling circle transcription, effectively processed by Dicer resulting in siRNA production for the inhibition of mRNA expression.[87] The complementary RNA nanocubes formed an interesting class of nanostructures incorporating six dsRNA Dicer substrates, when cleaved produced six siRNAs which resulted in the suppression of the reporter, enhanced green fluorescent protein (eGFP) for up to twelve days in breast cancer cells using Lipofectamine as a transfection reagent.[78] In a related study, RNA nanorings containing multiple siRNAs within the nanoparticle formulation resulted in eGFP knockdown.[88] In a recent application, a synthetic supramolecular RNA nano-architecture was used to template the design of a novel truncated tetrahedral siRNA scaffold.[89] The modular pieces of complementary RNA self-assembled into a tetrahedral siRNA scaffold with enhanced cellular uptake and RNAi efficacy. siRNA nanoparticles have also been functionalized with RNA

aptamers for selective binding to the epidermal growth factor receptor overexpressed on human breast cancer cells. Cell uptake of the RNA nanoparticles led to persistent eGFP knockdown. Branched siRNA nanostructures self-assembled into three- and four-way junctions have also been designed and developed for targeting the luciferase reporter gene for up to five days in HeLa cells.[90] Thus, the ability for higher-ordered siRNA nanostructures to behave as Dicer substrates, resulting in the release of multiple siRNAs that ultimately results in potent gene knockdown effects underscores the potential utility of siRNA nanostructures in RNAi screening and gene therapy applications.

In our contributions to RNA nanotechnology, we have developed a novel synthetic method for the generation of linear, V, and Y-shape RNA templates that can self-assemble into high-order siRNA nanostructures.[91,80] In this work, higher-order branch and hyper branch siRNAs were synthesized by solid-phase RNA synthesis incorporating an orthogonally protected RNA branchpoint nucleotide which enabled selective construction of the branch RNA templates.[91] The branch RNA templates were designed with sequence composition targeting the Glucose Regulated Protein of 78 kilodaltons (GRP78) which has been classified as a clinically relevant biological marker in the treatment of cancer. The branch siRNAs were found to be stable in annealing buffer and Lipofectamine-based transfections in HepG2 liver cancer cells resulted in suppression of GRP78 expression and to a more significant extent compared to treatment with the control, linear siRNA. Our efforts to expand the repertoire of functional siRNA nanostructures culminated with the application of the previously described linear, V-shape, and Y-branch RNA templates to self-assemble with complementary RNA to form a variety of siRNA nanostructures.[80] The siRNA nanostructures were genetically encoded to target multiple GRPs and were applied in RNAi screening in cancer cell lines of the cervix, breast, and endometrium.

The siRNA nanostructures revealed the influence of GRP activity on cancer cell viability, whereby GRP silencing with the multi-GRP targeting siRNA nanostructures resulted in the most potent anti-cancer effects. Interestingly, GRP silencing in a non-tumorigenic lung cell line displayed modest toxicity effects, underscoring the importance of GRP overexpression and function in cancer biology while providing some insights into tumor treatment specificity.

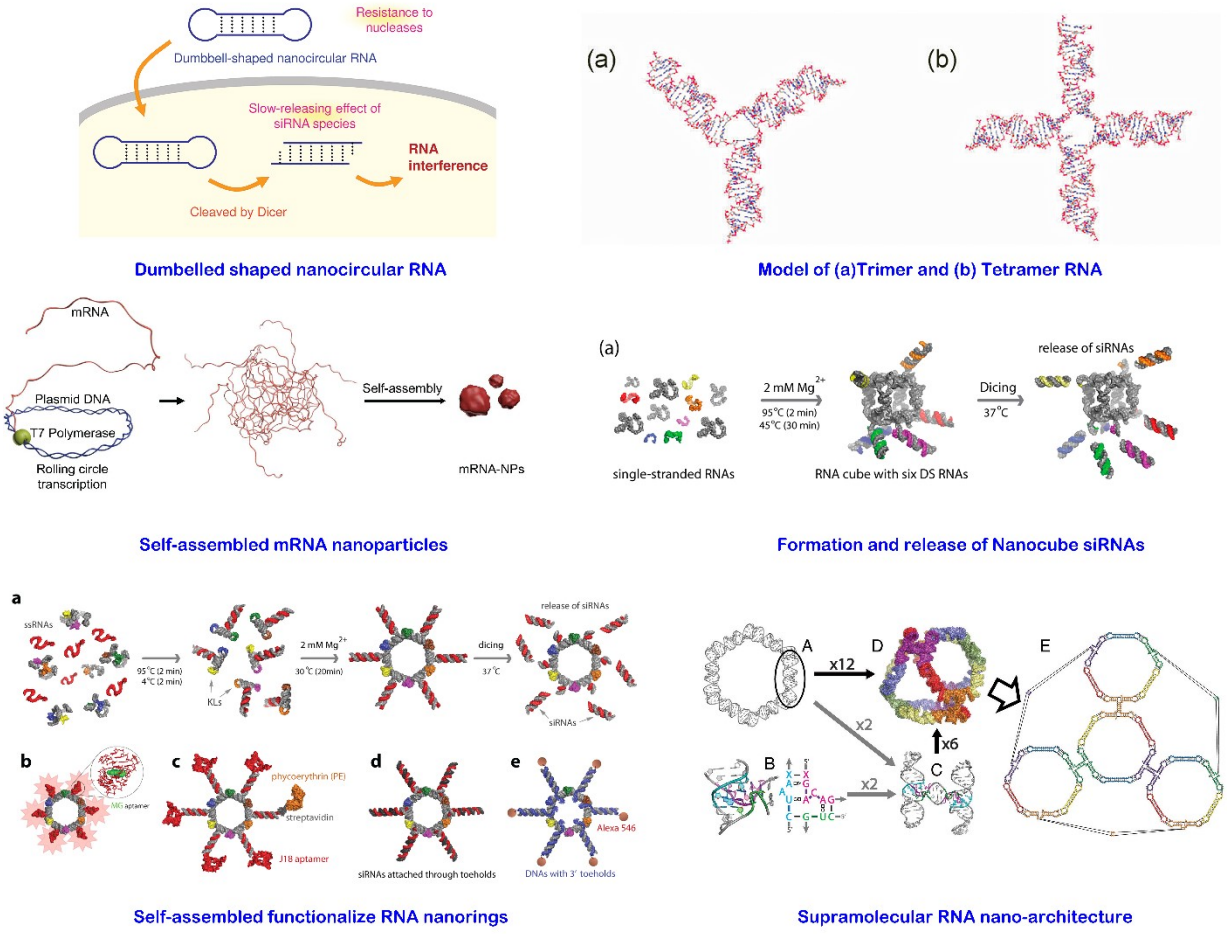

Figure 1.5. Representative examples of siRNA nanostructures. Figure adapted with permission from Refs. 78, 81, 85, 87-89 (Afonin, K.A.; Viard, M.; Kagiampakis, I.; Case, C.L.; Dobrovolskaia, M.A.; Hofmann, J.; Vrzak, A.; Kireeva, M.; Kasprzak, W.K.; Kewal Ramani, V.N.; Shapiro, B.A. Triggering of RNA Interference with RNA–RNA, RNA–DNA, and DNA–RNA Nanoparticles. *ACS Nano*. **2015,** *9(1)*, 251-259); (Abe, N.; Abe, H.; Ito, Y. Dumbbell-shaped nanocircular RNAs for RNA interference *J. Am. Chem. Soc.* **2007**, *129*,(49) 15108-15109); (Nakashima, Y.; Abe, H.; Abe, N.; Aikawa, K.; Ito, Y. Branched RNA nanostructures for RNA interference. *Chem. Commun*. (*Camb),* **2011**, *47(29)*, 8367-8369); (Kim H, Lee JS, Lee JB. Generation of siRNA Nanosheets for Efficient RNA Interference. *Sci Rep.* **2016**; *6*, 25146) ;(Afonin, K.A.; Viard, M.; Koyfman, A.Y.; Martins, A.N.; Kasprzak, W.K.; Panigaj, M.; Desai, R.; Santhanam, A.; Grabow, W.W.; Jaeger, L.; Heldman, E.; Reiser, J.; Chiu, W.; Freed, E.O.; Shapiro, B.A. Multifunctional RNA Nanoparticles. *Nano Lett*. **2014**, *14*, 5662-5671); (Zakrevsky, P.; Kasprzak, W.K.; Heinz, W.F.; Wu, W.; Khant, H.; Bindewald, E.; Dorjsuren, N.; Fields, E.A.; de Val, N.; Jaeger, L.; Shapiro, B.A. Truncated tetrahedral RNA nanostructures exhibit enhanced features for delivery of RNAi substrates. *Nanoscale.* **2020**, *12(4)*, 2555-2568).

Although we have developed a versatile strategy for the rapid construction of higher-order siRNA nanostructures, the inherent challenges associated with cellular RNA delivery and stability continue to limit its *in vitro* and *in vivo* efficacy, thereby increasing the demand for more effective RNA delivery carriers and transfection methods.

1.8 siRNA Delivery Systems

The rapidly emerging applications of gene therapy and therapeutic nucleic acids for the replacement or silencing of target malignant genes have increased the demand for the development of effective delivery strategies. Several biological barriers restrict the delivery and release of siRNAs into target cells for efficient RNAi activity **(Figure 1.6)**. Among the various extra- and intra-cellular barriers dampening siRNA efficacy are the endothelial and epithelial barriers, as well as tight junctions in selective tissues (e.g., the blood-brain barrier) that limits siRNA permeability. Furthermore, changes in pH, enzymatic digestion, and scavenging by the immune system may significantly impact siRNA biodistribution and therapeutic index. These barriers affect siRNA cellular targeting and penetration, intracellular trafficking, endosomal escape, and RNAi activity which ultimately leads to diminished therapeutic activity in the absence of an effective delivery system.[92,93] Therefore, it is difficult to achieve the desired therapeutic effect by direct, fusogenic siRNA delivery due to several biological and cellular barriers present in the body.

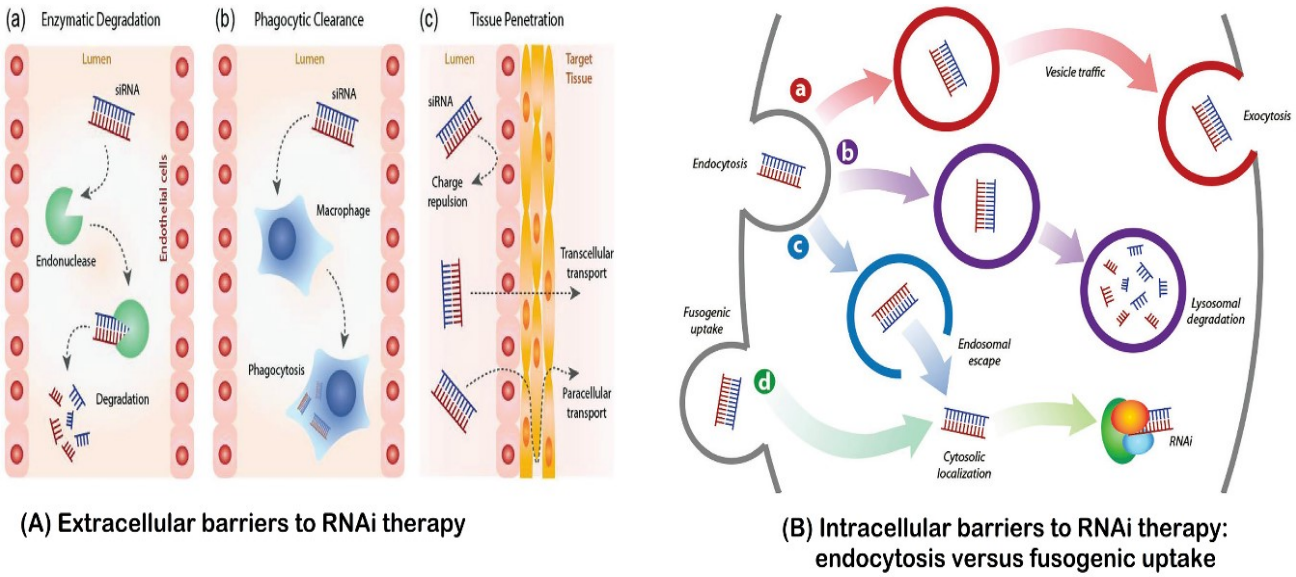

Figure 1.6. Biological barriers **(A)** Extracellular barriers to RNAi therapy. (a) Endonucleases degrade siRNA in circulation; (b) mononuclear phagocytic system, in particular, the macrophages remove siRNA within the major clearance organs (such as liver, lungs, and spleen); (c) tissue penetration of siRNA is hindered by charge repulsion between the anionic siRNA and the plasma membrane of endothelial/epithelial cells, as well as tight junctions in selective regions (e.g., the blood-brain barrier) that require transcellular or paracellular transport to reach the target tissue. **(B)** Intracellular barriers to RNAi therapy: endocytosis versus fusogenic uptake. (a) Endocytosis of siRNA, which eventually is excreted via vesicle trafficking and exocytosis, leads to negligible efficacy. (b) Endocytosis of siRNA, which carries the siRNA through early to late-stage endosomes, and lysosomes for acidification and degradation, also gives minimal efficacy. (c) siRNA can escape from the early endosomes to undergo RNA interference (RNAi) within the cytoplasm, but at attenuated potency due to inefficiency of the escape mechanism. (d) Fusogenic uptake of siRNA that leads to immediate cytosolic localization and RNAi. Figure adapted with permission from: Subhan, M.A.; Torchilin, V.P. siRNA-based drug design, quality, delivery, and clinical translation. *Nanomedicine: Nanotechnology, Biology, and Medicine.* **2020,** *29(102239)*, 1-20.[92]

The intracellular delivery of siRNAs is a challenging task requiring optimization of biological or synthetic vectors which can facilitate efficient cell uptake for RNAi activity.[93] Cell translocation of siRNA is a multi-step process that requires: i) cell-specific binding, ii)

internalization, iii) escape from endocytic vesicles, iv) transport through the cytoplasm and release of siRNA to complex with RISC and activate the RNAi pathway for silencing mRNA expression **(Figure 1.7)**.[94] The selection of effective delivery vehicles that may facilitate siRNA bio-activity require A) selection of a proper administration route, e.g. oral *vs* intravenous or infusion injections; B) a colloidal delivery system capable of efficiently condensing siRNA into small, monodispersed nanoparticles (≤ 80nm) to penetrate the biological barriers; C) cell-penetration and release of the siRNA into the cytoplasm for RNAi activity; which may produce a desirable D) efficacy and safety response upon administration.[94]

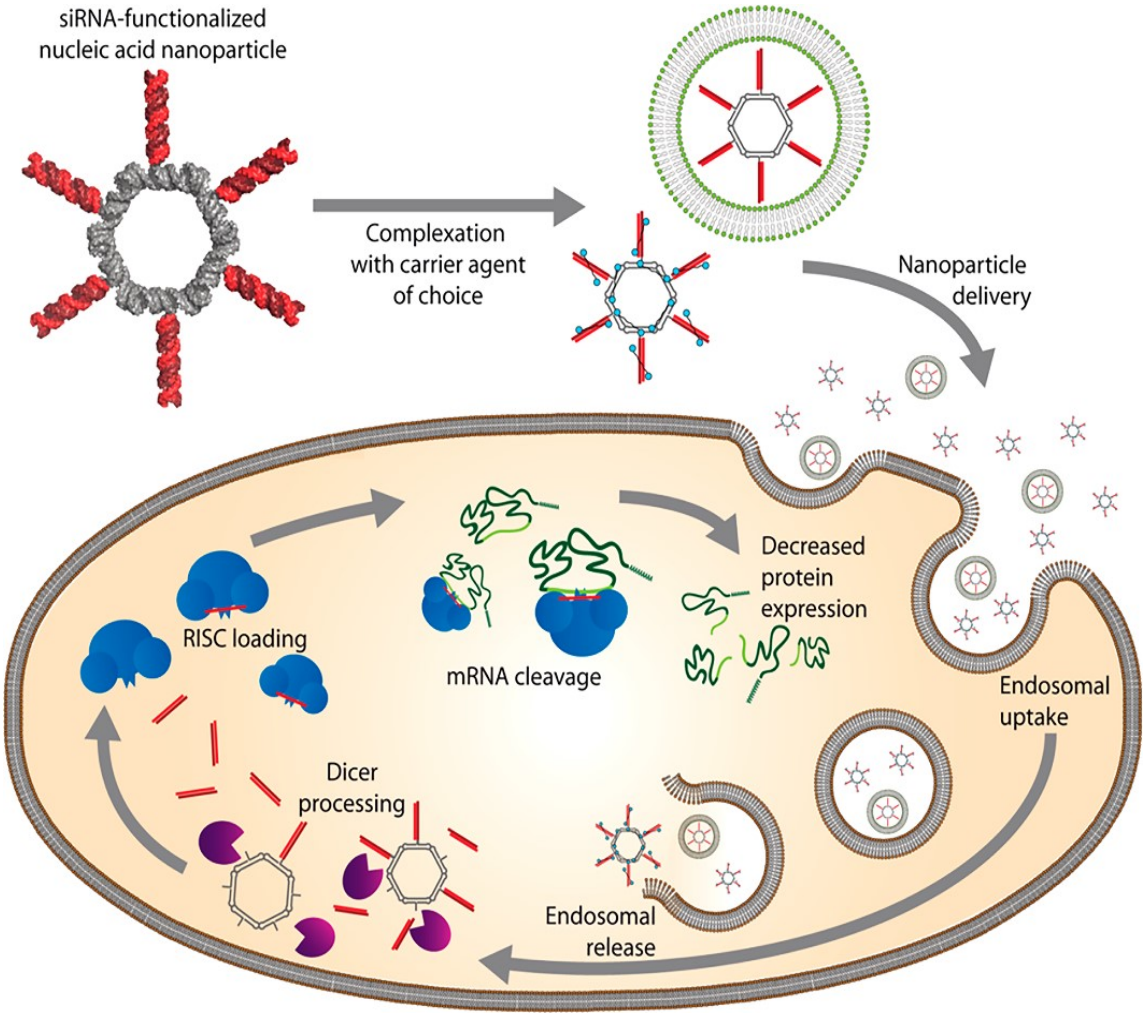

Figure 1.7. Schematic representation of siRNA nanoparticle delivery, uptake, and release into the cytoplasm for RNAi activity. siRNA nanoparticles may be encapsulated or complexed with a suitable delivery agent for cell uptake. Following cell uptake by endocytosis, siRNA triggers endosomal escape and recruitment of the RNAi components, Dicer enzyme (purple) processes siRNA substrates for RISC (blue) which recruits mRNA leading to inhibition of protein translation and mRNA degradation. Figure reproduced with permission from: Parlea, L.; Puri, A.; Kasprzak, W.; Bindewald, E.; Zakrevsky, P.; Satterwhite, E.; Joseph, K.; Afonin, K.A.; Shapiro, B.A. *ACS Comb. Sci*. **2016**; *18*, 527-547.[94]

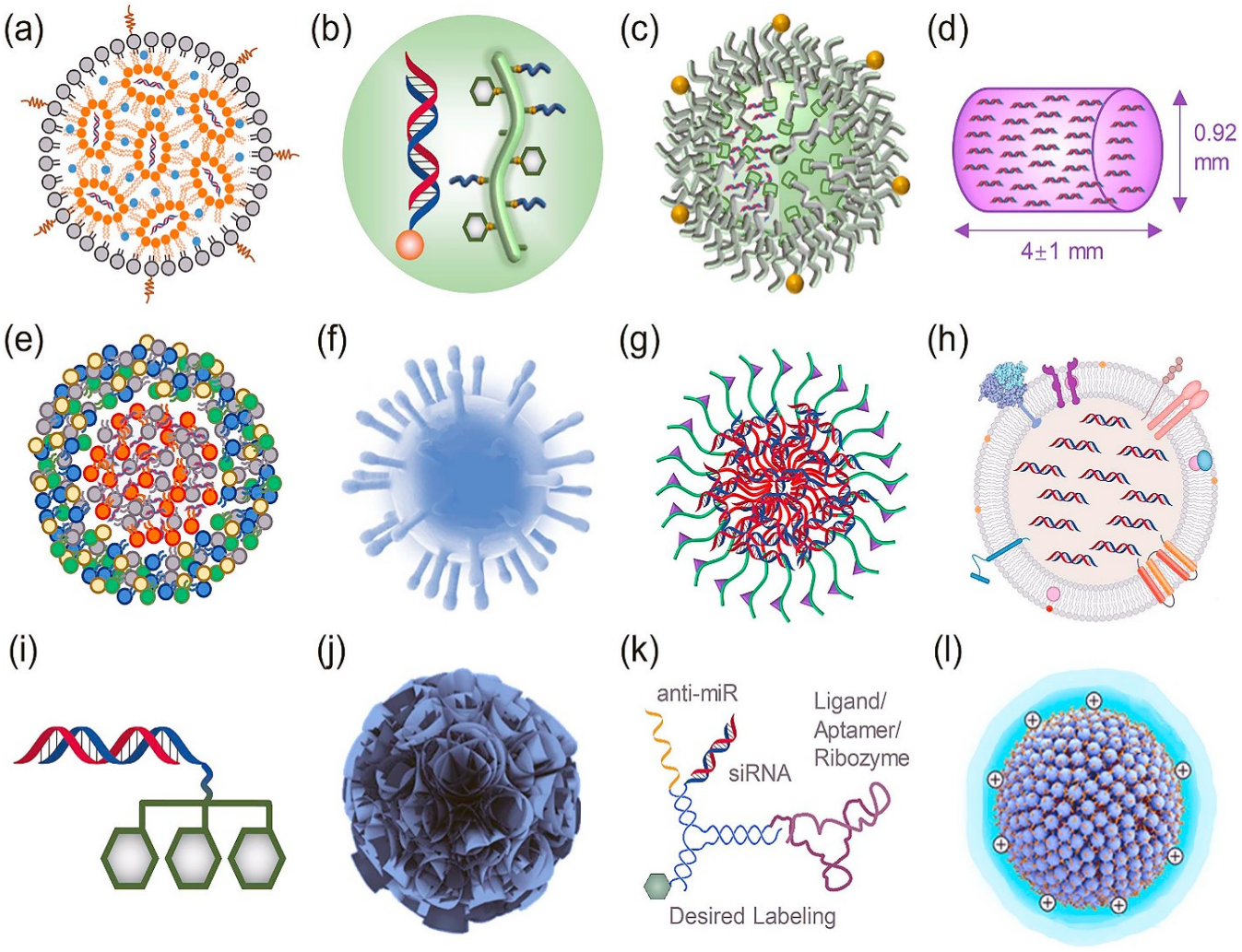

Figure 1.8. Representative siRNA delivery systems for RNAi drug development. Canonical liposome formulations (a), DPCiv™ (b), RONDEL™ (c), LODER polymer (PLGA matrix) (d), EnCore liposome (e), EDV™ nano cell (f), peptide nanoparticle (g), exosome (h), GalNAc-oligo conjugate (i), Multi-RNAi-microsponge (j), pRNA-3WJ (k) and fluorinated oligoethylenimine nano assembly (l) Figure reproduced with permission from: Weng, Y.; Xiao, H.; Zhang, J.; Liang, X.J.; Huang, Y. *Biotechnology Adv.* **2019**; *37*, 801-825.[95]

Multiple delivery systems based on viral and non-viral vectors have been developed to introduce siRNA safely and effectively within their cell targets **(Figure 1.8)**.[95] Successful examples of viral-based siRNA formulation are based on retroviral, adenoviral, adeno-

associated, and poxvirus vectors, among others. However, viral vectors are limited by significant immunogenicity, toxicity, and transgenic capacity size restrictions for efficient cell uptake.[96,97] Nonviral vectors are based on physical and chemical systems, which generally include chemical modifiers introduced by bioconjugation strategies that may facility siRNA delivery (e.g. lipid or GalNac functionalization) or self-assembly techniques involving: cationic liposomes, polymers, peptides, antibodies, and nanomaterials.[98,99] Physical methods have also been developed for direct transfection of siRNA into target cells. These strategies include particle bombardment, magnetofection, and ultrasound electroporation[100] or hydrodynamic injection,[101] applications. However, these physical methods have failed in commercial gene therapy due to their tendencies to drastically affect/alter cell-based compositions.[102] Therefore, nonviral vectors have gained the most traction in recent years due to favorable pharmacological properties while providing efficient and safe siRNA delivery. These synthetic delivery systems include: nanoparticles (NPs), liposomes, dendrimers, and cationic polymers due to their efficient siRNA condensation/release profiles *in vitro* and *in vivo*.[103] Liposomes and lipid-like materials, based on unilamellar, multilamellar, solid-lipid nanomaterials, and lipidoids have been commonly used for nucleic acid delivery vehicles. The cationic lipid DOTMA (N-[1-(2,3-dioleyloxy)propyl]-N, N, N trimethyl ammonium chloride) has been applied in siRNA transfections into the mouse, rat, and human cell lines.[104] Despite their utility, liposomes possess safety and toxicity concerns due to off-target gene silencing effects as these types of formulations are dispersed in most cell types and immunostimulatory side-effects have been reported *in vitro* and *in vivo.*[104] Modified liposomes have been engineered to address these limitations. Application of PEGylated liposomes bearing dialkyl and trialkyl cationic lipids were used for generating siRNA lipoplexes with enhanced systemic stability, decreased agglutination with erythrocytes, however, with a

marked decrease in gene silencing effects relative to control conditions.[105] To address this limitation, cell targeting/penetrating reagents, have been added to functionalized lipid-siRNA formulations. For example, a breast cancer binding peptide has been conjugated to the PEGylated liposome for efficient siRNA delivery within MCF-7 breast cancer cells.[106] The targeting peptide ligand, DMPGTVLP, displayed selective binding and cell uptake within MCF-7 cells resulting in significant down-regulation of *PRDM14* gene expression and PRDM14 protein synthesis, underscoring its potential utility in cancer-targeted gene therapy. Similarly, cell-targeting cationic polymers, such as polyethyleneimine (PEI) have been used as suitable siRNA delivery agents due to their ability to condense siRNA and facilitate endocytosis and endosomal escape due to the 'proton-sponge' effect.[107] In this release mechanism, the ionic PEI-siRNA cargo within the endosome leads to an accumulation of ions and an osmotic pressure effect that eventually bursts the endosome and releases the siRNA for RNAi activity.[108] In a clinically relevant application, co-delivery of the potent chemotherapeutic, doxorubicin, and siRNA targeting VEGF expression was formulated within a cholic acid conjugated PEI copolymer containing folic acid as targeting ligand for direct delivery in nude mice bearing human colorectal adenocarcinoma.[109,110] Tumor regression as a result of the combined chemotherapeutic and gene therapy effects were observed and specifically related to higher levels of apoptosis and necrosis detected from the histological analysis. In this manner, various targeting ligands such as small molecules (e.g. folate) peptides and proteins (e.g. transferrin, cell-targeting peptides) and biologics (e.g. monoclonal and polyclonal antibodies) have been formulated with siRNA-delivery agents for more effective and selective gene delivery.[111-115] As a representative example, a multi-component delivery system has recently been described and composed of the peptide (linear or cyclic fatty acyl peptide conjugates and hybrid cyclic/linear

peptides) and several lipids (DOTAP, DOPE, cholesterol, and phosphatidylcholine) to form a nanoparticle which enabled siRNA encapsulation and release profile and cellular uptake for RNAi activity.[115] The formulation effectively silenced Src and RPS6KA5 in the triple-negative human breast cancer cell line MDA-MB-231, compared to naïve cells, underscoring their potential utility in cancer gene therapy. Compared to their organic/synthetic counterparts, inorganic nanoparticles have also been applied in siRNA-mediated transfections and offer a wide range of beneficial properties. For example, the high luminescence of quantum dots (QDs),[116] superparamagnetic behavior of iron oxide nanoparticles[117,] and localized surface plasmon resonance of gold nanorods,[118] have enabled theranostic (therapy+diagnostic) utility in siRNA delivery applications. For example, poly(acrylic acid) and quantum dot excipients were combined with a PEGylated cationic polymer for the condensation and release of therapeutic siRNA.[119] Significantly, the quantum dots enabled stable polyplex formation which was visualized by cryogenic transmission electron microscopy (cryo-TEM) and promoted selective siRNA release upon polyplex disassembly according to Förster resonance energy transfer (FRET). The application of multifunctional and responsive materials in siRNA delivery has thus significantly increased their therapeutic utility.

1.9 Thesis Objectives

The research work described in this thesis is based on selected types of synthetic RNA motifs including linear, V, and Y-shaped RNA templates with the ability to self-assemble into higher-order siRNA nanostructures.[80,91] These multi-functional siRNAs enabled the knockdown of the Glucose Regulated Proteins (GRPs) in selected tumor cell lines to explore the influence of these chaperone proteins on tumor viability. This RNAi screening approach provides an important tool to investigate the impact of oncogene targets on cancer biology while enhancing

siRNA therapeutic activity by the synergistic action of silencing multiple oncogenes concurrently. Our synthetic RNA work has also enabled the bioconjugation or assembly of cell-penetrating and cell-targeting peptides,[120] lipids,[121] fluorescent probes[122,] and inorganic nanoparticles[123] for enhancing siRNA delivery and detection while maintaining potent knockdown of oncogenic GRP targets for gene therapy in cancer cells.[124,125] The novel synthetic biology approaches described in this thesis advances these preliminary studies, and serves to effectively improve the utility of siRNA-based biomaterial formulations for successful RNAi applications in the detection and treatment of cancer.

Chapter 2 of this thesis describes a novel synthetic strategy for the incorporation of a small set of fatty acids into chemically derived siRNAs to improve their metabolic stability and cancer cell permeability for RNAi activity. The linear, V- and Y-shape RNA templates (sense and antisense strands), were functionalized with a hexylamino linker which was also used as a nucleophile in the solid-phase bioconjugation of saturated and unsaturated fatty acids with RNA templates **(Figure 1.9).** The RNA-fatty acid bioconjugates were successfully synthesized following an optimized HCTU coupling procedure, purified, and hybridized with complementary RNA single strands to afford the amphiphilic self-assembled branch siRNA bioconjugates. The bioconjugates were characterized by RP HPLC, MS, DLS, and TEM to confirm the structural and biophysical properties. Furthermore, the self-transfection of the siRNA-fatty acid bioconjugates and their biological activities within a model PC-3 prostate cancer cell line revealed partial cell uptake, which contributed to modest RNAi activity when compared to the siRNA controls delivered with the commercially available Lipofectamine transfection reagent. Nonetheless, this solid-phase RNA bioconjugation approach provides an important entry point for the incorporation of various hydrophobic and amphiphilic functional groups for the

development of new RNAi molecules for screening important oncogene targets and for improving cancer gene therapy applications.

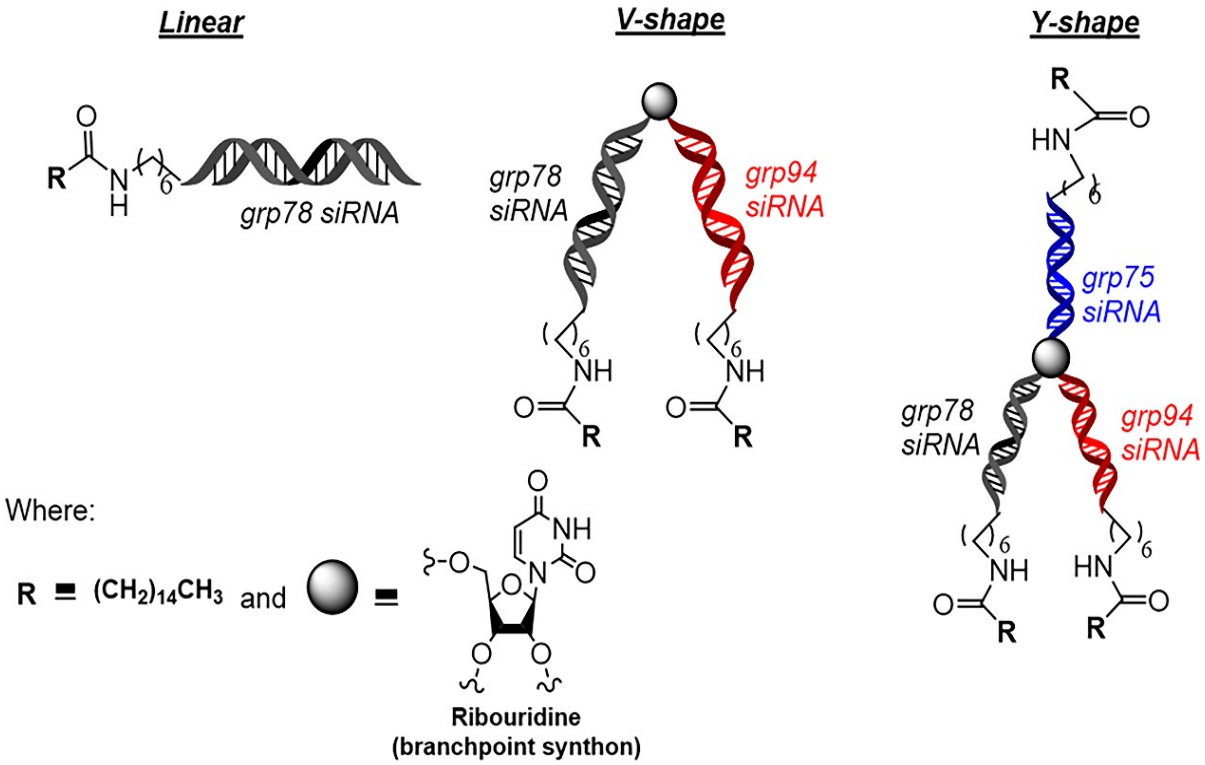

Figure 1.9 Graphical representation of linear, V-, and Y-shape siRNA templates covalent bioconjugation strategy for the introduction of fatty acid or fluorescent probes. Figure reproduced with permission from: Shah, S.S.; Cultrara, C.N.; Kozuch, S.D.; Patel, M.R.; Ramos, J.A.; Samuni, U.; Zilberberg, J.; Sabatino, D. *Bioconjugate Chem.,* **2018,** 29, 3638–3648.[121]

Chapter 3 describes a simple, bottom-up approach for templating RNAs onto gold (Au) surfaces for the generation of produce stable Au-siRNA nanoparticles. Further functionalization of the RNA strands using our bioconjugation approaches facilitated the incorporation of a fluorescent reporter (FITC) or a fatty acid (palmitic acid) used to track cell uptake in PC-3 prostate cancer (PCa) cells, **(Figure 1.10)**. The resulting Au-functionalized RNA particles were

found to be stable under reducing conditions, and self-assembled into primarily small (~10-40 nm) spherical shaped nanoparticles. The incorporation of FITC within the Au-RNA nanoparticles produced a bifunctional probe, which facilitated cell uptake detection in a time-dependent manner. The dual encapsulation-release profiles of the FITC-labeled Au-RNA nanoparticles were validated by time-dependent UV-Vis spectroscopy and spectrofluorimetry which showed increases in FITC absorption (λ_{abs}: 494 nm) and fluorescence emission (λ_{em}: 522 nm) with increased sample incubation times, under physiological conditions. Cell biology revealed the release of siRNA functionalized Au nanoparticles in prostate cancer (PC-3) cells which resulted in concomitant knockdown of GRP75, and detectable levels of cell death. The direct transfection of multi-functional Au-siRNA nanoparticles may thus have important utility in the early detection and treatment in PCa and related solid tumors.

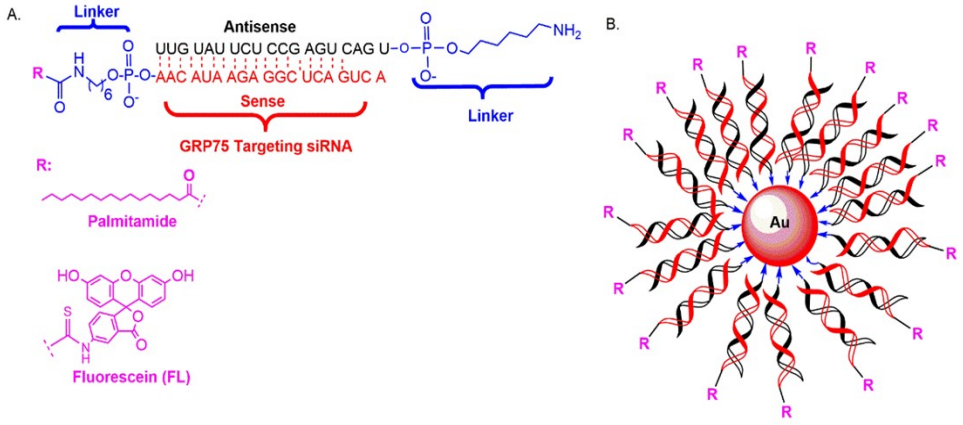

Figure 1.10. Graphical representation of the rational design of A) RNA sequence and B) bifunctional Au templated RNA particles. Figure reproduced with permission from: Shah, S.S.; Cultrara, C.N.; Ramos, J.A.; Samuni, U.; Zilberberg, J.; Sabatino, D. *J. Mater. Chem. B,* **2020,** 8, 2169-2176.[123]

In conclusion, Chapter 4 of this thesis will provide a general overview of current and on-going work aimed at the production of the Au-siRNA nanoparticle formulation bearing cell-targeting peptides (CTPs), for effective targeting and cell uptake in $PSMA^+$ prostate cancer cells (**Figure 1.11**).

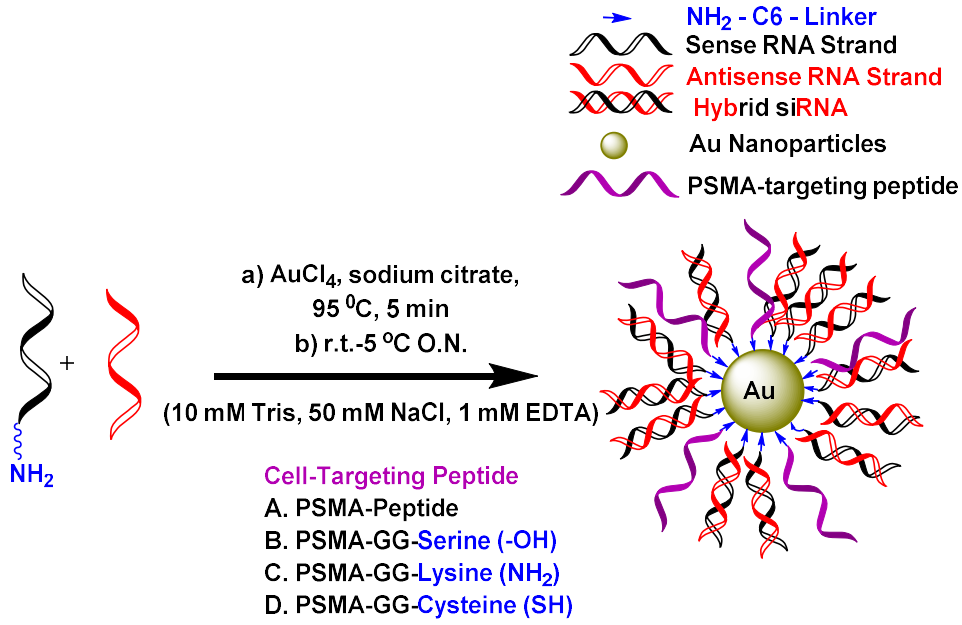

Figure 1.11. Graphical representation of PSMA-specific bifunctional Au templated RNA particles with varying cell-targeting peptides. Figure Drawn using Chemdraw Professional Software Version 16.0.1.4(77).

1.10 References

1. Lee, R.C.; Feinbaum, R.L.; Ambros, V. The C. elegans heterochronic gene lin-4 encode small RNAs with antisense complementarity to lin-14. *Cell* **1993,** *75(5)*, 843-854.
2. Fire, A.; Albertson, D.; Harrison, S.W.; Moerman, D.G. Production of antisense RNA leads to effective and specific inhibition of gene expression in C. elegans muscle. *Development* **1991,** *113(2)*, 503-514.
3. Guo, S. and Kemphues, K.J. Par-1, a Gene Required for Establishing Polarity in C. elegans Embryo, Encodes a Putative Ser/Thr Kinase That Is Asymmetrically Distributed. *Cell* **1995,** *81(4),*611-620.
4. Fire, A.; Xu, S.; Montgomery, M. K.; Kostas, S. A.; Driver, S. E.; Mello, C. C. Potent and specific genetic interference by double-stranded RNA in Caenorhabditis elegans. *Nature* **1998,** *391(6669),* 806-811.
5. NobelPrize.org. Nobel Media AB (2018). The Nobel Prize in Physiology or Medicine 2006. Available at: https://www.nobelprize.org/prizes/medicine/2006/press-release/.
6. Kurreck, J. siRNA efficiency: structure or sequence-that is the question. *J Biomed Biotechnol*. **2006**, *2006(4) 83757*, 1-7. DOI: 10.1155/JBB/2006/83757.
7. Fakhr, E.; Zare, F.; Teimoori-Toolabi, L. Precise and efficient siRNA design: a key point in competent gene silencing. *Cancer Gene Ther*. **2016,** *23(4)*, 73–82..
8. Harborth, J.; Elbashir, S.M.; Vandenburgh, K.; Manning, H.; Scaringe, S.A.; Weber, K.; Tuschl, T. Sequence, chemical, and structural variation of small interfering RNAs and short hairpin RNAs and the effect on mammalian gene silencing. *Antisense Nucleic Acid Drug Dev.* **2003**, *13(2)*, 83-105.
9. Jagla, B.; Aulner, N.; Kelly, P.D.; Song D.; Volchuk, A.; Zatorski, A.; Shum, D.; Mayer, T.; De Angelis, D.A.; Ouerfeli, O.; Rutishauser, U.R.S.; Rothman, J Sequence characteristics of functional siRNAs. *RNA* **2005,** *11(6),* 864–872.
10. Setten, R. L.; Rossi, J. J.; Han, S. P. The current state and future directions of RNAi-based therapeutics. *Nat. Rev. Drug Discov.* **2019,** *18*, 421–446.
11. Napoli, C.; Lemieux, C.; Jorgensen, R. Introduction of a Chimeric Chalcone Synthase Gene into Petunia Results in Reversible Co-Suppression of Homologous Genes in trans. *Plant Cell.* **1990**, *2(4)*, 279–289.
12. Hu, B.; Zhong, L.; Weng, Y.; Peng, L.; Huang, Y.; Zhao, Y.; Liang, X.J. Therapeutic siRNA: state of the art. *Signal Transduct. Targeted Ther.* **2020,** *5(1)*, 101..
13. Snead, N. M.; Wu, X.; Li, A.; Cui, Q.; Sakurai, K.; Burnett, J. C.; Rossi, J. J. Molecular basis for improved gene silencing by Dicer substrate interfering RNA compared with other siRNA variants. *Nucleic Acids Res*. **2013**, *41(12)*, 6209–6221.
14. Dana, H.; Chalbatani, G. M.; Mahmoodzadeh, H.; Karimloo, R.; Rezaiean, O.; Moradzadeh, A.; Mehmandoost, N.; Moazzen, F.; Mazraeh, A.; Marmari, V.; Ebrahimi, M.; Rashno, M. M.; Abadi, S. J.; Gharagouzlo, E. Molecular Mechanisms and Biological Functions of siRNA. *Int. J. Biomed. Sci.,* **2017**, *13(2)*, 48–57.

15. Rivas, F.V.; Tolia, N.H.; Song, J.J.; Aragon, J.P.; Liu, J.; Hannon, G.J.; Joshua-Tor, L. Purified Argonaute2 and an siRNA form recombinant human RISC. *Nat Struct Mol Biol.* **2005,** *12(4)*, 340-349.
16. Karagiannis, T.C.; El-Osta, A. RNA interference and potential therapeutic applications of short interfering RNAs. *Cancer Gene Ther*. **2005**, *12(10)*, 787-795.
17. Huang, Y. Y. The first RNA interference drug came out and the technological evolution in this field. *Prog. Biochem. Biophys.***2019,** *46(3)*, 313-322.
18. Agarwal, S.; Simon, A.R.; Goel, V.; Habtemariam, B.A.; Clausen, V.A.; Kim, J.B.; Robbie, G.J. Pharmacokinetics and Pharmacodynamics of the Small Interfering Ribonucleic Acid, Givosiran, in Patients with Acute Hepatic Porphyria. *Clin. Pharmacol. Ther.* **2020,** *108(1)*, 63-72.
19. Demirjian, S.; Ailawadi, G.; Polinsky, M.; Bitran, D.; Silberman, S.; Shernan, S.K.; Burnier, M.; Hamilton, M.; Squiers, E.; Erlich, S.; Rothernstein, D.; Khan, S.; Chawla, L.S. Safety and Tolerability Study of an Intravenously Administered Small Interfering Ribonucleic Acid (siRNA) Post On-Pump Cardiothoracic Surgery in Patients at Risk of Acute Kidney Injury. *Kidney Int. Rep*. **2017,** *2(5),* 836–843.
20. Thompson, J. D.; Kornbrust, D.J.; Foy, J.W-D.; Solano, E.C.R.; Schneider, D.J.; Feinstein, E.; Molitoris, B.A.; Erlich, S. Toxicological and pharmacokinetic properties of chemically modified siRNAs targeting p53 RNA following intravenous administration. *Nucleic Acid Ther*. **2012,** *22(4),* 255–264.
21. Titze-de-Almeida, R.; David, C.; Titze-de-Almeida, S.S. The Race of 10 Synthetic RNAi-Based Drugs to the Pharmaceutical Market. *Pharm. Res.* **2017,** *34(7),*1339–1363.
22. Solano, E.C.; Kornbrust, D.J.; Beaudry, A.; Foy, J.W.; Schneider, D.J.; Thompson, J.D. Toxicological and pharmacokinetic properties of QPI-1007, a chemically modified synthetic siRNA targeting caspase 2 mRNA, following intravitreal injection. *Nucleic Acid Ther.* **2014,** *24(4),* 258–266.
23. Ahmed, Z.; Kalinski, H.; Berry, M.; Almasieh, M.; Ashush, H.; Slager, N.; Brafman, A.; Spivak, I.; Prasad, N.; Mett, I.; Shalom, E.; Alpert, E.; Di Polo, A.; Feinstein, E.; Logan, A. Ocular neuroprotection by siRNA targeting caspase-2. *Cell Death Dis.* **2011,** *2(6),* e173.
24. Alvarez, R.; Elbashir, S.; Borland, T.; Toudjarska, I.; Hadwiger, P.; John, M.; Roehl, I.; Morskaya, S.S.; Martinello, R.; Kahn, J.; Van Ranst, M.; Tripp, R.A.; DeVincenzo, J.P.; Pandey, R.; Maier, M.; Nechev, L.; Manoharan, M.; Kotelianski, V.; Meyers, R. RNA interference-mediated silencing of the respiratory syncytial virus nucleocapsid defines a potent antiviral strategy. *Antimicrob Agents Chemother.* **2009**, *53(9),* 3952-3962.
25. DeVincenzo, J.; Cehelsky, J.E.; Alvarez, R.; Elbashir, S.; Harborth, J.; Toudjarska, I.; Nechev, L.; Murugaiah, V.; Van Vliet, A.; Vaishnaw, A.K.; Meyers, R. Evaluation of the safety, tolerability and pharmacokinetics of ALN-RSV01, a novel RNAi antiviral therapeutic directed against respiratory syncytial virus (RSV). *Antivial Res.* **2008**, *77(3)*, 225–231.
26. Zamora, M. R.; Budev M, Rolfe M, Gottlieb J, Humar A, Devincenzo J, Vaishnaw A, Cehelsky J, Albert G, Nochur S, Gollob JA, Glanville AR. RNA interference therapy in lung

transplant patients infected with respiratory syncytial virus. *Am J Respir Crit Care Med*. **2011**, 183(4), 531-538.

27. DeVincenzo, J.; Williams, R.L.; Wilkinson, T.; Cehelsky, J.; Nochur, S.; Walsh, E.; Meyers, R.; Gollob, J.; Vaishnaw, A. A randomized, double-blind, placebo-controlled study of an RNAi-based therapy directed against respiratory syncytial virus. *Proc. Natl Acad. Sci. USA.* **2010,** *107(19)*, 8800–8805.
28. Gottlieb, J.; Zamora, M.R. Hodges, T.; Musk, A.W. Sommerwerk, U.; Dilling, D.; Arcasov, S.; DeVincenzo, J.; Karsten, V.; Shah, S.; Bettencourt, B.R.; Cehelsky, J.; Nochur, S.; Gollob, J.; Vaishnaw, A.; Simon, A.; Glanville, A.R.; ALN-RSV01 for prevention of bronchiolitis obliterans syndrome after respiratory syncytial virus infection in lung transplant recipients. *J. Heart Lung Transpl.* **2016,** *35(2)*, 213–221.
29. Reagan-Shaw, S.; Ahmad, N. Silencing of polo-like kinase (Plk) 1 via siRNA causes induction of apoptosis and impairment of mitosis machinery in human prostate cancer cells: implications for the treatment of prostate cancer. *FASEB J. Express* **2005,** *19(6),* 1-14.
30. Tabernero J, Shapiro GI, LoRusso PM, Cervantes A, Schwartz GK, Weiss GJ, Paz-Ares L, Cho DC, Infante JR, Alsina M, Gounder MM, Falzone R, Harrop J, White AC, Toudjarska I, Bumcrot D, Meyers RE, Hinkle G, Svrzikapa N, Hutabarat RM, Clausen VA, Cehelsky J, Nochur SV, Gamba-Vitalo C, Vaishnaw AK, Sah DW, Gollob JA, Burris HA. 3rd. First-in-humans trial of an RNA interference therapeutic targeting VEGF and KSP in cancer patients with liver involvement. *Cancer Discov.* **2013**, *3(4)*, 406-417
31. Zuckerman, J.E.; Gritli, I.; Tolcher, A.; Heidel, J.D.; Lim, D.; Morgan, R.; Chmielowski, B.; Ribas, A.; Davis, M.E.; Yen, Y. Correlating animal and human phase Ia/Ib clinical data with CALAA-01, a targeted, polymer-based nanoparticle containing siRNA. *Proc Natl Acad Sci USA.* **2014**, *111(31)*, 11449-11454.
32. Golan, T.; Khvalevsky, E.Z.; Hubert, A.; Gabai, R.M.; Hen, N.; Segal, A.; Domb, A.; Harari, G.; David, E.B.; Raskin, S.; Goldes, Y.; Goldin, E.; Eliakim, R.; Lahav, M.; Kopleman, Y.; Dancour, A.; Shemi, A.; Galun, E. RNAi therapy targeting KRAS in combination with chemotherapy for locally advanced pancreatic cancer patients. *Oncotarget.* **2015**, *6(27),* 24560–24570.
33. Strumberg, D.; Schulthesis, B.; Traugott, U.; Vank, C.; Santel, A.; Giese, O.K.; Kaufmann, J.; Drevs, J. Phase I clinical development of Atu027, a siRNA formulation targeting PKN3 in patients with advanced solid tumors. *Int. J. Clin. Pharm. Ther.* **2012**, *50(1),* 76-78.
34. Schultheis, B.; Strumberg, D.; Santel, A.; Vank, C.; Gebhardt, F.; Keil, O.; Lange, C.; Giese, K.; Kaufmann, J.; Khan, M.; Drevs, J. First-in-human phase I study of the liposomal RNA interference therapeutic Atu027 in patients with advanced solid tumors. *J Clin Oncol*. **2014**, *32(36),* 4141-4148.
35. Rolle, K.; Nowak, S.; Wyszko, E.; Nowak, M.; Zukiel, R.; Piestrzeniewicz, R.; Gawronska, I.; Barciszewska, M.Z.; Barciszewsk, J. Promising human brain tumors therapy with interference RNA intervention (iRNAi). *Cancer Biol Ther.* **2010,** *9(5),* 396-406.

36. Yin, J.Q.; Gao, J.; Shao, R.; Tian, W.N.; Wang, J.; Wan, Y. J. siRNA agents inhibit oncogene expression and attenuate human tumor cell growth. *Exp. Ther. Oncol*. **2003**, *3(4),* 194–204.
37. Zhang, L.; Yang, N.; Mohamed-Hadley, A.; Rubin, S.C.; Coukos, G. Vector-based RNAi, a novel tool for isoform-specific knock-down of VEGF and anti-angiogenesis gene therapy of cancer. *Biochem. Biophys. Res. Commun.* **2003,** *303(4)*, 1169–1178.
38. Aigner, A. Perspectives, issues and solutions in RNAi therapy: the expected and the less expected. *Nanomedicine (Lond)*. **2019**, *14(21)*, 2777-2782.
39. Bora, R. S.; Gupta, D.; Mukkur, T. K.; Saini, K. S. RNA interference therapeutics for cancer: Challenges and opportunities (Review) *Mol. Med. Rep*. **2012,** *6(1)*, 9-15.
40. Gilmore, I.R.; Fox, S.P.; Hollins, A.J.; Akhtar, S. Delivery strategies for siRNA-mediated gene silencing. *Curr. Drug. Deliv*. **2006**, *3(2)*, 147-155.
41. Cao Z, Xiao H, Li L, Liu M, Lin G, Zhai P, Yong KT, Wang X, Xu G. The Codelivery of siRNA and QDs by pH-Responsive Micelle for Hepatoma Cancer Cells. *Front Pharmacol.* **2019**; *10*, 1194.
42. Kim MW, Jeong HY, Kang SJ, Jeong IH, Choi MJ, You YM, Im CS, Song IH, Lee TS, Lee JS, Lee A, Park YS. Anti-EGF Receptor Aptamer-Guided Co-Delivery of Anti-Cancer siRNAs and Quantum Dots for Theranostics of Triple-Negative Breast Cancer. *Theranostics*. **2019**; *9(3)*, 837-852.
43. Ma F, Jiang S, Zhang CY. SiRNA-directed self-assembled quantum dot biosensor for simultaneous detection of multiple microRNAs at the single-particle level *Biosensor Bioelectronics.* **2020**; *157*, 112177.
44. Li N, Yang H, Yu Z, Li Y, Pan W, Wang H. Nuclear-targeted siRNA delivery for long-term gene silencing. *Chem Sci*. **2017**, *8*(4), 2816-2822.
45. Jang M, Han HD, Ahn HJ. A RNA nanotechnology platform for a simultaneous two-in-one siRNA delivery and its application in synergistic RNAi therapy. *Sci Rep.* **2016**, *6*, 32363
46. Watts, J. K.; Deleavey, G. F.; Damha, M. J. Chemically modified siRNA: tools and applications. *Drug Discovery Today* **2008**, *13*, 842-855.
47. Sioud, M.; Furset, G.; Cekaite, L.Suppression of immunostimulatory siRNA-driven innate immune activation by 2'-modified RNAs. *Biochem Biophys. Res.Commun* **2007**, *361(1),* 122-126.
48. Song, X, Wang X, Ma Y, Liang Z, Yang Z, Cao H. Site-Specific Modification Using the 2' Methoxyethyl Group Improves the Specificity and Activity of siRNAs. *Mol. Ther. Nucleic Acids* **2017,** *9*, 242-250.
49. Fluiter, K.; Mook, O. R.; Baas, F. The therapeutic potential of LNA-modified siRNAs: reduction of off-target effects by chemical modification of the siRNA sequence. *Methods Mol. Biol*. **2009,** *487*, 189-203.
50. Bramsen, J. B., Pakula, M.M.; Hansen, T.B.; Bus, C.; Langkjaer, N.; Odadzic, D.; Smicius, R.; Wengel, S.L.; Chattopadhyaya, J.; Engels, J.W. A screen of chemical modifications

identifies position-specific modification by UNA to most potently reduce siRNA off-target effects. *Nucleic Acids Res.* **2010,** *38*, 5761-5773.
51. Detzer, A.; Sczakiel, G. Phosphorothioate-stimulated uptake of siRNA by mammalian cells: a novel route for delivery. *Curr. Top. Med. Chem*. **2009**, *9(12)*, 1109-1116.
52. Shaw BR, Moussa L, Sharaf M, Cheek M, Dobrikov M. Boranophosphate siRNA-aptamer chimeras for tumor-specific downregulation of cancer receptors and modulators. *Nucleic Acids Symp Ser (Oxf).* **2008**, *52*, 655-656.
53. Jin W, Jain A, Liu H, Zhao Z, Cheng K. Noncovalent Attachment of Chemical Moieties to siRNAs Using Peptide Nucleic Acid as a Complementary Linker. *ACS Appl Bio Mater.* **2018**, *1*(3), 643-651.
54. Iwase R, Kurokawa R, Ueno J. Synthesis of modified double stranded RNAs containing duplex regions between amide-linked RNA and RNA at both ends and enhanced nuclease resistance. *Nucleic Acids Symp Ser (Oxf).* **2009**, 53, 119-120.
55. Puri, N.; Wang, X.; Varma, R.; Burnett, C.; Beauchamp, L.; Batten, D.M.; Young, M.; Sule, V.; Latham, K.; Sendra, T.; Echeverri, C.; Sachse, C.; Magdaleno, S. LNA incorporated siRNAs exhibit lower off-target effects compared to 2'-OMethoxy in cell phenotypic assays and microarray analysis. *Nucleic Acids Symp Ser (Oxf)*. **2008**, *52*, 25-26.
56. Peacock, H.; Kannan, A.; Beal, P. A.; Burrows, C. J. Chemical modification of siRNA bases to probe and enhance RNA interference. *J. Org. Chem*. **2011,** *76(18)*, 7295-7300.
57. Jackson, A. L.; Burchard, J.; Leake, D.; Reynolds, A.; Schelter, J.; Guo, J.; Johnson, J. M.; Lim, L.; Karpilow, J.; Nichols, K.; Marshall, W.; Khvorova, A.; Linsley, P. S. Position-specific chemical modification of siRNAs reduces "off-target" transcript silencing. *RNA* **2006**, *12(7)*, 1197-1205.
58. Patel, P.L.; Rana, N.K.; Patel, M.R.; Kozuch, S.D.; Sabatino, D. Nucleic Acid Bioconjugates in Cancer Detection and Therapy. *ChemMedChem.* **2016**, *11(3),* 252-269.
59. Yamada, T.; Peng, C.G.; Matsuda, S.; Addepalli, H.; Jayaprakash, K.N.; Alam, M.R.; Mills, K.; Maier, M.A.; Charisse, K.; Sekine, M.; Manoharan, M.; Rajeev, K.G. Versatile Site-Specific Conjugation of Small Molecules to siRNA Using Click Chemistry. *J. Org. Chem*. **2011**, *76(5)*, 1198-1211.
60. Dohmen, C.; Fröhlich, T.; Lächelt, U.; Röhl, I.; Vornlocher, H.P.; Hadwiger, P.; Wagner, E. Defined Folate-PEG-siRNA Conjugates for Receptor-specific Gene Silencing. *Mol. Ther. Nucleic Acids*. **2012**, *1(1)*, e7.
61. Guo, J.; Ogier, J.R.; Desgranges, S.; Darcy, R.; O'Driscoll, C. Anisamide-targeted cyclodextrin nanoparticles for siRNA delivery to prostate tumours in mice. *Biomaterials,* **2012**, *33(31)*, 7775-7784.
62. Nair, J.K.; Willoughby, J.L.; Chan, A.; Charisse, K.; Alam, M.R.; Wang, Q.; Hoekstra, M.; Kandasamy, P.; Kel'in, A.V.; Milstein, S.; Taneja, N.; O'Shea, J.; Shaikh, S.; Zhang, L.; van der Sluis, R.J.; Jung, M.E.; Akinc, A.; Hutabarat, R.; Kuchimanchi, S.; Fitzgerald, K.; Zimmermann, T.; van Berkel, T.J.; Maier, M.A.; Rajeev, K.G.; Manoharan, M. Multivalent

N-acetylgalactosamine-conjugated siRNA localizes in hepatocytes and elicits robust RNAi-mediated gene silencing. *J Am Chem Soc*. **2014,** *136(49),* 16958-16961.

63. Sharma, V.K.; Osborn, M.F.; Hassler, M.R.; Echeverria, D.; Ly, S.; Ulashchik, E.A.; Martynenko-Makaev, Y.V.; Shmanai, V.V.; Zatsepin, T.S.; Khvorova, A.; Watts, J.K. Novel Cluster and Monomer-Based GalNAc Structures Induce Effective Uptake of siRNAs in Vitro and in Vivo. *Bioconjug Chem.* **2018**, *29(7),* 2478-2488.
64. Xu, W.; Pan, R.; Zhao, D.; Chu, D.; Wu, Y.; Wang, R.; Chen, B.; Ding, Y.; Sadatmousavi, P.; Yuan, Y.; Chen, P. Design and Evaluation of Endosomolytic Biocompatible Peptides as Carriers for siRNA Delivery. *Mol. Pharm.* **2015**, *12*, 56-65.
65. Alam, M.R.; Ming, X.; Fisher, M.; Lackey, J.G.; Rajeev, K.G.; Manoharan, M.; Juliano, R.L. Multivalent Cyclic RGD Conjugates for Targeted Delivery of Small Interfering RNA. *Bioconjug. Chem.* **2011**, *22*, 1673-1681.
66. Lu, H.; Wang, H.D.; Kazane, S.; Javahishvili, T.; Tian, F.; Song, F.; Sellers, A.; Barnett, B.; Schultz, P.G. Site-Specific Antibody–Polymer Conjugates for siRNA Delivery. *J. Am. Chem. Soc.* **2013**, *135(37)*, 13885-13891.
67. Huschka, R.; Barhoumi, A.; Liu, Q.; Roth, J.A.; Ji, L.; Halas, N.J. Gene Silencing by Gold Nanoshell-Mediated Delivery and Laser-Triggered Release of Antisense Oligonucleotide and siRNA *ACS Nano*. **2012**, *6*, 7681-7691.
68. Patel, D. J.; Ma, J.B.; Yuan, Y.R.; Ye, K.; Pei, Y.; Kuryavyi, V.; Malinina, L.; Meister, G.; Tuschl, T. Structural Biology of RNA Silencing and Its Functional Implications. *Cold Spring Harb. Symp. Quant. Biol.* **2006,** *71*, 81–93.
69. Wu, M. and Tinoco, I Jr. RNA folding causes secondary structure rearrangement. *Proc Natl Acad Sci U S A*. **1998**, *95(20)*, 11555-11560.
70. Afonin, K.A.; Bindewald, E.; Yaghoubian, A.J.; Voss, N.; Jacovetty, E.; Shapiro, B.A.; Jaeger, L. In vitro assembly of cubic RNA-based scaffolds designed in silico. *Nat. Nanotechnol*. **2010**, *5(9),* 676-682.
71. Bindewald, E.; Hayes, R.; Yingling, Y.G.; Kasprzak, W.; Shapiro, B.A. RNAJunction: a database of RNA junctions and kissing loops for three-dimensional structural analysis and nanodesign. *Nucleic Acids Res.* **2008**, *36(1)*, D392-D397.
72. Grabow, W.W.; Zakrevsky, P.; Afonin, K.A.; Chworos, A.; Shapiro, B.A.; Jaeger, L. Self-assembling RNA nanorings based on RNAI/II inverse kissing complexes. *Nano Lett.* **2011**, *11(2)*, 878-887.
73. Bindewald, E.; Afonin, K.; Jaeger, L.; Shapiro, B.A. Multistrand RNA Secondary Structure Prediction and Nanostructure Design Including Pseudoknots. *ACS Nano* **2011**, *5(12)*, 9542-9551.
74. Afonin, K.A.; Desai, R.; Viard, M.; Kireeva, M.L.; Bindewald, E.; Case, C.L.; Maciag, A.E.; Kasprzak, W.K.; Kim, T.; Sappe, A.; Stepler, M.; Kewalramani, V.N.; Kashlev, M.; Blumenthal, R.; Shapiro, B.A. Co-transcriptional production of RNA-DNA hybrids for simultaneous release of multiple split functionalities. *Nucleic Acids Res.* **2014**, *42(3)*, 2085-2097.

75. Afonin, K.A.; Viard, M.; Martins, A.N.; Lockett, S.J.; Maciag, A.E.; Freed, E.O.; Heldman, E.; Jaeger, L.; Blumenthal, R.; Shapiro, B.A. Activation of different split functionalities on re-association of RNA-DNA hybrids. *Nat. Nanotechnol.* **2013**, *8(4)*, 296-304.
76. Afonin, A.K.; Grabow, W.W.; Walker, M.F.; Bindewald, E.; Dobrovolskaia, A.M.; Shapiro, A.B.; Jaeger, L. Design and self-assembly of siRNA-functionalized RNA nanoparticles for use in automated nanomedicine. *Nat. Protoc.* **2011**, *6(12)*, 2022-2034.
77. Afonin, K.A.; Kasprzak, W.K.; Bindewald, E.; Kireeya, M.; Viard, M.; Kashlev, M.: Shapiro, B.A. In silico design and enzymatic synthesis of functional RNA nanoparticles *Acc. Chem. Res.* **2014,** *47(6)*, 1731-1741.
78. Afonin, K.A.; Viard, M.; Kagiampakis, I.; Case, C.L.; Dobrovolskaia, M.A.; Hofmann, J.; Vrzak, A.; Kireeva, M.; Kasprzak, W.K.; Kewal Ramani, V.N.; Shapiro, B.A. Triggering of RNA Interference with RNA–RNA, RNA–DNA, and DNA–RNA Nanoparticles. *ACS Nano*. **2015,** *9(1)*, 251-259.
79. Guo, P. The Emerging Field of RNA Nanotechnology. *Nat. Nanotechnology*. **2010,** *5*, 833-842.
80. Patel, M.R.; Kozuch, S.D.; Cultrara, C.N.; Yadav, R.; Huang, S.; Samuni, U.; Koren, J., Chiosis, G.; Sabatino, D. RNAi Screening of the Glucose-Regulated Chaperones in Cancer with Self-Assembled siRNA Nanostructures. *Nano Lett.* **2016,** *16(10)*, 6099–6108.
81. Abe, N.; Abe, H.; Ito, Y. Dumbbell-shaped nanocircular RNAs for RNA interference *J. Am. Chem. Soc.* **2007**, *129*,(49) 15108-15109.
82. Abe, N.; Abe, H.; Ohshiro, T.; Nakashima, Y.; Maeda, M.; Ito, Y. Synthesis and characterization of small circular double stranded RNAs. *Chem. Commun. (Camb).* **2011**, *47*, 2125-2127.
83. Abe, N.; Abe, H.; Nagai, C.; Harada, M.; Hatakeyama, H.; Harashima, H.; Ohshiro, T.; Nishihama, M.; Furukawa, K.; Maeda, M.; Tsuneda, S.; Ito, Y. Synthesis, structure, and biological activity of dumbbell-shaped nanocircular RNAs for RNA interference. *Bioconjug. Chem*. **2011**, *22(10),* 2082-2090.
84. Chang, C.I.; Lee, T.Y.; Kim, S.; Sun, X.; Hong, S.W.; Yoo, J.W.; Dua, P.; Kang, H.S.; Kim, S.; Li, C.J.; Lee, D.K. Enhanced intracellular delivery and multi-target gene silencing triggered by tripodal RNA structures. *J. Gene Med.* **2012**, *14(2)*, 138-146.
85. Nakashima, Y.; Abe, H.; Abe, N.; Aikawa, K.; Ito, Y. Branched RNA nanostructures for RNA interference. *Chem. Commun*. (*Camb),* **2011**, *47(29)*, 8367-8369.
86. Yingling YG, Shapiro BA. Computational design of an RNA hexagonal nanoring and an RNA nanotube. *Nano Lett.* **2007**; *7*(8), 2328-2334.
87. Kim H, Park Y.; Lee JB. Self-assembled Messenger RNA Nanoparticles (mRNA-NPs) for Efficient Gene Expression. *Sci Rep.* **2015**; *5*, 12737.
88. Afonin, K.A.; Viard, M.; Koyfman, A.Y.; Martins, A.N.; Kasprzak, W.K.; Panigaj, M.; Desai, R.; Santhanam, A.; Grabow, W.W.; Jaeger, L.; Heldman, E.; Reiser, J.; Chiu, W.; Freed, E.O.; Shapiro, B.A. Multifunctional RNA Nanoparticles. *Nano Lett*. **2014**, *14*, 5662-5671.

89. Zakrevsky, P.; Kasprzak, W.K.; Heinz, W.F.; Wu, W.; Khant, H.; Bindewald, E.; Dorjsuren, N.; Fields, E.A.; de Val, N.; Jaeger, L.; Shapiro, B.A. Truncated tetrahedral RNA nanostructures exhibit enhanced features for delivery of RNAi substrates. *Nanoscale.* **2020**, *12(4)*, 2555-2568.
90. Afonin, K.A.; Dobrovolskaia, M.A.; Church, G.; Bathe, M. Opportunities, Barriers, and a Strategy for Overcoming Translational Challenges to Therapeutic Nucleic Acid Nanotechnology. *ACS Nano* **2020**, *14*(8), 9221-9227.
91. Maina, A.; Blackman, B.A.; Parronchi, C.J.; Morozko, E.; Bender, M.E.; Blake, A.D.; Sabatino, D. Solid-phase synthesis, characterization and RNAi activity of branch and hyperbranch siRNAs. *Bioorg Med Chem Lett.* **2013,** *23(19),* 5270-5274.
92. Subhan, M.A.; Torchilin, V.P. siRNA-based drug design, quality, delivery and clinical translation. *Nanomedicine: Nanotechnology, Biology, and Medicine.* **2020,** *29(102239)*, 1-20
93. Yin, H.; Kanasty, R.L.; Eltoukhy, A.A.; Vegas, A.J.; Dorkin, J.R.; Anderson, D.G. Non-viral vectors for gene-based therapy. *Nat Rev Genet.* **2014**, *15(8)*, 541-555.
94. Parlea, L; Puri, A.; Kasprzak, W.; Bindewald, E.; Zakrevsky, P.; Satterwhite, E.; Joseph, K.; Afonon, K.A.; Saapiro, B.A. Cellular Delivery of RNA Nanoparticles. *ACS Comb. Sci*. **2016**, *18*(9), 527–547.
95. Weng, Y.; Xiao, H.; Zhang, J.; Liang, X.J.; Huang, Y. RNAi therapeutic and its innovative biotechnological evolution. *Biotechnology Adv.* **2019**, *37*, 801-825.
96. Molnar-Kimber, K.L.; Sterman, D.H.; Chang, M.; Kang, E.H.; ElBash, M.; Lanuti, M.; Elshami, A.; Gelfand, K.; Wilson, J.M.; Kaiser, L.R.; Albelda, S.M. Impact of preexisting and induced humoral and cellular immune responses in an adenovirus-based gene therapy phase I clinical trial for localized mesothelioma. *Hum Gene Ther*. **1998**, *9(14),* 2121-33.
97. Gardlik, R.; Palffy, R.; Hodosy, J.; Lukacs, J.; Turna, J.; Celec, P. Vectors and delivery systems in gene therapy. *Med Sci Monit* **2005,** *11(4),* RA110-121.
98. Hirai, H.; Satoh, E.; Osawa, M.; Inaba, T.; Shimazaki, C.; Kinoshita, S.; Nakagawa, M.; Mzda, O.; Imanishi, J. Use of EBV-Based Vector/HVJ-Liposome Complex Vector for Targeted Gene Therapy of EBV-Associated Neoplasms. *Biochem Biophys Res Commun.* **1997**, *241(1)*, 112-118.
99. Kanasty R, Dorkin JR, Vegas A, Anderson D. Delivery materials for siRNA therapeutics. *Nat Mater.* **2013**; *12*(11), 967-977.
100. Heller, L.C.; Ugen, K.; Heller, R. Electroporation for targeted gene transfer. *Expert Opin Drug Deliv* **2005**, *2*, 255-268.
101. Knapp, J.E.; Liu, D. Hydrodynamic delivery of DNA. *Methods Mol Biol* **2004,** *245,* 245-250.
102. Mellott AJ, Forrest ML, Detamore MS. Physical non-viral gene delivery methods for tissue Engineering. *Ann Biomed Eng.* **2013**; *41*(3), 446-468.
103. Vasir, J.K.; Labhasetwar, V. Polymeric nanoparticles for gene delivery. *Expert Opin Drug Deliv.* **2006**, *3*, 325-444.

104. Manunta MDI, Tagalakis AD, Attwood M, Aldossary AM, Barnes JL, Munye MM, Weng A, McAnulty RJ, Hart SL. Delivery of ENaC siRNA to epithelial cells mediated by a targeted nanocomplex: a therapeutic strategy for cystic fibrosis. *Sci Rep.* **2017**, *7*(1), 700.
105. Hattori, Y.; Tamaki, K.; Sakasai, S.; Ozaki, K.I.; Onishi, H. Effects of PEG anchors in PEGylated siRNA lipoplexes on in vitro gene-silencing effects and siRNA biodistribution in mice. *Mol Med Rep.* **2020**, *22(5),* 4183-4196.
106. Bedi, D.; Musacchio, T.; Fagbohun, O.A.; Gillespie, J.W.; Deinnocentes, P.; Bird, R.C.; Bookbinder, L.; Torchilin, V. P.; Petrenko, V.A. Delivery of siRNA into breast cancer cells via phage fusion protein-targeted liposomes. *Nanomedicine:Nanotechnology, Biology and Medicine*. **2011,** *7(3)*, 315–323.
107. Sajeesh, S.; Lee, T. Y.; Kim, J. K.; Son, D. S.; Hong, S. W.; Kim, S.; Yun, W. S.; Kim, S.; Chang, C.; Li, C.; Lee, D. K. Efficient intracellular delivery and multiple-target gene silencing triggered by tripodal RNA based nanoparticles: A promising approach in liver-specific RNAi delivery. *J of Control Release.* **2014,** *196*, 28-36.
108. Wojnilowicz M, Glab A, Bertucci A, Caruso F, Cavalieri F. Super-resolution Imaging of Proton Sponge-Triggered Rupture of Endosomes and Cytosolic Release of Small Interfering RNA. *ACS Nano.* **2019**; *13*(1), 187-202.
109. Chen, J.; Sun, X.; Shao, R.; Xu, Y.; Gao, J.; Liang, W. VEGF siRNA delivered by polycation liposome-encapsulated calcium phosphate nanoparticles for tumor angiogenesis inhibition in breast cancer. *Int J Nanomedicine*. **2017**, *12*, 6075-6088.
110. Huang, H.Y.; Kuo, W.T.; Chou, M.J.; Huang, Y.Y. Co-delivery of anti-vascular endothelial growth factor siRNA and doxorubicin by multifunctional polymeric micelle for tumor growth suppression. *J Biomed Mater Res A.* **2011**, *97(3),* 330-338.
111. Deshayes, D.; Morris, M. C.; Divita, G.; Heitz, F. Cell-penetrating peptides: tools for intracellular delivery of therapeutics *Cell Mol. Life. Sci.* **2005,** *62(16),* 1839-1849.
112. Boisguérin, P.; Deshayes, S.; Gait, M. J.; O'Donovan, L.; Godfrey, C.; Betts, C. A.; Wood, M. J.; Lebleu, B. Delivery of therapeutic oligonucleotides with cell penetrating peptides. *Adv. Drug. Del. Rev.* **2015,** *87*, 52-67.
113. Lehto, T.; Kurrikoff, K.; Langel, U. Cell-penetrating peptides for the delivery of nucleic acids. *Expert Opin. Drug Disc.* **2012,** *9*, 823-836.
114. Toloue MM, Ford LP. Antibody targeted siRNA delivery. In: Goodchild J. (eds) Therapeutic Oligonucleotides. *Methods in Molecular Biology (Methods and Protocols*), 764. Humana Press.
115. Hall, R.; Alasmari, A.; Mozaffari, S.; Mahdipoor, P.; Parang, K.; Montazeri Aliabadi, H. Peptide/Lipid-Associated Nucleic Acids (PLANAs) as a Multicomponent siRNA Delivery System. *Mol Pharm.* **2021**, online ahead of print. DOI: 10.1021/acs.molpharmaceut.0c00969
116. Onoshima, D.; Yukawa, H.; Baba, Y. Multifunctional nanobiodevices in medical sciences. *Adv. Drug Delivery Rev.* **2015**, *95,* 1-14.

117. Laurent, S.; Saei, A. A.; Behzadi, S.; Panahifar, A.; Mahmoudi, M. Superparamagnetic iron oxide nanoparticles for delivery of therapeutic agents: opportunities and challenges. *Expert Opin. Drug Delivery.* **2014,** *11*, 1449-1470.
118. Bonoiu AC, Bergey EJ, Ding H, Hu R, Kumar R, Yong KT, Prasad PN, Mahajan S, Picchione KE, Bhattacharjee A, Ignatowski TA. Gold nanorod--siRNA induces efficient in vivo gene silencing in the rat hippocampus. *Nanomedicine (Lond).* 2011, *6*(4), 617-630.
119. Greco, C.T.; Andrechak, J.C.; Epps, T.H.; Sullivan, M.O. Anionic Polymer and Quantum Dot Excipients to Facilitate siRNA Release and Self-Reporting of Disassembly in Stimuli-Responsive Nanocarrier Formulations. *Biomacromolecules*. **2017**, *18(6),*1814-1824.
120. Cultrara, C.N.; Shah, S.; Antuono, G.; Heller, C.J.; Ramos, J.A.; Samuni, U.; Zilberberg, J.; Sabatino, D. Size Matters: Arginine-Derived Peptides Targeting the PSMA Receptor Can Efficiently Complex but Not Transfect siRNA. *Mol. Ther. Nucleic Acids,* **2019,** *18*, 863–870.
121. Shah, S.S.; Cultrara, C.N.; Kozuch, S.D.; Patel, M.R.; Ramos, J.A.; Samuni, U.; Zilberberg, J.; Sabatino, D. Direct Transfection of Fatty Acid Conjugated siRNAs and Knockdown of the Glucose-Regulated Chaperones in Prostate Cancer Cells. *Bioconjugate Chem.,* **2018,** *29*, 3638–3648.
122. Kozuch, S.D.; Cultrara, C.N.; Beck, A.E.; Heller, C.J.; Shah, S.S.; Patel, M.R.; Zilberberg, J.; Sabatino, D. Enhanced Cancer Theranostic with Self-Assembled, Multilabeled siRNAs. *ACS Omega,* **2018,** *3,* 12975–12984.
123. Shah, S.S.; Cultrara, C.N.; Ramos, J.A.; Samuni, U.; Zilberberg, J.; Sabatino, D. Bifunctional Au-templated RNA nanoparticles enable direct cell uptake detection and GRP75 knockdown in prostate cancer. *J. Mater.Chem. B,* **2020,** *8*, 2169-2176.
124. Cultrara, C.N.; Kozuch, S.D.; Ramasundaram, P.; Heller, C.J.; Shah, S.S.; Beck, A.E.; Zilberberg, J.; Sabatino, D. GRP78 modulates cell adhesion markers in prostate Cancer and multiple myeloma cell lines. *BMC Cancer,* **2018**, *18*, 1–14.
125. Cultrara, C.N.; Shah, S.S.; Kozuch, S.D.; Patel, M.R.; Sabatino, D. Solid phase synthesis and self-assembly of higher-order siRNAs and their bioconjugates. *Chem.Biol.Drug Des.* **2019,** *93*, 999-1010.

Chapter 2: Direct Transfection of Fatty Acid Conjugated siRNAs and Knockdown of the Glucose-Regulated Chaperones in Prostate Cancer Cells

2.1 Abstract

RNA interference has led to rapid advances in the therapeutic applications of siRNAs including recent clinical candidates that have been approved for treatment of rare hereditary diseases. In this thesis chapter's contribution towards the development of therapeutic siRNAs, an efficient bioconjugation approach has been developed for the ligation of linear, V and Y-shaped RNA templates with a small set of saturated and unsaturated fatty acids. This bioconjugation approach is hypothesized to improve siRNA cell uptake and knockdown efficacy of the glucose regulated proteins (GRPs) in prostate cancer cells. An optimized HCTU-coupling procedure was developed and used for the amidation of saturated and unsaturated fatty acids onto the 5'-ends of linear and V-shape RNA templates functionalized with an alkylamino linker that enabled solid-phase conjugation. Reverse phase ion pairing HPLC was used to validate product conversions, while providing trends in amphiphilic properties. Hybridization and self-assembly of complementary linear RNA strands yielded linear, V- and Y-shape fatty acid-conjugated siRNAs which were characterized by native PAGE, CD spectroscopy, DLS and TEM which confirmed multi-component self-assembled structures that were prone towards aggregation. The fatty acid conjugated siRNA bioconjugates were evaluated for RNAi activity within GRP overexpressing prostate cancer (PC-3). The siRNA bioconjugates with sense strand fatty acid conjugation provided more potent GRP knockdown when compared to the antisense strand modified siRNAs. However, less GRP knockdown efficacy was observed when compared to the unconjugated siRNA transfected with the commercial Trans-IT X2® dynamic delivery system. Flow cytometry

revealed limited cell uptake of the fatty acid conjugated siRNAs which likely contributed to decreased RNAi activity of the fatty acid conjugated siRNAs without additional transfection vector delivery. Regardless, these constructs represent a new contribution higher-order siRNA modification that may lead to more efficient siRNA bioconjugates for cancer gene therapy applications.

2.2 Introduction

In the gene therapy of cancer, therapeutic siRNAs have been used for screening oncogene markers and gene therapy applications of malignant oncogenes.[1,2] Their therapeutic effects by silencing oncogenes that are critically important for tumor survival, proliferation and invasion offers renewed hope in the clinical treatment of resilient tumors.[3,4] However, the clinical utility of siRNAs remains off-set by a wide range of limitations, including poor metabolic stability, limited cell uptake, reduced therapeutic efficacy at the localized tumor site and off-target gene silencing effects, which limits their utility and increases side-effects.[5] In order to address these limitations, chemical modifications or conjugation of siRNAs with biologically active functional groups or molecular probes have been applied in the diagnosis and therapy (theranostics) of maligant oncogene targets in cancer.[6]

The Glucose Regulated Proteins (GRPs) are a family of chaperone proteins expressed in all cell types where they function in the unfolded protein response associated with protein folding under physiological or pathological stress conditions in the lumen of the endoplasmic reticulum.[7] In cancer, GRPs are overexpressed and may be trafficked to the cell surface where they confer tumor proliferation, metastatic spread and resistance towards drug treatment.[8] The GRPs have thus been classified as clinically relevant markers in the detection and treatment of cancer. Many

therapeutic strategies have been developed to inhibit or silence the GRPs in cancer,[9-11] however, off-target side-effects, immunogenicity, poor cell uptake and serum stability have limited their therapeutic efficacy raising the need for new and improved leads. Towards this goal, our group has previously established a synthesis method for linear, V-, Y- and hyper-branch shaped siRNAs. The siRNAs were designed with sequence compositions that target a single and multiple mRNA expression sites related to GRP78 expression.[12] The GRP78-silencing siRNAs triggered notable GRP78 knockdown (50-60%) but only limited (10-20%) cell death in a pediatric liver hepatoblastoma cell line (HepG2). In order to improve the therapeutic activity of the siRNAs, the higher-order siRNA nanostructures targeting GRP-75, 78 and 94, led to a more potent knockdown (50-95%) followed by more significant increases in cell death (50-60%) across a wider panel of tumor types.[13] Thus, a multi-GRP silencing approach has been proven to be an effective anti-cancer strategy in both hematological and solid tumor types. In spite of these promising results, synthetic strategies that can help improve siRNA metabolic stability, cell uptake, and targeted delivery, are still in widespread demand and a focal point of the study described in this thesis chapter.

siRNA bioconjugates have shown the potential to improve pharmalogical properties in preclinical and clinical studies related to cancer treatment.[5,6,14-18] The incorporation of lipids (fatty acids, terpenes and steroids) are among the most widespread siRNA modifications that have improved metabolic stability, enhanced cell permeability and effected longer duration of action when compared to the control, non-labeled siRNA treatment conditions.[19-28] Combinatorial libraries of lipid-functionalized (lipidoid) siRNAs have also been found to be effective within *in vivo* models, including the observation of potent, specific and durable gene silencing effects in three distinct species, including nonhuman primates.[29] Therapeutic efficacy was also observed in

liver, lung and peritoneal macrophages underscoring the potential clinical utility of lipidoid siRNA. However, these examples are typically limited in scope and the efficiency of lipid-siRNA functionalization as well as the location of incorporation, which is typically restricted to either 3' or 5' conjugation.[30-34] Thus, new synthetic approaches that may effectively serve to increase the scope and functionality of modified lipid-siRNA bioconjgates may lead to the discovery of more potent RNAi therapeutics in the treatment of cancer and other morbidities.

Despite their utility, lipid siRNA bioconjugates remain limited by their safe and effective delivery for potent and long-lasting suppression of malignant gene expression. In this study, we have built upon our previous work and that described by others in the literature[19-34] by expanding the scope of lipidated siRNAs while attempting to address some of their limitations in RNAi applications. More specifically, the GRP-targeting linear, V- and Y-shape RNA templates were used for the incorporation of fatty acids to investigate their effects on the direct transfection, cell uptake and GRP knockdown in prostate cancer (PC-3) cells.

2.3 Chapter Objectives

This thesis chapter describes the design, synthesis, characterization, and biological evaluation of lipidated siRNA nanostructures within human cancer cells. The work described within this chapter forms part of our on-going efforts in developing effective anti-cancer approaches via collaborative, multidisciplinary research. Based on our previous work on the branching RNA chemistry, we have expanded the scope of synthetic siRNA constructs with the development of high-order lipidated siRNAs while attempting to address some of the shortcomings of siRNAs in RNAi applications. The project objectives begin with the selection of the GRP-targeting linear, V- and Y-shaped RNA templates that can be self-assembled with their complementary strands to

afford the GRP-silencing siRNAs. These siRNA sequences have been selected to target two sites of oncogenic GRP78 and those related to the GRP-75 and 94 mRNA sequences. The incorporation of a small library of fatty acids (saturated, unsaturated and polyunsaturated) at the 5' ends of the antisense and sense strands of linear, V- and Y-shape RNA templates provides lipidated RNA with variable structural and amphiphilic properties. These trends will be investigated by a combination of reverse-phase ion-pairing HPLC and UV-Vis spectrophotometry. Moreover, experimental studies conducted in collaboration with Drs. Jorge Ramos and Uri Samuni at Queen's College, CUNY, will be based on dynamic light scattering (DLS) and transmission electron microscopy (TEM) which will provide valuable insights into the sizes, shapes, charge distribution and aggregation potential of the lipid-RNA particles. Furthermore, annealing with complementary RNA strands will facilitate the formation of lipidated siRNA with and without a fluorochrome (fluorescein isothiocyanate, FITC) label for investigating the influence of these functional probes on siRNA secondary structure (CD spectroscopy) and stability (thermal denaturation, native polyacrylamide gel electrophoresis and serum digestion) which is anticipated to have a direct impact on biological activity. The lipidated siRNAs will then be investigated in direct transfection and cell uptake studies (fluorescence microscopy and flow cytometry) as well as GRP knockdown at the mRNA (real time polymerase chain reaction, qRT-PCR) and protein (western blot) levels of expression within a metastatic prostate cancer (PC-3) cell line to determine their utility in cancer gene therapy applications. These biological assays will be conducted in collaboration with Drs. Christopher Cultrara and Jenny Zilberberg located at the Center for Discovery and Innovation at Hackensack-Meridian Health. The results and data presented in this chapter are published and adapted with permission from the co-authored publication: Shah, S.S.; Cultrara, C.N.; Kozuch, S.D.; Patel, M.R.; Ramos,

J.A.; Samuni, U.; Zilberberg, J.; Sabatino, D. *Bioconjugate Chem.,* **2018,** *29*, 3638–3648 (Figure 2.1).[35]

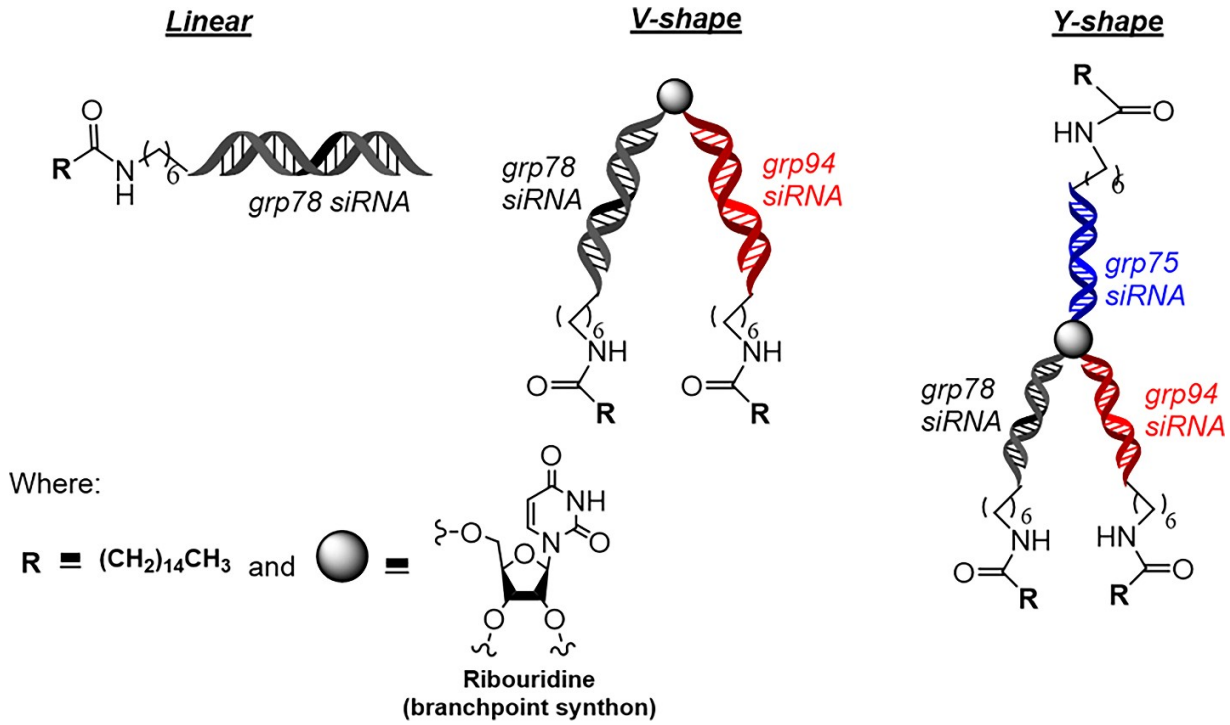

Figure 2.1. Rational design of lipidated-siRNA bioconjugates with Linear, V-shape and Y-branch GRP silencing siRNAs. Figure reproduced with permission from: Shah, S.S.; Cultrara, C.N.; Kozuch, S.D.; Patel, M.R.; Ramos, J.A.; Samuni, U.; Zilberberg, J.; Sabatino, D. Direct Transfection of Fatty Acid Conjugated siRNAs and Knockdown of the Glucose-Regulated Chaperones in Prostate Cancer Cells. *Bioconjugate Chem.,* **2018**, *29*, 3638–3648.[35]

2.4. Results and Discussion

2.4.1 Solid-Phase Bioconjugation

The synthetic siRNA bioconjugates described in this chapter (**Table 2.1**) are based on the sequence compositions used for silencing GRP-75, 78, and 94 expressions in human cancer cells.[12,13] The linear, V- and Y-shaped RNA templates bearing the nucleophilic 5'-hexamethylene amino linker within the antisense (A) or sense (S) strands were synthesized by automated solid-phase RNA synthesis. Using our previously established synthetic

procedures,[12,13] RNA synthesis on a controlled pore glass support also enabled the incorporation of an orthogonally protected 5'-OLv 2'-OMMT ribouridine phosphoramidite as branchpoint synthon. Selective deprotections and RNA synthesis facilitated the production of the V- and Y-shape RNA templates on solid supports. Following RNA synthesis, an O-(1H-6-chlorobenzotriazole-1-yl)-1,1,3,3-tetramethyluronium hexafluorophosphate, HCTU-based peptide (amide) coupling reaction was designed and optimized for the incorporation of hydrophobic modifiers (i.e., fatty acids) by solid phase RNA bioconjugation, which has been found to be useful for the incorporation of hydrophobic molecules onto oligonucleotide strands.[36] More specifically, short and long-chain (C_{12}-C_{18}) fatty acids with saturated, unsaturated, and polyunsaturated long chain alkyl groups were coupled onto the amino-linked RNA template strands using HCTU as activator, *N, N'*-diisopropylethylamine (DIEA) as base and *N, N'*-dimethylformamide (DMF) as reaction solvent (**Scheme 2.1**). Following solid phase bioconjugation, RNA samples were cleaved and deprotected from the solid support and analyzed by RP IP HPLC to determine reaction conversions. The conjugation reactions proceeded with good product conversions (52-75%) in the case of antisense linear RNA functionalization. The V- and Y-shape RNA templates were subjected to the HCTU/DIEA coupling reaction for the incorporation of palmitic acid which produced good conversions in the case of the V-shape RNA bioconjugate (69 %). However, little conjugated product (<5%) was detected in the case of the Y-shape RNA template. The latter may be attributed to poor reactivities associated with conjugation of fatty acids onto more complex, higher-order RNA templates. We have observed similar restrictions with the bioconjugation of fluorescent probes (fluorescein) onto Y-shape RNA templates.[37] In order to address these limitations, an alternative approach was developed in which the 5'-alkylamino group of the linear RNA sense strands were coupled with palmitic acid

using our established HCTU/DIEA coupling reaction, followed by hybridization to the linear, V- and Y-shape antisense RNA templates (**Scheme 2.2**). This self-assembly approach enabled the production of linear, V- and Y-shape GRP targeting siRNAs containing single, double, and triple palmitamide incorporations to explore the influence of fatty acid conjugation on the structure-activity properties of the siRNA bioconjugates.

Table 2.1. Characterization data of RNA templates and their fatty acid bioconjugates.

Sample #	Sample Name	Targeting Gene	Sequence[a]	rt[b] (min)	Mass[c] (Cal/Obs)
1	78A	GRP78	5' rArUrC rArGrA rArUrC rUrUrC rCrArA rCrArC rU 3'	5.7	5949.6/5949.6
2	78S	GRP78	5' rArGrU rGrUrU rGrGrA rArGrA rUrUrC rUrGrA rA 3'	5.7	6104.0/6103.7
3	94S	GRP94	5'-rGrArA rGrArA rGrCrA rUrCrU rGrArU rUrArC rC-3'	5.5	6068.8/6069.0
4	75S	GRP75	5'-rArCrU rGrArC rUrCrG rGrArG rArArU rArCrA rA-3'	5.9	6091.8/6092.3
5	78AC12	GRP78	(Lauric Acid))C12COOH/5AmMC6/5' rArUrC rArGrA rArUrC rUrUrC rCrArA rCrArC rU 3'	17.3	6311.0/6311.1
6	78AC16	GRP78	(Palmitic Acid)C16COOH/5AmMC6/5' rArUrC rArGrA rArUrC rUrUrC rCrArA rCrArC rU 3'	21.9	6367.3/6367.2
7	78AC18:1	GRP78	(Oleic Acid)C18:1COOH/5AmMC6/5' rArUrC rArGrA rArUrC rUrUrC rCrArA rCrArC rU 3'	22.5	6394.0/6393.3
8	78AC18:2	GRP78	(Linoleic Acid)C18:2COOH/5AmMC6/5' rArUrC rArGrA rArUrC rUrUrC rCrArA rCrArC rU 3'	21.3	6391.2/6391.2
9	78AC18:3	GRP78	(Linolenic Acid)C18:3COOH/5AmMC6/5' rArUrC rArGrA rArUrC rUrUrC rCrArA rCrArC rU 3'	20.3	6389.3/6389.2
10	7894VA	GRP78 GRP94	2'3' rCrUrU rCrUrU rCrGrU rArGrA rCrUrA rArUrC rG 5' rU 3'5'-rArUrC rArGrA rArUrC rUrUrC rCrArA rCrArC rU-3'	6.0	12318.0/12318.0
11	757894YA	GRP78 GRP94 GRP75	2'3'-rCrUrU rCrUrU rCrGrU rArGrA rCrUrA rArUrG rG-5' 5'-rUrUrG rUrArU rUrCrU rCrCrG rArGrU rCrArG rU-3'5'-rU 3'5'-rArUrC rArGrA rArUrC rUrUrC rCrArA rCrArC rU-3'	6.1	18356.3/18356.3
12	7894VC16	GRP78 GRP94	2'3' rCrUrU rCrUrU rCrGrU rArGrA rCrUrA rArUrC rG 5'/5AmMC6/C16COOH rU 3'5'-rArUrC rArGrA rArUrC rUrUrC rCrArA rCrArC rU-3'	19.0	12723.4/12723.3
13	78SC16	GRP78	C16COOH/5AmMC6/5' rArGrU rGrUrU rGrGrA rArGrA rUrUrC rUrGrA rA 3'	22.1	6522.2/6521.2

14	94SC16	GRP94	C16COOH/5AmMC6/5'-rGrArA rGrArA rGrCrA rUrCrU rGrArU rUrArC rC-3'	20.8	6496.1/6496.3
15	75SC16	GRP75	C16COOH/5AmMC6/5'-rArCrU rGrArC rUrCrG rGrArG rArArU rArCrA rA-3'	21.1	6520.1/6519.3

[a]Linear sequence number 1, 5, 6, 7 and 8 represents antisense (A) RNA sequence and the corresponding fatty acid bioconjugate to its complimentary sense (S) sequence 2. V-shaped siRNA sequences 10 and 12 contains two siRNA sequences targeting GRP78 and GRP94 mRNA to its complimentary sense (S) sequences 2 and 3. Y-shaped RNA sequence 11 contains three RNA sequences targeting three different sites of GRP78, GRP94 and GRP75 mRNA to its complimentary sense (S) sequences 2, 3, 4 along with 13, 14 and 15 as a palmitic acid bioconjugate. [b]Obtained by RP-IP-HPLC using 0.1 mM TEAA in TEAA with 7-70% MeCN, pH: 7.1 over 40 min. [c]Calculated mass (observed mass) by ESI-MS in negative mode (Novatia LLC, Newton, PA). Table reproduced with permission from: Shah, S.S.; Cultrara, C.N.; Kozuch, S.D.; Patel, M.R.; Ramos, J.A.; Samuni, U.; Zilberberg, J.; Sabatino, D. Direct Transfection of Fatty Acid Conjugated siRNAs and Knockdown of the Glucose-Regulated Chaperones in Prostate Cancer Cells. *Bioconjugate Chem.,* **2018**, *29*, 3638–3648.[35]

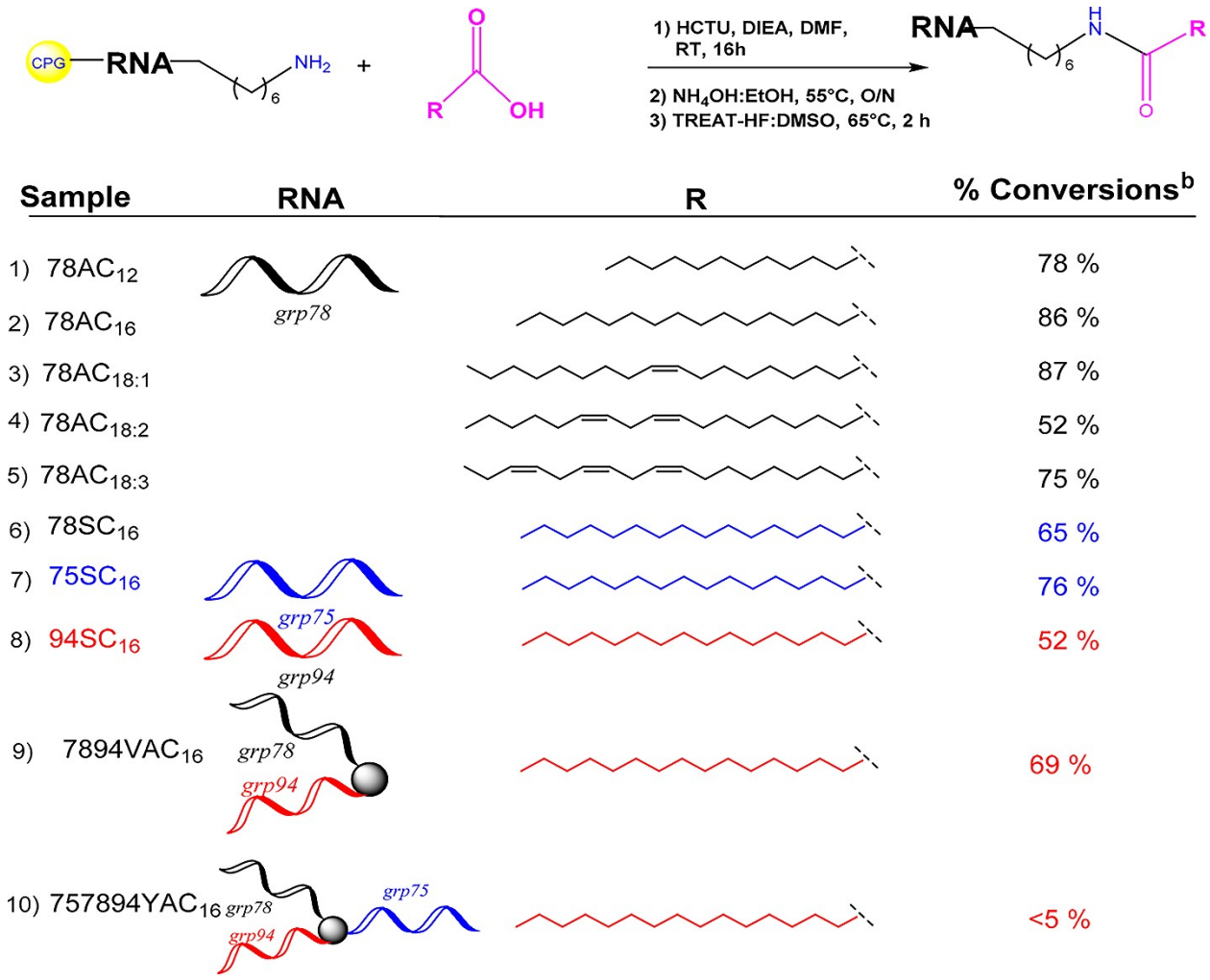

Scheme 2.1. Solid-phase bioconjugation of the amino-linked linear, V-, and Y-Shaped RNA templates with various fatty acids to afford the amide-linked fatty acid-RNA bioconjugates. Scheme reproduced with permission from: Shah, S.S.; Cultrara, C.N.; Kozuch, S.D.; Patel, M.R.; Ramos, J.A.; Samuni, U.; Zilberberg, J.; Sabatino, D. Direct Transfection of Fatty Acid Conjugated siRNAs and Knockdown of the Glucose-Regulated Chaperones in Prostate Cancer Cells. *Bioconjugate Chem.,* **2018**, *29*, 3638–3648.[35]

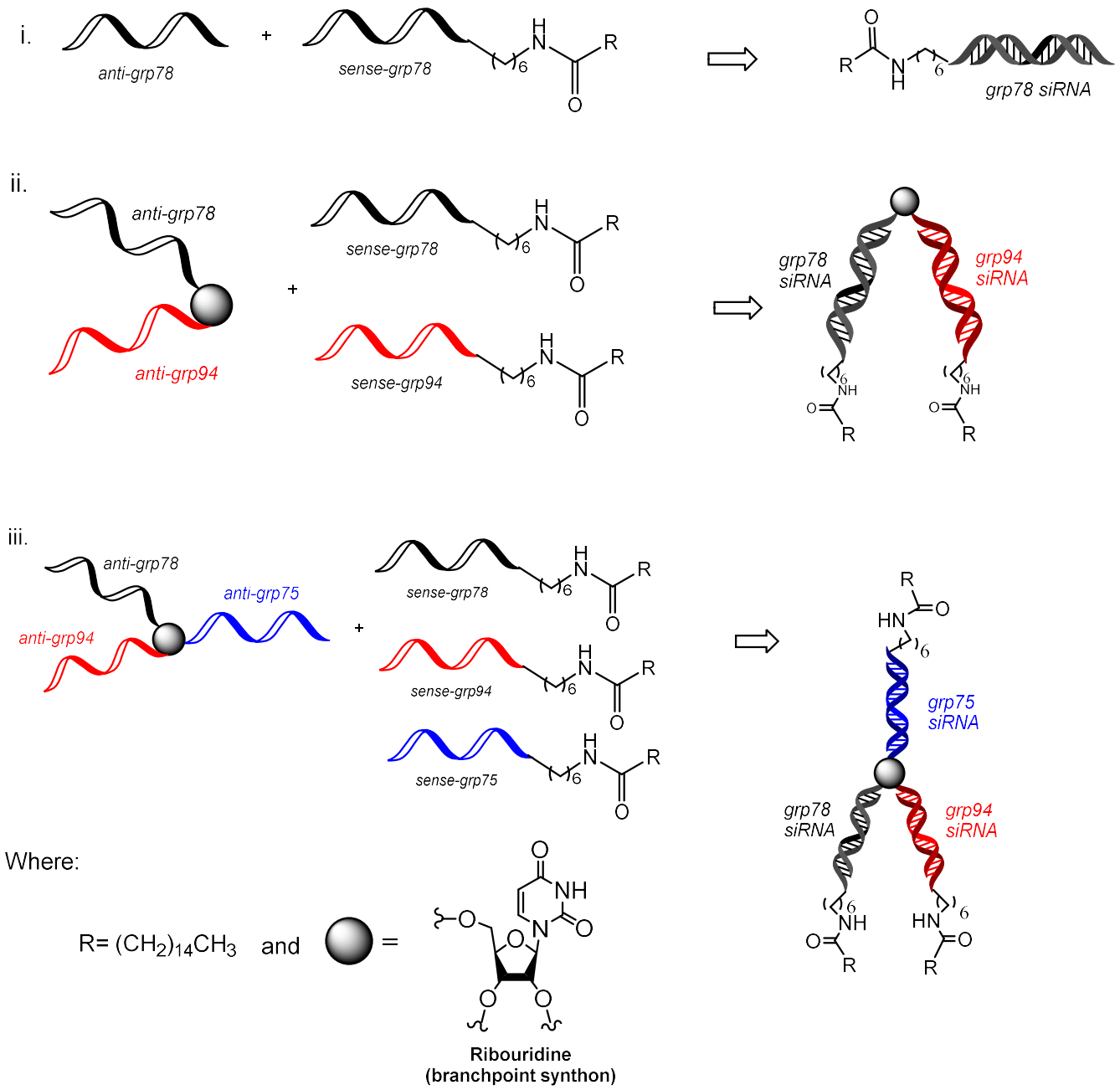

Scheme 2.2. Self-assembly of i. linear, ii. V- and iii. Y-shape multi-palmitamide labeled siRNA constructs. Scheme reproduced with permission from: Shah, S.S.; Cultrara, C.N.; Kozuch, S.D.; Patel, M.R.; Ramos, J.A.; Samuni, U.; Zilberberg, J.; Sabatino, D. Direct Transfection of Fatty Acid Conjugated siRNAs and Knockdown of the Glucose-Regulated Chaperones in Prostate Cancer Cells. *Bioconjugate Chem.,* **2018**, *29*, 3638–3648.[35]

2.4.2 Analysis and Purification of Fatty acid conjugated RNA Templates.

Following synthesis, the fatty acid conjugated RNA templates (**Table 2.1**) were purified by analytical Reverse-Phase Ion-Pairing High Performance Liquid Chromatography (RP IP HPLC) in ≥90% purities. Further, their identities were confirmed by electrospray ionization mass spectrometry (ESI MS) in negative mode using the LC/MS facilities at Novatia LLC (Newton, PA). Purified RNA templates with and without fatty acid conjugations were also analyzed by denaturing (urea) polyacrylamide gel electrophoresis (PAGE) (**Figure 2.2**) which confirmed sample purities and provided a first indication of the structural influence of the fatty acid groups, generating more retained bands compared to the unconjugated RNA templates. This trend underscores the potential impact of the fatty acid group in increasing the hydrophobicity, size, and structure composition of the functionalized RNA. UV-Visible (UV-Vis) spectroscopy was also used for sample quantitation at λ_{max}: 260 nm.

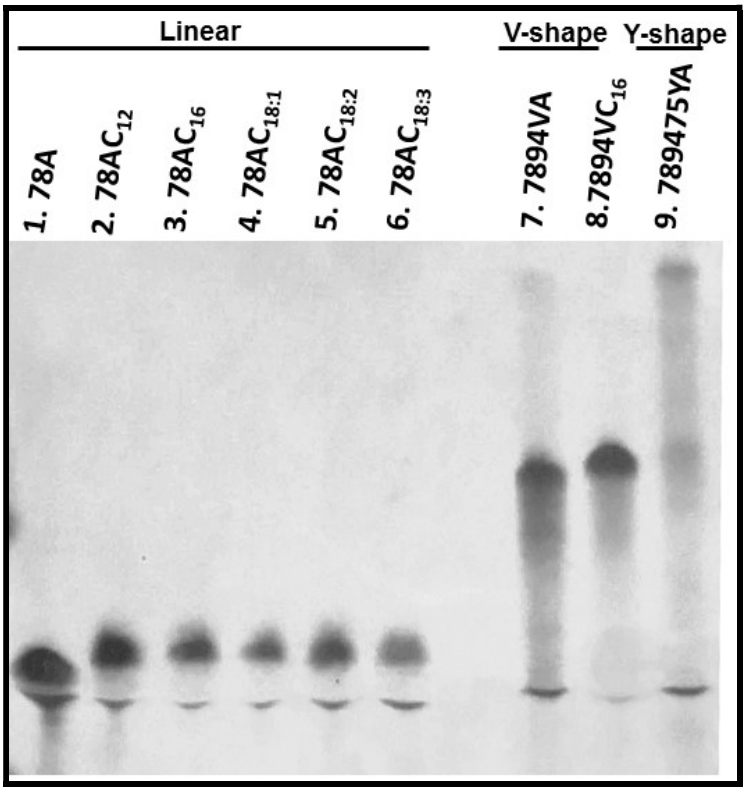

Figure 2.2. Denaturing PAGE of fatty acid conjugated linear (78AC12, 78AC16, 78AC18:1, 78AC18:2, 78AC:3), and V-shape (7894VC16) RNA templates and the unconjugated RNA controls (linear 78A, V-shape 7894VA, Y-shape 789575YA). Figure reproduced with permission from: Shah, S.S.; Cultrara, C.N.; Kozuch, S.D.; Patel, M.R.; Ramos, J.A.; Samuni, U.; Zilberberg, J.; Sabatino, D. Direct Transfection of Fatty Acid Conjugated siRNAs and Knockdown of the Glucose-Regulated Chaperones in Prostate Cancer Cells. *Bioconjugate Chem*., **2018**, *29*, 3638–3648.[35]

2.4.3 RP IP HPLC analysis of fatty acid conjugated siRNAs

The fatty acid conjugated RNA samples along with their native RNA templates were analyzed by RP IP HPLC with a Symmetry C-18 reverse phase column (4.6 x 250 mm, 5 μm particle size) using a gradient elution method of 7-70 % (MeCN in 0.1 M triethylammonium acetate, TEAA) over 40 minutes **(Figure 2.3)**. These analytical HPLC conditions were used to analyze the amphiphilic trends of the linear RNA templates conjugated with a small set of saturated, monounsaturated, and polyunsaturated fatty acids (**Scheme 2.1**, Samples 1-8) with varying chain lengths along with the V-shape RNA bioconjugate (**Scheme 2.1**, Sample 9). However, no detectable fatty acid conjugated product was observed with Y-shape RNA (**Scheme 2.1**, Sample 10). RP IP HPLC analyses confirmed greater retention (22.5 min) of the lengthier (Sample 3, $78AC_{18:1}$) fatty acid conjugated RNA when compared to the shorter (Sample 1, $78AC_{12}$) fatty acid bioconjugate (17.3 min) confirming that increasing fatty acid chain length increases hydrophobicity onto the RNA sequence, thus providing greater retention on the reverse phase column(**Figure 2.3**). Alternatively, increasing the degree of unsaturation with the polyunsaturated fatty acid-RNA conjugates resulted in the shortest retention times (Sample 5, $78AC_{18:3}$, 20.1 min) when compared to the monounsaturated (Sample 3, $C_{18:1}$, 22.5 min) and saturated (Sample 2, $78AC_{16}$, 21.9 min) counterparts (**Figure 2.3**).

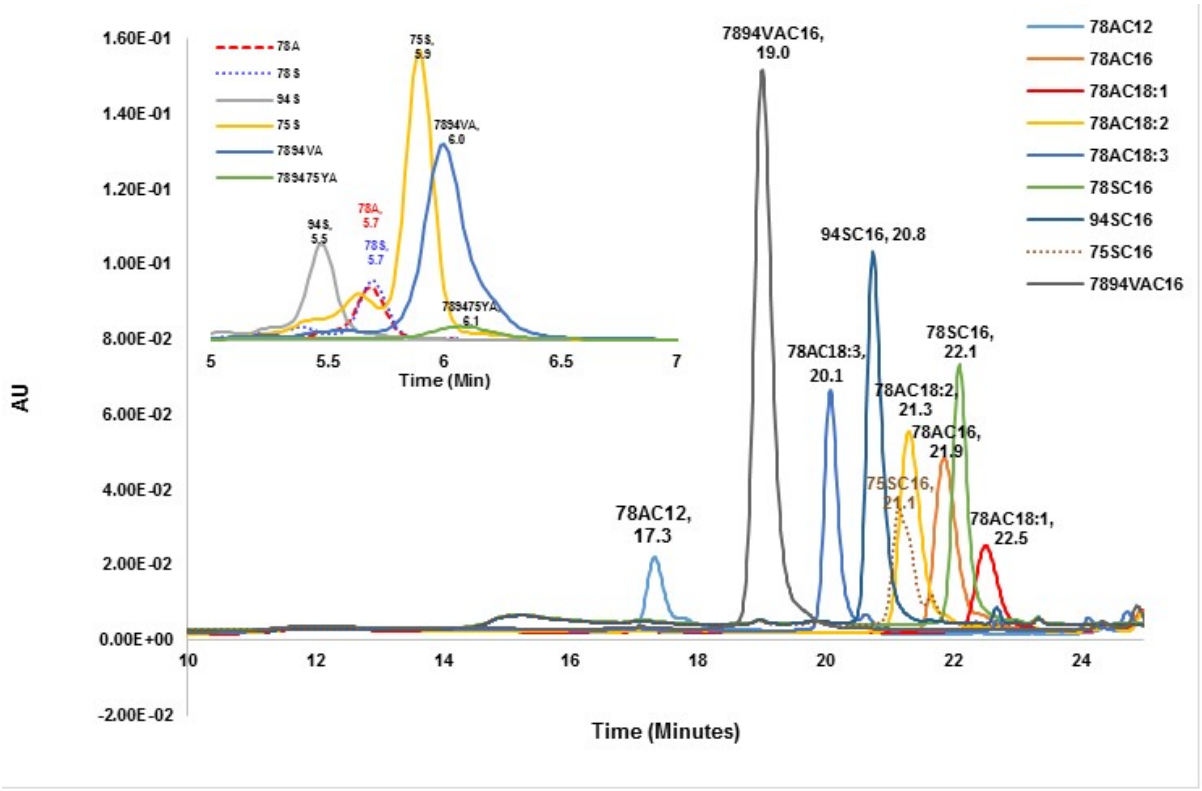

Figure 2.3. HPLC chromatogram of linear and V-shaped fatty acid-RNA bioconjugates along with their corresponding RNA templates (inset) and retention times (min). Figure reproduced with permission from: Shah, S.S.; Cultrara, C.N.; Kozuch, S.D.; Patel, M.R.; Ramos, J.A.; Samuni, U.; Zilberberg, J.; Sabatino, D. Direct Transfection of Fatty Acid Conjugated siRNAs and Knockdown of the Glucose-Regulated Chaperones in Prostate Cancer Cells. *Bioconjugate Chem*., **2018,** *29*, 3638–3648.[35]

It is hypothesized that increasing the cis-double bond character within the polyunsaturated fatty acids is expected to minimize their packing arrangement contributing to reduced hydrophobicity of the conjugated RNA sequences according to NMR and HPLC data of related saturated and unsaturated fatty acid conjugated siRNA.[38] Similarly palmitic acid conjugated V-shaped RNA template (Sample 10, 7894VC$_{16}$, 19 min) eluted with comparable retention times when compared

to the linear sense strands that were also functionalized with palmitic acid (Samples 6-8, GRP75, 78, 94 SC_{16}, 20-22 min). Thus, fatty acid chain length and double bond character influences RNA hydrophobicity, which in turn may influence RNA hybridization, structure, and biophysical properties.

2.4.4 Non-denaturing (native) PAGE analysis of fatty acid conjugated siRNAs

The purified RNA templates and their complementary RNA strands in their lipidated and non-lipidated form were hybridized in annealing buffer (10 mM Tris, 50 mM NaCl, 1 mM EDTA, pH 7.5–8.0) using equimolar concentrations (1.25 μM) of the pairing strands. Samples were hybridized by heating the complementary sequences at 95 °C (5 min) followed by slow cooling to room temperature (22 °C) for 1 h, and overnight storage at 4 °C. siRNA hybridization was confirmed by native, non-denaturing 16% polyacrylamide gel electrophoresis (PAGE). In this assay (**Figure 2.4A**), the native, linear siRNA hybrid (**Figure 2.4A**, Lane 1) migrated fastest on the gel when compared to the related linear siRNA-fatty acid bioconjugates (**Figure 2.4A**, Lanes 2-6). Comparatively to the HPLC analyses (**Figure 2.3**), linear fatty acid functionalized siRNAs displayed a gel migration pattern that was consistent with the lengths of the hydrocarbon tails, with the lengthier fatty acids (**Figure 2.4A**, 78AC16-C18, Lanes 3-6) being most retained when compared to the shorter one (**Figure 2.4A**, 78AC12, Lane 2). Similar retention trends were observed on RP IP HPLC (**Figure 2.3**). Similarly, the V and Y-shaped RNA templates (**Figure 2.4A**, Lanes 7 and 9) were more retained on the gel when compared to their linear counterparts, whereas the palmitamide conjugated V-shape siRNA (**Figure 2.4A**, Lane 8) was also found to be more retained on gel when compared to the corresponding V-shape unconjugated RNA template (**Figure 2.4A**, Lane 7). These results confirmed efficient siRNA

hybridization of the linear, V- and Y-shape motifs, with the linear and V-shape siRNA conferring more retained gel migration when conjugated with their corresponding fatty acids. In the case of the V- and Y-shape siRNA bioconjugates, linear sense strand palmitamide conjugation facilitated the self-assembly and hybridization of the V-and Y-shape siRNA (**Scheme 2.2**). This one-pot self-assembly strategy enabled the rapid formation of V- and Y-shape siRNA bioconjugates functionalized with a single, double, and triple palmitamides to explore the influence of multiple fatty acid groups on siRNA structure and amphiphilicity (**Figure 2.4B**, Lanes 6, 7 and 9-11). In the native PAGE analysis, the linear siRNA hybrid control (**Figure 2.4B**, Lane 1) migrated fastest on the gel, followed by its palmitamide bioconjugate functionalized on either sense or antisense strands (**Figure 2.4B**, Lanes 2 and 3). Similarly, the native V- and Y-shaped siRNA hybrids (**Figure 2.4B**, Lane 4 and 8) also migrated fastest on the gel when compared to the palmitic acid conjugated V-shaped RNA template (**Figure 2.4B**, Lane 5) followed by the more retained V-shape siRNA conjugated with a single and double palmitamides (**Figure 2.4B**, Lane 6 and7). For the Y-shape series, analogous migration trends were observed on native gel, with the Y-shape RNA template migrating the fastest (**Figure 2.4B**, Lane 8) followed by the palmitamide conjugated RNA template (**Figure 2.4B**, Lane 9) and siRNA hybrids incorporating double and triple palmitamides (**Figure 2.4B**, Lanes 10 and 11, respectively). Taken together, the native gel data confirmed the hybridization and self-assembly of linear, V- and Y-shape siRNA bioconjugates incorporating single or multiple fatty acids (**Figures 2.4A** and **B**).

2.4.5. Circular dichroism (CD) analysis of lipidated siRNAs.

Circular dichroism (CD) spectroscopy was used to investigate whether the fatty acid conjugated siRNA hybrids preserved the prerequisite A-type helix geometry for RNAi applications.[39] The CD spectra (**Figure 2.4C**) confirmed the A-type structure for the lipidated linear, V- and Y-shaped siRNA bioconjugates with a minimum peak at 240 nm and broad maxima in between 250-290 nm. Though, small variations in the amplitudes of the molar ellipticities at these distinctive wavelengths were observed for the higher-order V- and Y-shape bioconjugates representing some perturbation of the fatty acid on siRNA helical geometry.

2.4.6 Thermal Denaturation (Tm)

The siRNA hybrid thermal stabilities were measured by thermal denaturation (Tm) experiments to examine the influence (if any) of the fatty acid groups on siRNA hybridization (**Figure 2.4D**). The Tm data indicates the melting temperature at which 50% of the hybrid siRNA will denature to RNA single strands, thereby causing an increase in the observed RNA absorption at λ_{max}: 260nm.[40] The melting curves for native and fatty acid conjugated siRNAs indicated that the incorporation of various fatty acids generated stable siRNA hybrids (Tm: 60-64 ^{o}C) which were comparable to the native, unconjugated controls (Tm: 58-64 ^{o}C).

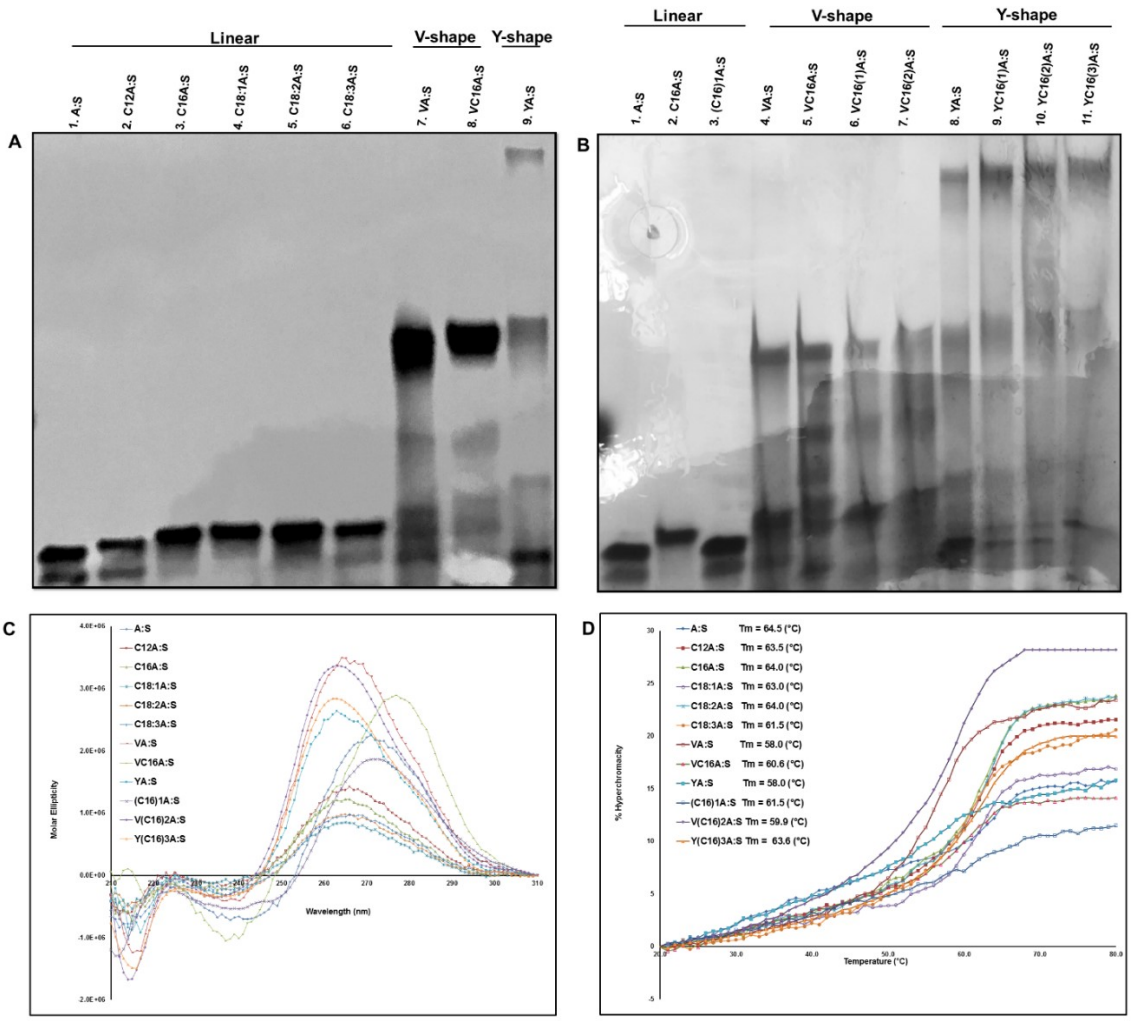

Figure 2.4 (A) Native, nondenaturing 16% PAGE of native linear, V and Y-shaped siRNA hybrids (Lanes 1, 7 and 9); saturated, unsaturated, and polyunsaturated fatty acid conjugated linear siRNA hybrids (Lanes 2-6) along with palmitamide conjugated V-shape siRNA (Lane 8). (B) Native, nondenaturing 16% PAGE of native linear, V and Y-shaped siRNA hybrids (Lanes 1, 4 and 8); palmitamide conjugated linear and V-shaped siRNA (Lanes 2 and 5, respectively); palmitamide conjugated linear sense (S) strands hybridized to complementary antisense (A) linear, V and Y-shaped RNA templates (Lane 3, 6, 7, 9-11) (C) Circular dichroism spectroscopy of linear, V- and Y-shaped siRNAs and their lipid bioconjugates (1.25 μM) in annealing buffer (1 mL, 10 mM Tris, 50 mM NaCl, 1 mM EDTA, pH 7.5). (D) Thermal denaturation linear, V- and Y-shaped siRNAs and their corresponding lipid bioconjugates (1.25 μM) hybridized in annealing buffer (1 mL, 10 mM Tris, 50 mM NaCl, 1 mM EDTA, pH 7.5). Figure reproduced with permission from: Shah, S.S.; Cultrara, C.N.; Kozuch, S.D.; Patel, M.R.; Ramos, J.A.; Samuni, U.; Zilberberg, J.; Sabatino, D. Direct Transfection of Fatty Acid Conjugated siRNAs and Knockdown of the Glucose-Regulated Chaperones in Prostate Cancer Cells. *Bioconjugate Chem.*, **2018,** *29*, 3638–3648.[35]

2.4.7. Serum Stability analysis of siRNAs.

Fatty acids such as palmitic acid have been used to improve siRNA half-life in biological serum and stability towards enzymatic digestion.[41,42] In order to explore the influence of fatty acid conjugation on siRNA serum stability, the palmitamide conjugated linear siRNA hybrids with antisense (C16A:S) and sense (C16)1A:S) strand modifiers in the presence of 10% FBS revealed improved stability and resistance towards degradation for up to 24 h when compared to the native, unconjugated siRNA hybrid (A:S) (**Figure 2.5**). These results underscore the potential therapeutic utility of the fatty acid siRNAs that may lead to long-lasting gene silencing activity in biological systems.

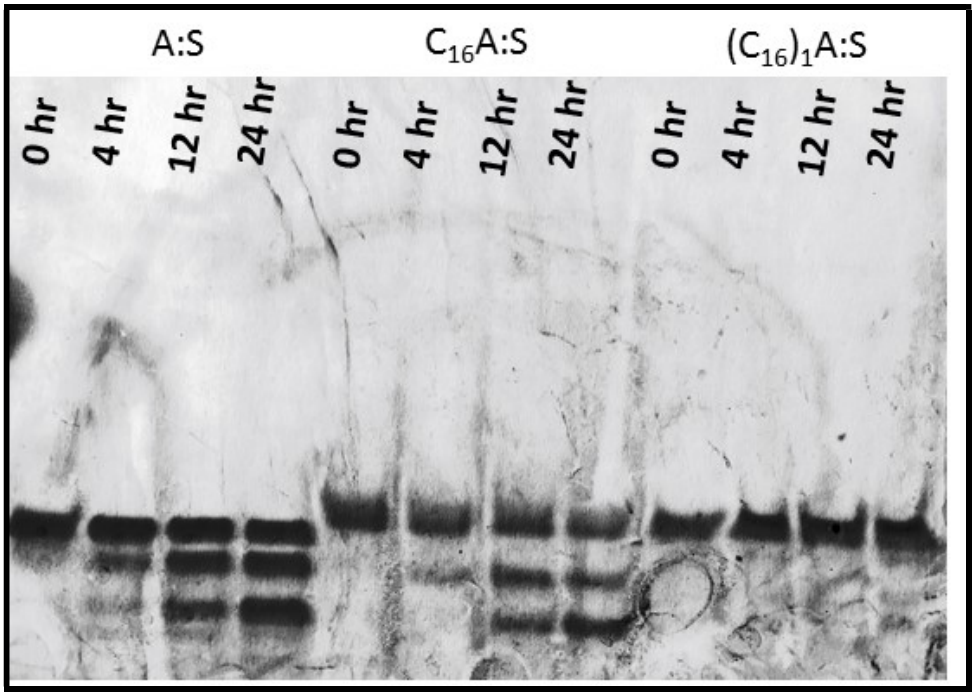

Figure 2.5. Serum stability study (10% FBS) of linear siRNA control (A1:S1), palmitamide conjugated both antisense and sense linear siRNA (C_{16} A:S and $(C_{16})_1$A:S). Figure reproduced with permission from: Shah, S.S.; Cultrara, C.N.; Kozuch, S.D.; Patel, M.R.; Ramos, J.A.; Samuni, U.; Zilberberg, J.; Sabatino, D. Direct Transfection of Fatty Acid Conjugated siRNAs and Knockdown of the Glucose-Regulated Chaperones in Prostate Cancer Cells. *Bioconjugate Chem*., **2018,** *29*, 3638–3648.[35]

2.4.8. DLS and TEM analysis of fatty acid conjugated siRNAs

Dynamic light scattering (DLS), and transmission electron microscopy (TEM) were used as instrumental tools to investigate the influence of fatty acid conjugation on siRNA morphology, size, structure and aggregation as well as zeta potential values demonstrating charge distributions (**Figure 2.6 and Table 2.2**). TEM images of saturated (**Figure 2.6A**) and unsaturated fatty acid conjugated (**Figure 2.6B**) to linear siRNAs indicated large, spherical aggregates of about 300 nm. DLS measurements of these samples showed multimodal size distribution suggesting formation of large aggregates. Zeta potential measurements of these samples showed an overall reduction in charge density when compared to the native, unconjugated siRNA (**Table 2.2**). Similarly, palmitic acid conjugated to higher-order V-shaped RNA displayed a propensity for aggregation, however, without formation of well-defined structures (**Figure 2.6C**). The palmitic acid conjugated to sense strand formed the linear palmitamide conjugated siRNA which formed spherical aggregates of about 300 nm (**Figure 2.6D**) similar to the ones observed for the antisense strand functionalized palmitic acid-siRNA bioconjugate (**Figure 2.6A**). The palmitamide conjugated sense RNA strands hybridized with the V-shape RNA template to form the V-shape siRNA bioconjugate with double palmitic acid incorporations (**Figure 2.6E**). Similarly, the palmitamide conjugated sense RNA strands hybridized with the Y-shape RNA template to form the Y-shape siRNA bioconjugate with triple palmitic acid incorporations (**Figure 2.6F**). These multi-labeled higher-order siRNA bioconjugates displayed large irregular amorphous aggregates (> 300 nm). Thus, the incorporation of multiple fatty acids within siRNA triggers formation of larger, and typically undefined aggregates that may have profound effects on siRNA cell biology. Furthermore, the tabulated average data for particle size, polydispersity index and zeta potentials from triplicate

measurements are provided in **Table 2.2**, which supports the observed particle characteristics from the TEM and DLS measurements.

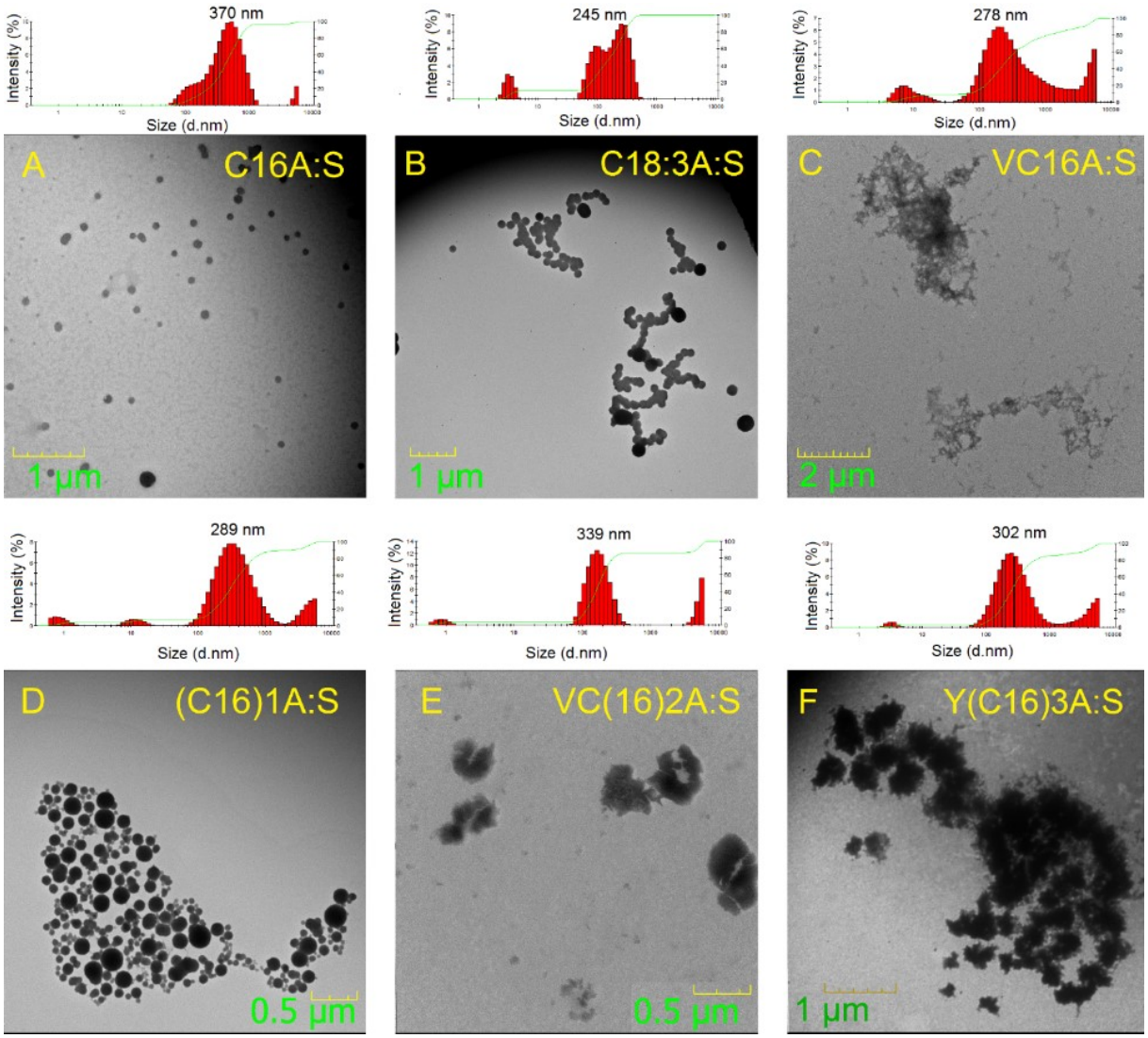

Figure 2.6. Representative DLS derived size distribution and corresponding TEM images of (A) saturated (C16), (B) unsaturated (C18:3) linear siRNA and (C) palmitic acid (C16) conjugated V shaped siRNA bioconjugates. Palmitic acid (C16) conjugated sense strands were used to generate the multi-functionalized linear (single), V (double) and Y-shaped (triple) palmitamide-siRNA bioconjugates (D-F). Figure reproduced with permission from: Shah, S.S.; Cultrara, C.N.; Kozuch, S.D.; Patel, M.R.; Ramos, J.A.; Samuni, U.; Zilberberg, J.; Sabatino, D. Direct Transfection of Fatty Acid Conjugated siRNAs and Knockdown of the Glucose-Regulated Chaperones in Prostate Cancer Cells. *Bioconjugate Chem*., **2018,** *29*, 3638–3648.[35]

Table 2.2. Particle size and zeta potential measurements of linear, V and Y shaped RNA-fatty acid bioconjugates determined by DLS and TEM.

Sample Details	Sample Name	Particle Size (nm)		Polydispersity Index	Zeta Potential (mV)
		DLS[a]	TEM		
Linear Control	A1:S1	480	NA	0.502	-15
Dodecanoic Acid Conjugated	78AC12	600	NA	0.516	-13
Palmitic Acid Conjugated	78AC16A	370	130	0.507	-14
Oleic Acid Conjugated	78AC18:1	370	NA	0.538	-10
Linoleic Acid Conjugated	78AC18:2	690	450	0.610	-8.3
Linolenic Acid Conjugated	78AC18:3	240	350	0.472	-7.2
V shaped RNA Control	7894VA:S	760	NA	0.707	-3.6
Palmitic Acid Conjugated	7894SVC16	280	500-750	0.644	-4.1
Y-Shaped RNA control	757894YA:S	340	NA	0.580	-6.9
Palmitic Acid Conjugated (Sense)	$78S(C16)_1$	290	250-424	0.463	-5.9
Palmitic Acid Conjugated (Sense)	$7894SV(C16)_2$	340	240-450	0.363	-2.4
Palmitic Acid Conjugated (Sense)	$757894SY(C16)_3$	300	200-230	0.322	-16

. [a]DLS analysis data presented are triplicate and having a range of standard deviation of 30-100 nm in terms of size depending on the type of samples. Table reproduced with permission from: Shah, S.S.; Cultrara, C.N.; Kozuch, S.D.; Patel, M.R.; Ramos, J.A.; Samuni, U.; Zilberberg, J.; Sabatino, D. Direct Transfection of Fatty Acid Conjugated siRNAs and Knockdown of the Glucose-Regulated Chaperones in Prostate Cancer Cells. *Bioconjugate Chem*., **2018**, *29*, 3638–3648.[35]

2.4.9. Biological Activity of siRNA Bioconjugates

Following evaluation of the biochemical and physical properties, the biological activity of the fatty acid conjugated linear, V- and Y-shape siRNAs was examined in a PC-3 prostate cancer cell line.[43] The PC-3 prostate cancer cell line (ATCC® CRL-1435™) was used as a GRP overexpressing cell line model to examine the knockdown efficiency of the lipidated siRNA constructs.[44] The *Trans*-IT X2® Dynamic Delivery System (Mirusbio®) was used as suitable siRNA transfection reagent within the PC-3 cell culture to establish the baseline GRP knockdown activity of the unconjugated linear, V- and Y-shape siRNA controls. In this assay, the control sequences exhibited potent (60-80%) GRP mRNA knockdown according to RT PCR (**Figure 2.7A**). Comparatively, the antisense fatty acid functionalized linear siRNAs (**Scheme 2.1**, Samples 1-5) transfected directly and without the use of the *Trans*-IT X2® transfection reagent triggered GRP78 mRNA knockdown, albeit to a lesser extent (20-40%) relative to the linear siRNA control (80%) transfected with the *Trans*-IT X2® dynamic delivery system (**Figure 2.7B**). Interestingly, the length of the hydrophobic fatty acid tail and the degree of unsaturation did not have any significant impact on siRNA activity. Thus, palmitic acid (C_{16}) which has been found to be well tolerated in siRNA applications,[19-27] was chosen to functionalize the higher-order V- and Y- shape siRNAs for silencing multiple GRPs. In this direct transfection assay, GRP78 knockdown (~40%) was noted with the palmitamide conjugated linear, V- and Y-shape siRNAs, however, with little effects on GRP75 and 94 mRNA levels (**Figure 2.7C**). In an effort to improve GRP knockdown activity, the palmitamide-functionalized sense strand RNAs were hybridized and self-assembled to the complementary antisense strand linear, V- and Y-shape RNA templates to afford the siRNA bioconjugates incorporating single, double and triple palmitamides (**Scheme 2.2**). The sense strand modifiers known to be better tolerated and

processed in RISC[45] were found to improve GRP mRNA knockdown efficacy (~5-60%) upon direct transfection within the PC-3 cells (**Figure 2.7D**); albeit, to a lesser extent when compared to the unconjugated siRNAs transfected with the *Trans*-IT X2® dynamic delivery system (**Figure 2.7A**). To provide some rationale for this discrepancy, a cell uptake assay was performed by flow cytometry (**Figure 2.8**). To assess the influence of fatty acid conjugation on siRNA transfection efficacy the lipidated siRNA bioconjugates were compared with native, unconjugated siRNA transfections with the *Trans*-IT X2® dynamic delivery system. In this assay, linear, sense strand RNAs were functionalized with either palmitic acid or fluorescein isothiocyanate (FITC) functioning as reporter probe and hybridized to complementary antisense linear, V- and Y-shape RNA templates to afford the multi-labeled siRNA bioconjugates. Flow cytometry revealed partial (6 h) cell uptake of the palmitamide-functionalized siRNAs. Comparatively, the native siRNAs transfected with the *Trans*-IT X2® dynamic delivery system maintained FITC cell signaling up to 24 h. Thus, partial cell uptake is likely a contributing factor in the modest GRP mRNA knockdown (KD) effects observed for the palmitamide-functionalized siRNAs. This may be in part due to the larger size aggregates (≥ 300 nm) observed from the DLS and TEM studies which may altogether restrict cell permeability.[46,47] Additional hydrophobic or amphiphilic carriers may be explored in future studies to help improve cell uptake of the functionalized siRNAs for more potent RNAi activity.[48]

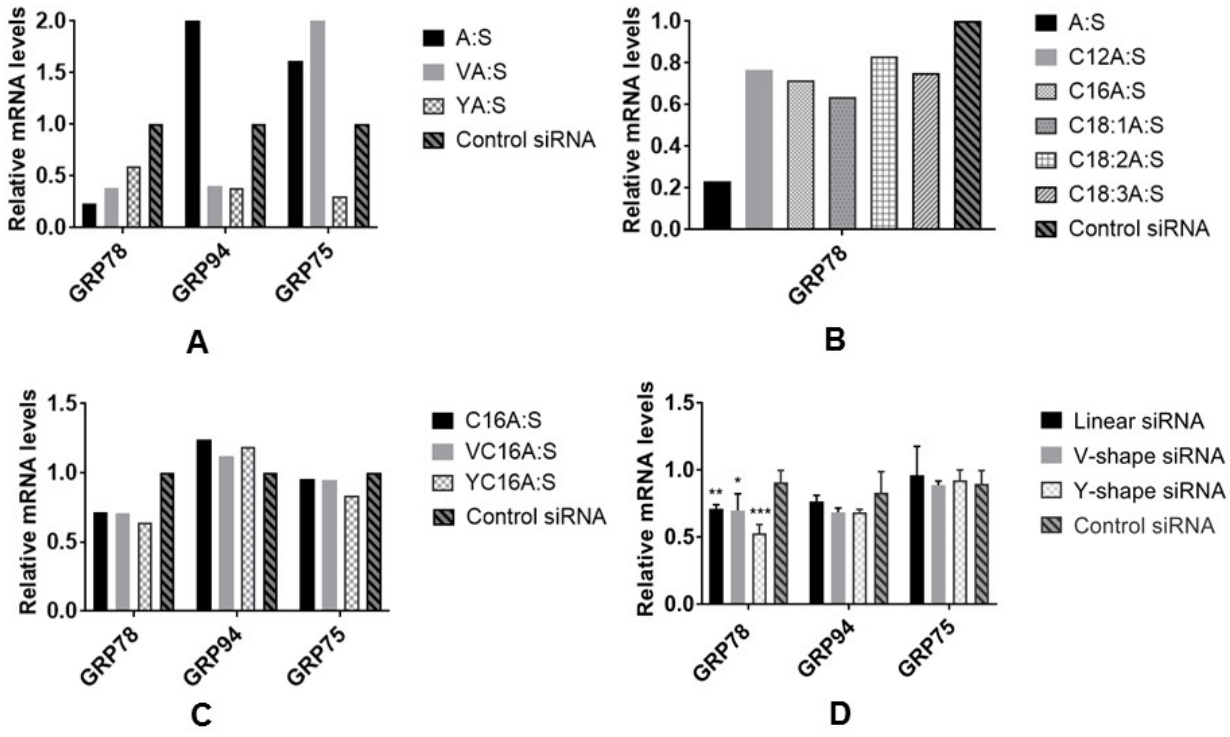

Figure 2.7. qRT-PCR analysis of GRP mRNA levels in PC-3 cells following (A) transfection of linear, V and Y shaped siRNAs with the Trans-IT X2® dynamic delivery system, (B) direct transfection of saturated, unsaturated and polyunsaturated fatty acid-siRNA bioconjugates, (C) direct transfection of palmitamide conjugated linear, V and Y-shaped siRNA bioconjugates, (D) direct transfection of linear, V and Y-shaped siRNA bioconjugates respectively containing a single, double and triple palmitamides. Target mRNA levels are relative to a control siRNA and represented as the mean fold change ± SD of 3 separate trials. *P<0.05 and ***P <0.001 in PC3 cells for GRP78 KD. Figure reproduced with permission from: Shah, S.S.; Cultrara, C.N.; Kozuch, S.D.; Patel, M.R.; Ramos, J.A.; Samuni, U.; Zilberberg, J.; Sabatino, D. Direct Transfection of Fatty Acid Conjugated siRNAs and Knockdown of the Glucose-Regulated Chaperones in Prostate Cancer Cells. *Bioconjugate Chem*., **2018**, *29*, 3638–3648.[35]

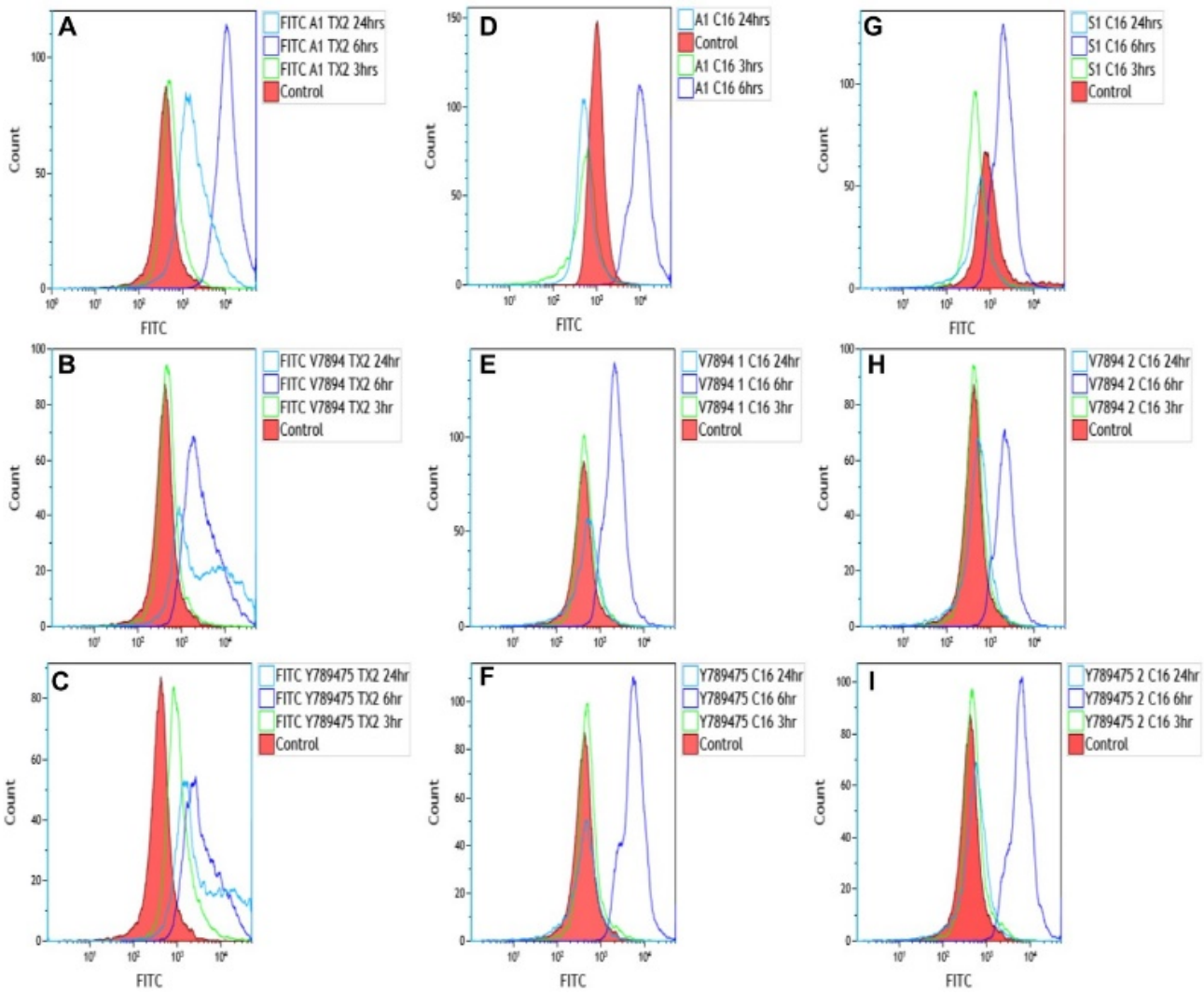

Figure 2.8. Time dependent (6-24 h) flow cytometric analysis of linear, V and Y shaped FITC labeled siRNAs transfected with the Trans-IT X2® dynamic delivery system (A-C). Direct transfection of linear, V- and Y-shape FITC-labeled siRNA containing single (D-F) and multiple (G-I) palmitamides within the PC-3 prostate cancer cell line. Figure reproduced with the permission from: Shah, S.S.; Cultrara, C.N.; Kozuch, S.D.; Patel, M.R.; Ramos, J.A.; Samuni, U.; Zilberberg, J.; Sabatino, D. Direct Transfection of Fatty Acid Conjugated siRNAs and Knockdown of the Glucose-Regulated Chaperones in Prostate Cancer Cells. *Bioconjugate Chem.*, **2018**, *29*, 3638–3648.[35]

2.5. Conclusions

In conclusion, short and long-chain fatty acids containing saturated, unsaturated and polyunsaturated long chain hydrocarbon groups were successfully incorporated within the GRP-silencing siRNAs by solid phase RNA synthesis. The siRNA-fatty acid bio-conjugates were characterized according to their structural and biophysical properties which revealed amphiphilic aggregates with stable hybrid and serum stabilities as well as A-type helical secondary structures applicable to RNAi activity. Their biological activity in a metastatic (PC-3) prostate cancer cell line revealed partial cell uptake, which contributed to modest RNAi activity when compared to the siRNA controls, likely due to the formation of large, aggregated particles. Nonetheless, the solid-phase RNA bio-conjugation approach reported in this study provides an important entry point for the incorporation of various hydrophobic and amphiphilic functional groups onto higher-order, multifunctional siRNA constructs. This strategy may enable the development of new generation RNAi molecules for screening important oncogene targets and for improving cancer gene therapy applications.

2.6 Experimental Section

2.6.1 Methods and Materials

Chemical synthesis reagents and solvents were obtained from ChemGenes, Aldrich and VWR and used as received. Solid phase RNA synthesis reagents were obtained from ChemGenes or Glen Research Inc. and used without further purification. Analytical thin-layer chromatography (TLC) was performed on aluminum-backed silica gel plates (Merck 60 F254). TLCs were visualized under UV shadowing (260 nm) or staining (10% H_2SO_4/MeOH). Compound purification using silica gel chromatography was performed on 230-400 mesh silica (Sorbent Technologies). Molecular weights for the branchpoint uridine phosphoramidite was

measured by direct injections on a Hewlett Packard series 1100 MSD equipped with ESI as ion-source in positive mode using 50/50 v/v MeOH/H_2O at a flowrate of 0.5 mL/min. Nuclear magnetic resonance spectra (^{1}H, ^{13}C, ^{31}P COSY NMR) were recorded on a Varian NMR AS500 spectrophotometer. NMR spectra were obtained at ambient temperature using an indirect pulse field gradient (ID-PFG) probe. The obtained data was processed using VNMRJ software (version 2.2). Materials for cell biology were obtained from Thermofisher Scientific, Cell Signaling, Bio-legend, Mirus and Invitrogen Life Technologies.

2.6.2 Solid-Phase Oligonucleotide Synthesis

Synthesis of alkyl (C_6) amino linker GRP78 antisense RNA (5'-AUC AGA AUC UUC CAA CAC U-3') and sense RNA (5'- AGU GUU GGA AGA UUC UGA U -3') were performed on a 2000 Å UnyLinker controlled pore glass (CPG) support (ChemGenes) using a 1 µmol scale automated synthesis cycle on an ABI 3400 DNA synthesizer. All phosphoramidites were dissolved in anhydrous MeCN yielding 0.15 M solutions. The coupling times were 5 minutes using 0.25 M 5-ethylthiotetrazole (ETT) in MeCN as the activator. The detritylation times were set to 2 min using a solution of 3% dichloroacetic acid in CH_2Cl_2 (DCM). Capping and oxidation steps were performed using a mixture of acetic anhydride/N-methyl imidazole in MeCN and a solution of 0.01 M iodine in pyridine/THF/H_2O respectively. Following synthesis, oligonucleotides were cleaved from the CPG and deprotected with NH_4OH: EtOH (3:1 v/v) for 16 hours at 55 ºC. The crude oligonucleotides were evaporated to dryness and re-suspended in a mixture of 1:1.5 v/v DMSO:triethylaminetrihydrofluoride(TEA:THF) (250µL) to complete the 2'-desilylation reaction at 65 °C for 2 h. The crude RNA was precipitated from the reaction mixture with 3 M NaOAc (35µL) in n-BuOH (1 mL). Precipitation was completed in a -80°C freezer 30 min prior to centrifugation (~12,000 rpm, 2 min) leaving the crude oligonucleotides as

a solid white pellet. Crude oligonucleotides were re-suspended in autoclaved water (1 mL) and the yields were determined by UV absorbance measurements at 260 nm. Crude RNA was purified by reverse-phase HPLC on a Waters 2695 Alliance system equipped with a Symmetry/XTerra RP-C_{18} reverse phase column (4.6 x 250 mm, 5 μm particle size) and gradient elution method of 7-70% MeCN in 0.1M TEAA over 40 minutes.

2.6.3 Solid-Phase RNA Bioconjugation

The RNA bioconjugates were produced on solid-phase, by combining the fatty acids (7 mg, 27.3 μmol, 25 eq) with the oligonucleotide-bound resin (0.106 μmol,). A coupling reagent (HCTU, 10 mg, 27.3 μmol, 25 eq) was added, and the mixture was suspended in minimum DMF (1 mL) and a base (DIEA, 8 μL, 50 eq) was added to initiate the reaction. Reactions were conducted in screw-cap Eppendorf tube and performed overnight (16 hrs.) at room temperature on a shaker. The CPG was subsequently washed with DMF/DCM/MeOH and dried *in vacuo*. The fatty acid oligonucleotide-bound resin was cleaved and deprotected using NH_4OH:EtOH (3:1 v/v) for 16 hours at 55 ºC. The crude oligonucleotides were evaporated to dryness and re-suspended in a mixture of 1:1.5 v/v DMSO: triethylaminetrihydrofluoride (250 μL) to complete the 2'-desilylation reaction at 65 °C for 2 hours. The crude RNA bioconjugates were precipitated from the reaction mixture with 3 M NaOAc (35 μL) in n-BuOH (1 mL). Precipitation was completed in -80°C freezer 30 min prior to centrifugation (~10,000 rpm, ~5 minutes) leaving the crude oligonucleotides as a solid white pellet. The fatty acid RNA bioconjugates was extracted in autoclaved water (1 mL), quantitated by UV-Vis spectrophotometry, analyzed, and purified by ion pairing reverse-phase HPLC as described above.

2.6.4 UV-Vis Spectroscopy

Following cleavage and deprotection, samples were evaporated to dryness on a Speedvac concentrator and then re-suspended in 1 mL autoclaved deionized water for analysis. Optical absorption spectra were acquired with a HP 8452A Diode Array UV-Vis spectrophotometer. Absorption measurements were recorded in between 210-310 nm for RNA samples, which were quantified according to the Beer-Lambert law.

2.6.5. Reverse Phase Ion Pairing High Performance Liquid Chromatography (RP IP HPLC)

The crude RNA templates were analyzed by Reverse Phase Ion Pairing High Performance Liquid Chromatography (RP IP HPLC) to determine crude purities. Briefly, HPLC analyses (~0.1 OD) and purifications (1 OD) were performed on a Waters 2695 Alliance Separations Module. Crude RNA templates were dissolved in autoclaved water (1 mL) and injected into a Waters Symmetry/XTerra RP C_{18} reverse phase column (4.6 x 250 mm, 5 μm particle size) heated at 60 °C. HPLC analyses and purifications were conducted using a gradient of 7-70% eluent C (100% acetonitrile) in eluent A (0.1 M triethylammonium acetate) with a flow rate of 1 mL/min, run times of 40 minute and with absorbance detection at 260 nm using a Waters 2489 UV/Visible detector. Retention times (min.) and peak areas (% area) were integrated with Empower II software and used to confirm RNA purities >90% following sample purifications.

2.6.6 Electrospray Ionization Mass Spectrometry (ESI MS)

All oligonucleotides (0.1-0.4 μM) were dissolved in Millipore water (1 mL) and all the mass spectra analyzed by Dr. Mark Hail at Novatia, LLC, Newtown, PA. Samples were analyzed

on an Oligo HTCS LCMS system equipped with ESI/MS in negative mode. The data was processed by a ProMass software. Theoretical molecular weights were calculated using IDT mass analyzer https://www.idtdna.com/calc/analyzer.

2.6.7 Hybridization of fatty acid-siRNA bioconjugates

Equimolar concentrations of fatty acid-RNA bioconjugates and complementary RNA were combined with 15 µL of annealing buffer (10 mM Tris, pH 7.5-8.0, 50 mM NaCl, 1 mM EDTA) in a 1.5 mL screw-cap Eppendorf tube. The mixture was vortexed briefly and placed on a standard heat block at 95 ± 1 °C for 5 minutes. The samples were then allowed to slowly cool to room temperature before placing in a 4 °C fridge for 24 h. before further hybrid analysis.

2.6.8 Native Polyacrylamide Gel Electrophoresis (PAGE)

Hybrid siRNA samples (as described above) were removed from the fridge and diluted with 15 µL 30% sucrose loading buffer (30% sucrose in 5X TAE buffer). The hybrid samples were analyzed using 16% native PAGE. Gels were run at 500 V (60 W) for 3-4 h and visualized under short wave UV light. Gels were subsequently placed in a Stains-All® (Sigma) solution (25 mg S8 Stains-All®, 50 mL isopropyl alcohol, 25 mL formamide, 125 mL water). After 2 h, gels were removed from the Stains-All® solution and exposed to light to de-stain.

2.6.9 Circular Dichroism (CD) Spectroscopy

Annealed siRNA samples (1.25 µM) were diluted to 1 mL with annealing buffer and transferred to fused quartz cells with a 1 cm path length and maintained within the cell holder at RT under N_2 for 10 minutes prior to spectral acquisition. Spectra were collected using an Olis RSM CD 1000 spectrophotometer as an average of three scans. Spectra were analyzed between 210-310 nm and raw data were processed using Olis Global Works data analysis software and

correcting by subtracting the buffer followed by smoothing the data points. The data was then exported onto Windows Excel™ spreadsheet software for plotting the CD spectra as changes in molar ellipticities with increasing wavelengths.

2.6.10 Thermal Denaturation (T_m)

Annealed siRNA samples (1.25 μM) in annealing buffer were transferred to a fused quartz cells with a 1 cm path length and maintained within the cell holder at RT under N_2 for 10 minutes prior to spectral acquisition. Spectra were measured on a CARY 3E, UV-Vis spectrophotometer equipped with a temperature controller regulating the changes in hyperchromicities at 260 nm with increasing temperatures (20-80°C at 1 °C/min) under N_2. The melting temperatures (T_m) were calculated from the first derivative plots of the melting curves, representing the temperature at which 50 % of the duplex has denatured to the corresponding single strands. This data was exported into an Excel™ spreadsheet for plotting the T_m curves.

2.6.11 Dynamic Light Scattering (DLS)

A Malvern Zetasizer, Nano-ZS (Malvern Instruments, UK) employing a 173° scattering angle and a 4mW incident He-Ne laser (633 nm) was used to measure the particle sizes (hydrodynamic diameter), size distributions and zeta potentials of the siRNA hybrid control and siRNA-fatty acid bioconjugates. Samples were measured in triplicates at 25 ºC. All samples were loaded into folded capillary cells (DTS1070) equipped with electrodes on both sides to allow measurement of their zeta potentials and by extension, the stability and degree of aggregation. Particle suspensions with highly positive or highly negative zeta potentials are considered stable because the electrical repulsion between the particles tends to counter the van der Waals forces that would otherwise result in aggregation and precipitation.

2.6.12 Transmission Electron Microscopy (TEM)

TEM analyses of the linear, V and Y-shaped siRNA bioconjugates were performed with a JEOL 1200EX Transmission Electron Microscope (JEOL Ltd, Japan) at an accelerating voltage of 80 kV. A mixture of 1:1 volume ratio 1% uranyl acetate and sample suspension were prepared and 10 µL of this solution placed on a TEM carbon-film-coated copper grid of 300 mesh (Electron Microscopy Sciences Inc., Hatfield, PA). Each sample was allowed to sit for five minutes on the grid before wicking the excess liquid followed by storage of one week to allow the samples to dry. Images were taken with a SIA-L3C CCD camera (Scientific Instruments and Applications, Inc.) using the software Maxim DL5 (Diffraction Limited, Ottawa, Canada).

2.6.13 Serum Stability Assay

siRNA hybrid samples (A:S, C16A:S and A:S(C16)1) were hybridized using the protocol described in section 2.6.7 in annealing buffer. An aliquot (50 µL, 30 µM) was added to a 10% FBS solution (50 µL in phosphate buffer). The mixtures were incubated at 37 ºC and periodically (0 – 48 h) sample aliquots (15 µL) were removed, frozen at -80 ºC prior to analyses. Samples were thawed to room temperature (22 ºC) and diluted by 30 % sucrose loading buffer and analyzed on a 16% native, non-denaturing PAGE for 2.5 h. The gel was then visualized with a Stains-All (Sigma-Aldrich™) solution.

2.6.14 Cell Culture

Prostate cancer cell line PC-3 (ATCC® CRL-1435™) was cultured in RPMI-1640 complete growth medium supplemented with 10% (v/v) fetal bovine serum (FBS), and 1% (v/v) penicillin/streptomycin (P/S) under 5% CO_2 at 37 ºC. For passaging, PC-3 cells were detached with 0.25% trypsin and re-suspended with complete culture medium.

2.6.15 siRNA Transfections in PC-3 Cells and Flow Cytometry

PC-3 cells were seeded at a density of 9.0 x 10^4 cells/well, were plated in 24-well culture plates containing RPMI complete culture media with 10% FBS. Cells were cultured in a humidified incubator set at 37 ºC with 5% CO_2. Prior to transfections, the cocktail and control siRNA hybrids (7.5 µL, 10 µM, in Opti-MEM, 133 µL) were mixed with the transfection reagent (*Trans*IT-X2® Dynamic Delivery System, 9 µL, in Opti-MEM, 250 µL) according to the manufacture's recommendation and the fatty acid–siRNA bioconjugates were transfected directly with final concentration of 50 nM. The mixtures were incubated (15 min, 22 ºC) then added to the PC-3 cell culture and incubated at 37 ºC with 5% CO_2 over a three-day (72 h) period. Samples were tested at 3, 6 and 24 h post-transfection to determine internalization efficiency. Cells were removed from the well using trypsin and diluted in RPMI-1640 media. A Cytomics FC 500 flow cytometer was used for determining time dependent cell uptake.

2.6.16 mRNA Isolation and Gene Knockdown via Quantitative Real-Time Polymerase Chain Reaction (qRT-PCR)

Total mRNA was isolated following transfection (48-72 hr) from TriZol (Ambion) preserved cells using a TriRNA Pure Kit (Geneaid), following the manufacturer's instructions. The collected mRNA was then quantitated on a Qubit 3.0 fluorimeter using the Qubit Broad Range (BR) assay kit (Thermo Fisher Scientific). mRNA (200 ng) was reverse transcribed into cDNA using a high-capacity cDNA kit (Applied Biosystems). RT-PCR was performed using pre-developed TaqManTM gene expression primer-probes for GRP78 (assay ID Hs99999174_m1), GRP94 (assay ID Hs00437665_g1), GRP75 (Hs00269818_m1), and GAPDH (Hs99999905_m1) and TaqManTM fast advanced master mix. qPCR fast assay was carried out

on a StepOnePlus (Applied Biosystems). Fold changes were calculated with the ΔΔCt method using GAPDH as endogenous control and the negative siRNA as the control sample.

2.6.17 Statistical Analysis

All data were plotted and analyzed using the GraphPad Prism software, V 7.0d (La Jolla, CA). Each experiment was performed in triplicates (N=3). Data is represented as the mean ± SD. Comparisons between two groups were analyzed using unpaired Student's *t*-tests. A probability (P) value of less than 0.05 was considered statistically significant.

2.7. References

1. Elbashir, S.M.; Harborth, J.; Lendeckel, W.; Yalcin, A.; Weber, K.; Tuschl, T. Duplexes of 21-nucleotide RNAs mediate RNA interference in cultured mammalian cells. *Nature*, **2001**, *411*, 494-498.
2. Jinek, M.; Doudna, J.A. A three-dimensional view of the molecular machinery of RNA interference. *Nature*, **2009,** *457*, 405-412.
3. Aliabadi, H.M.; Mahdipoor, P.; Bisoffi, M.; Hugh, J.C.; Uludag, H. Single and Combinational siRNA Therapy of Cancer Cells: Probing Changes in Targeted and Nontargeted Mediators after siRNA Treatment. *Mol. Pharm*. **2016,** *13,* 4116-4128.
4. Ku, S.H., Kim, K., Choi, K., Kim, S.H., Kwon, I.C. Tumor-Targeting Multifunctional Nanoparticles for siRNA Delivery: Recent Advances in Cancer Therapy. *Adv. Healthcare Mater*. **2014,** *3*, 1182-1193.
5. Zuckerman, J.E.; Gritli, I.; Tolcher, A.; Heidel, J.D.; Lim, D.; Morgan, R.; Chmielowski, B.; Ribas, A.; Davis, M.E.; Yen, Y. Correlating animal and human phase Ia/Ib clinical data with CALAA-01, a targeted, polymer-based nanoparticle containing siRNA. *Proc. Natl. Acad. Sci. U.S.A.* **2014,** *111*, 11449-11454.
6. Patel, P.L.; Rana, N.K.; Patel, M.R.; Kozuch, S.D.; Sabatino, D. Nucleic acid bioconjugated in cancer detection and therapy. *Chem. Med. Chem*. **2016**, *11*, 252-269.
7. Lee, A.S. The glucose-regulated proteins: stress induction and clinical applications. *Trends Biochem. Sci.* **2001**, *26*, 504-510.
8. Lee, A. S. Glucose-regulated proteins in cancer: molecular mechanisms and therapeutic potential. *Nat. Rev. Cancer.* **2014**, *14*, 263-276.
9. Matsumura, K.; Sakai, C.; Kawakami, S.; Yamashita, F.; Hashida, M. Inhibition of Cancer Cell Growth by GRP78 siRNA Lipoplex via Activation of the Unfolded Protein Response. *Biol. Pharm. Bull*. **2014**, *37*, 648-653.

10. Huang, K.H.; Kuo, K.L.; Chen, S.C.; Weng, T.I.; Chuang, Y.T.; Tsai, Y.C.; Pu, Y.S.; Chiang, C.K.; Liu, S.H. Down-regulation of glucose-regulated protein (GRP) 78 potentiates cytotoxic effect of celecoxib in human urothelial carcinoma cells. *PLoS One*. **2012**, *7,* e33615.
11. Maddalo, D.; Neeb, A.; Jehle, K.; Schmitz, K.; Muhle-Goll, C.; Shatkina, L.; Walther, T.V.; Bruchmann, A.; Gopal, S.M.; Wenzel, W.; Ulrich, A.S.; Cato, A.C. A peptidic unconjugated GRP78/BiP ligand modulates the unfolded protein response and induces prostate cancer cell death. *PLoS One*. **2012**, *7*, e45690.
12. Maina, A.; Blackman, B. A.; Parronchi, C. J.; Morozko, E.; Bender, M. E.; Blake, A. D.; Sabatino, D. Solid-phase synthesis, characterization and RNAi activity of branch and hyperbranch siRNAs. *Bioorg. Med. Chem. Lett*. **2013**, *23,* 5270-5274.
13. Patel, M.R.; Kozuch, S.D.; Cultrara, C.N.; Yadav, R.; Huang, S.; Samuni, U.; Koren, J.; Chiosis, G.; Sabatino, D. RNAi Screening of the Glucose-Regulated Chaperones in Cancer with Self-Assembled siRNA Nanostructures. *Nano Lett*. **2016**, *16*, 6099-6108.
14. Musacchio, T.; Vaze, O.; D'Souza, G.; Torchilin, V.P. Effective Stabilization and Delivery of siRNA: Reversible siRNA−Phospholipid Conjugate in Nanosized Mixed Polymeric Micelles. *Bioconjug. Chem*. **2010**, *21*, 1530-1536.
15. Lee, S.H.; Mok, H.; Lee, Y.; Park, T.G.J. A duplex oligodeoxynucleotide-dendrimer bioconjugate as a novel delivery vehicle for doxorubicin in in vivo cancer therapy. *J. Control. Release* **2011**, *155*, 88-95.
16. Qiu, J.; Kong, L.; Cao, X.; Li, A.; Wei, P.; Wang, L.; Mignani, S.; Caminade, A.M.; Majoral, J.P.; Shi, X. Enhanced Delivery of Therapeutic siRNA into Glioblastoma Cells Using Dendrimer-Entrapped Gold Nanoparticles Conjugated with β-Cyclodextrin. *Nanomaterials*. **2018,** *8*, 6519-6533.
17. Nishina, K.; Unno, T.; Uno, Y.; Kubodera, T.; Kanouchi, T.; Mizusawa, H.; Yokota, T. Efficient in vivo delivery of siRNA to the liver by conjugation of alpha-tocopherol. *Mol. Ther*. **2008**, *16*, 734-740.
18. Lv, H.; Zhang, S.; Wang, B.; Cui, S.; Yan, J. Toxicity of cationic lipids and cationic polymers in gene delivery. *J. Control. Release*. **2006***, 114*, 100-109.
19. Kubo, T.; Yanagihara, K.; Sato, Y.; Nishimura, Y.; Kondo, S.; Seyama, T. Gene-Silencing Potency of Symmetric and Asymmetric Lipid-conjugated siRNAs and its Correlation with Dicer Recognition. *Bioconjug. Chem*. **2013**, *24,* 2045-2057.
20. Kubo, T.; Yanagihara, K.; Takei, Y.; Maura, K.; Morita, Y.; Seyama. T. Palmitic Acid-Conjugated 21-Nucleotide siRNA enhances Gene-Silencing Activity. *Mol. Pharm*. **2011**, *8,* 2193-2203.
21. Kubo, T.; Yanagihara, K.; Takei, Y.; Mihara, K.; Sato, Y.; Seyama, T. Lipid-conjugated 27-nucleotide double stranded RNAs with dicer-substrate potency enhance RNAi-mediated gene silencing. *Mol. Pharm*. **2012**, *9*, 1374-1383.

22. Kubo, T.; Takai, Y.; Mihara, K.; Yanagihara, K.; Seyama, T. Amino-Modified and Lipid-Conjugated Dicer-Substrate siRNA enhances RNAi Efficacy. *Bioconjug. Chem*. **2012**, *23*, 164-173.
23. Kubo, T.; Zhelev, Z.; Ohba, H.; Bakalova, R. Modified 27-nt dsRNAs with dramatically enhanced stability in serum and long-term RNAi activity. *Oligonucleotides*. **2007,** *17*, 445-464.
24. Kubo, T.; Zhelev, Z.; Bakalova, R.; Ohba, H. Enhancement of gene silencing potency and nuclease stability by chemically modified duplex RNA. *Nucleic Acids Symp. Ser*. **2007**, *51*, 407-408.
25. Kubo, T.; Zhelev, Z.; Bakalova, R.; Ohba, H. Highly efficient gene suppression by chemically modified 27 nucleotide double-stranded RNAs. *Jpn. J. Appl. Phys*. **2008**, *47*, 1346-1350.
26. Kubo, T.; Zhelev, Z.; Ohba, H.; Bakalova, R. Chemically modified symmetric and asymmetric duplex RNAs: an enhanced stability to nuclease degradation and gene silencing effect. *Biochem. Biophys. Res. Commun*. **2008**, *365*, 54-61.
27. Kubo, T.; Yanagihara, K.; Sato, Y.; Morita, Y.; Seyama, T. Enhancement of gene silencing effect and membrane permeability by peptide-conjugated 27-nucleotide small interfering RNA. *Molecules*. **2012**, *17*, 11089-11102.
28. Rietwyk, S.; Peer, D. Next-Generation Lipids in RNA Interference Therapeutics. *ACS Nano*. **2017**, *11*, 7572-7586.
29. Akinc, A.; Zumbuehl, A.; Goldberg, M.; Leshchiner, E.S.; Busini, V.; Hossain, N.; Bacallado, S.A.; Nguyen, D.N.; Fuller, J.; Alvarez, R.; Borodovsky, A.; Borland, T.; Constien, R.; de Fougerolles, A.; Dorkin, J.R.; Narayanannair, J. K.; Jayaraman, M.; John, M.; Koteliansky, V.; Manoharan, M.; Nechev, L.; Qin, J.; Racie, T.; Raitcheva, D.; Rajeev, K.G.; Sah, D.W.; Soutschek, J.; Toudjarska, I.; Vornlocher, H.P.; Zimmermann, T.S.; Langer, R.; Anderson, D.G. A combinatorial library of lipid-like materials for delivery of RNAi therapeutics. *Nat Biotechnol.* **2008**, *26(5),* 561-569.
30. O'Loughlin, A.J.; Mäger, I.; de Jong, O.G.; Varela, M.A.; Schiffelers, R.M.; El Andaloussi, S.; Wood, M.J.A.; Vader, P. Functional delivery of lipid-conjugated siRNA by extracellular vesicles. *Mol. Ther*. **2017**, *25*, 1580–1587.
31. Didiot, M.C.; Hall, L.M.; Coles, A.H.; Haraszti, R.A.; Godinho, B.M.; Chase, K.; Sapp, E.; Ly, S.; Alterman, J.F.; Hassler, M.R.; et al. Exosome-mediated delivery of hydrophobically modified siRNA for Huntingtin mRNA silencing. *Mol. Ther*. **2016**, *24*, 1836–1847.
32. Nishina, T.; Numata, J.; Nishina, K.; Yoshida-Tanaka, K.; Nitta, K.; Pieo, W.; Iwata, R.; Ito, S.; Kuwahara, H.; Wada, T.; Mizusawa, H.; Yokota, T. Chimeric Antisense Oligonucleotide conjugated to alpha-tocopherol. *Mol. Ther. Nucleic Acid*. **2015**, *4,* e220.
33. Nikan, M.; Osborn, M.F.; Coles, A.H.; Godinho, B.M.; Hall, L.M.; Haraszti, R.A.; Hassler, M.R.; Echeverria, D.; Aronin, N.; Khvorova, A., et al. Docosahexaenoic acid conjugation enhances distribution and safety of siRNA upon local administration in mouse brain. *Mol. Ther. Nucleic Acids*. **2016,** *5(8),* e344.

34. Kubo, T.; Nishimura, Y.; Sato, Y.; Yanagihara, K.; Seyama, T. Sixteen Different Types of Lipid-Conjugated siRNAs Containing Saturated and Unsaturated Fatty Acids and Exhibiting Enhanced RNAi Potency. *ACS Chem Biol*. **2021,** *16(1),* 150-164.
35. Shah, S.S.; Cultrara, C.N.; Kozuch, S.D.; Patel, M.R.; Ramos, J.A.; Samuni, U.; Zilberberg, J.; Sabatino, D. Direct Transfection of Fatty Acid Conjugated siRNAs and Knockdown of the Glucose-Regulated Chaperones in Prostate Cancer Cells. *Bioconjugate Chem*., **2018**, *29*, 3638–3648.
36. Patel, P.; Patel, H.H.; Borland, E.; Gorun, S.M.; Sabatino, D. Chemically robust fluoro alkyl phthalocyanine-oligonucleotide bioconjugates and their GRP78 oncogene photo cleavage activity. *Chem Commun (Comb*). **2014**, *50,* 6309-6311.
37. Kozuch, S.D.; Cultrara, C.N.; Beck, A.E.; Heller, C.J.; Shah, S.S.; Patel, M.R.; Zilberberg, J.; Sabatino, D. Enhanced Cancer Theranostic with Self-Assembled, Multilabeled siRNAs. *ACS Omega*, **2018**, *3*, 12975–12984.
38. Alexandri, E.; Ahmed, R.; Siddiqui, H.; Choudhary, M.I.; Tsiafoulis, C.G.; Gerothanassis, I.P. High Resolution NMR Spectroscopy as a Structural and Analytical Tool for Unsaturated Lipids in Solution. *Molecules* **2017**, *22*, 1-72.
39. Li, Z.; Rana, T.M. Molecular mechanisms of RNA-triggered gene silencing machineries. *Acc Chem Res.* **2012**, *45(7),*1122-31.
40. Addepalli, H. M.; Peng, C. G.; Wang, G.; Fan, Y.; Charisse, K.; Jayaprakash, K. N.; Rajeev, K. G.; Pandey, R. K.; Lavine, G.; Zhang, L.; Jahn-Hofmann, K.; Hadwiger, P.; Manoharan, M.; Maier, M. A. Modulation of thermal stability can enhance the potency of siRNA. *Nucleic Acids Res.*, **2010**, *38(20),* 7320–7331.
41. Sarett, S.M.; Kilchrist, K.V.; Miteva, M.; Duvall, C.L. Conjugation of palmitic acid improves potency and longevity of siRNA delivered via endosomolytic polymer nanoparticles. *J Biomed Mater Res A*. **2015**, *103*, 3107-3116.
42. Sarett, S. M.; Werfel, T. A.; Chandra, I.; Jackson, M. A.; Kavanaugh, T. E.; Hattaway, M. E.; Giorgio, T. D.; Duvall, C. L. Hydrophobic Interactions between Polymeric Carrier and Palmitic Acid-Conjugated siRNA Improve PEGylated Polyplex Stability and Enhance In Vivo Pharmacokinetics and Tumor Gene Silencing. *Biomaterials.* **2016**, *97*, 122-132.
43. Rebollo, J.; Geliebter, J.; Reyes, N. ESM-1 siRNA Knockdown Decreased Migration and Expression of CXCL3 in Prostate Cancer Cells. *Int J Biomed Sci*. **2017**, *13*, 35-42.
44. Tormo, E.; Adam-Artigues, A.; Ballester, S.; Pineda, B.; Zazo, S.; González-Alonso, P.; Albanell, J.; Rovira, A.; Rojo, F.; Lluch, A., et al. The role of miR-26a and miR-30b in $HER2^+$ breast cancer trastuzumab resistance and regulation of the CCNE2 gene. *Sci Rep*., **2017**, *7*, 41309.
45. Pham, J.W.; Sontheimer, E.J. Molecular Requirements for RNA-induced Silencing Complex Assembly in the *Drosophila* RNA Interference Pathway. *J Biol Chem*. **2005,** *280*, 39278–39283.
46. Zheng, M., Yu, J. The effect of particle shape and size on cellular uptake. *Drug Deliv Transl Res***. 2016**, *6*, 67-72.

47. Cultrara C.N., Shah S., Antuono G., Heller C.J., Ramos J.A., Samuni U., Zilberberg J., Sabatino D. Size Matters: Arginine-Derived Peptides Targeting the PSMA Receptor Can Efficiently Complex but Not Transfect siRNA. *Mol Ther Nucleic Acids.* **2019**; *18*, 863-870.
48. Kim, J.B.; Lee, Y.M.; Ryu, J.; Lee, E.; Kim. W.J.; Keum, G.; Bang, E.K. Coordinative Amphiphiles as Tunable siRNA Transporters. *Bioconjug Chem*. **2016**, *27*, 1850-1856.

Chapter 3: Bifunctional Au-templated RNA Nanoparticles Enable Direct Cell Uptake Detection and GRP75 Knockdown in Prostate Cancer

3.1 Abstract

Nucleic acids templated on gold (Au) surfaces have led to a wide range of functional materials ranging from microarrays, sensors, and probes as well as applications in drug delivery and treatment. In this thesis chapter, we describe a simple and novel method for templating amino-functionalized RNA onto Au surfaces and their self-assembly into small, discrete nanoparticles for gene therapy applications in prostate cancer cells. In our method, sample hybridization with a complementary RNA strand with and without a fatty acid (palmitamide) produced palmitamide-functionalized double-stranded RNA on the Au surface. The resulting Au-RNA particles were found to be stable under reducing conditions according to UV-Vis spectroscopy. Sample characterization by DLS and TEM confirmed self-assembly into primarily small (~10-40 nm) spherical-shaped nanoparticles expected to be amenable to cell biology. However, fluorescence emission (λ_{exc}: 350 nm, λ_{em}: 650 nm) revealed radiative properties associated with gold nanoparticles, which restricted cell biology applications (i.e. cell uptake, and cytotoxicity) due to limitations with the emission/scattering detection of gold nanoparticles by flow-cytometry and high content screening microscopy. Introduction of fluorescein within the Au-RNA particles produced a bifunctional probe, in which fluorescein emission (λ_{exc}: 494 nm, λ_{em}: 522 nm) facilitated cell uptake detection, in a time-dependent manner. The dual encapsulation-release profiles of the fluorescein-labeled Au-RNA particles were validated by time-dependent UV-Vis spectroscopy and spectrofluorimetry. These experiments respectively indicated an increase in fluorescein absorption (λ_{abs}: 494 nm) and fluorescence emission (λ_{em}: 522 nm) with increased sample incubation times under physiological conditions. The release of

Au-functionalized siRNA particles in prostate cancer (PC-3) cells resulted in GRP75 knockdown, which led to detectable levels of cell death in the absence of a transfection vector. Thus, the formulation of stable, small, and discrete Au-RNA nanoparticles may prove to be valuable bifunctional probes in the theranostic study of cancer cells.

3.2 Introduction

The advancement of RNA nanomaterials has led to the development of new molecular tools capable of screening, detecting, and treating a wide range of malignancies, including cancer.[1-4] In the fight against cancer, RNA nanomaterials functioning as precision nanomedicines have improved target specificity, cell uptake, and anti-cancer activity relative to non-specific and toxic chemotherapy and radiative treatment regimens. More specifically, in recent years, metal nanoclusters have emerged as a promising class of theranostic agents due to their unique metal core and surface-layer properties which facilitate functionalization with bio-active probes for bioimaging, biosensing, and therapeutic applications.[5-13] Moreover, the recent generation of gold (Au) functionalized RNA has enabled the self-assembly of stable RNA nanoparticles that have been found to be compatible with cell biology applications.[14] These have included the structural assembly of molecular beacons,[15] and sensors for nucleic acid detection,[16] microarrays for gene screening and sequencing methods,[17] controlled and targeted RNA delivery for gene therapy in cells, tissues, and animal models.[18-21] Of specific interest, recent studies have demonstrated that Au nanoparticles, functionalized with polyethylene glycol (PEG) and polyethyleneimine (PEI), respectively applied as biocompatible and condensing agents for RNA cell uptake, along with transferrin (Tf) and folate (FA) as cell-targeting ligands have been effectively used to deliver siRNAs into LNCaP prostate cancer (PCa) cells.[22] Following the endolysosomal escape, the Au-

siRNA nanoparticles exhibited notable intracellular silencing of the RelA oncogene when compared to the non-targeted formulation, suggesting that Au-siRNA nanoparticles may have potential in the detection and treatment of PCa. It was also found to be the case with PEI-functionalized Au nanoparticles bearing anisamide (AA) as targeting ligand.[23] In this study, siRNA delivery into PC-3 PCa cells resulted in significant (~70%) knockdown (KD) of the RelA oncogene in a cell-line dependent manner which expresses the sigma (σ) receptor on the cell surface in the absence of serum media. Serum was found to obstruct the requisite ligand-receptor interaction required for cell uptake and KD activity. In addition to their theranostic activities, Au-functionalized siRNA nanoparticles have also been shown to 1) have enhanced serum stability when compared to their native siRNA counterparts,[24] 2) serve as stimuli-responsive materials for controlled siRNA intracellular release under glutathione-reducing cytosolic conditions,[25] and 3) possess desirable radiative and photothermal properties into the near-infrared (NIR) region which is advantageous in producing local heating and cavitation of endosomes, resulting in siRNA intracellular escape.[26] This is in contrast to siRNA-based formulations which are not amenable to cell transfection and *in vivo* delivery of siRNA due to their limited capabilities of 1) condensing and releasing siRNA at the target site for RNAi silencing activity, 2) conferring serum stability, 3) generating small, discrete and neutral nanoparticle formulations for efficient cell uptake and 4) limiting off-target silencing and toxicity effects.[27-29] Thus, Au-siRNA formulations have resulted in successful gene silencing applications and may form the basis for the development of potent therapeutic interventions against malignant oncogene targets.

Glucose-regulated proteins (GRPs), are a class of chaperone proteins that serve as the main regulators of the unfolded protein response under physiological and pathological stress conditions in cells.[30] GRPs in the lumen of the endoplasmic reticulum (ER) promote protein

folding activity, in the mitochondria, they interact with pro-apoptotic executors that regulate cell survival/death responses and at the cell surface, the direct signal transduction. Moreover, GRPs have been found to be over-expressed and cell surface localized in a wide range of cancer types, where they regulate cancer initiation, proliferation, adhesion, and invasion which contributes to metastatic spread and chemoresistance. Thus, the GRPs have been classified as clinically relevant biological markers in cancer detection and treatment.[30] Among the GRPs, the Glucose Regulated Protein of 75 kilodaltons (GRP75/Mortalin) has been classified as a homolog of the Heat Shock Protein of 70 kilodalton (HSP70) and functions primarily as a mitochondrial chaperone where it regulates cell growth and survival related to mitochondrial-dependent cell death pathways.[31] GRP75 is localized in the ER where it assists in protein folding and at the plasma membrane where it confers cell survival from complement-dependent cytotoxicity (CDC) pathways.[32] Moreover, GRP75 has been strongly associated with tumor resistance, survival, and proliferation, making it a clinical target for the detection and treatment of certain tumor types.[33-36] For example, GRP75 has been found to be overexpressed in tumors of the colon, liver, brain, breast, and skin, where it functions as an important regulator of tumor cell growth and survival.[37,38] In PCa, GRP75 has been detected by western blot and correlated with a visceral metastasis-derived (PC-3M) cell line.[39] Knockdown or inhibition of GRP75 was found to reverse its pro-survival effects resulting in tumor apoptosis.[40-42] Therefore, therapeutic targeting of GRP75 has potential anti-cancer implications.

3.3 Chapter Objectives

In this chapter, our objective is to develop a methodology that improves cell-uptake and GRP75 knockdown efficacy in PCa cells using Au-siRNA nanoparticle-formulations. Towards this goal, we have pioneered a versatile solid-phase synthesis strategy for the generation of the

linear, branch, and hyper-branch RNA templates for their self-assembly into higher-order siRNA nanostructures.[43,44] Significantly, these constructs silenced GRP75, GRP78, and GRP94 expressions in the liver (HepG2), endometrial (AN3CA), cervical (HeLa), and breast (MDA-MB-231) cells resulting in synergistic anti-cancer effects. Recent efforts to expand the scope and functionality of the siRNA nanostructures resulted in the formulation of fluorescently labeled[45] and fatty acid conjugated[46] constructs that exhibited modest KD and toxicity effects in PCa cells in the absence of a transfection vector. Overcoming this siRNA delivery challenge is a critical requirement for successful cell-based gene therapy applications.

To improve the cell uptake and theranostic utility of our multi-functional siRNA nanostructures in PCa cells, this thesis chapter will describe the rational design, synthesis, characterization, and biological evaluation of newly assembled bifunctional Au-templated RNA nanoparticles. The synthetic method for the formulation of Au-RNA particles will be based on a novel bottom-up approach for nucleating synthetic double-stranded (ds) RNA in which the antisense (A1) strand bearing a reactive alkylamino linker will used to template RNA onto the surface of reduced Au particles. The complementary sense (S1) strand will be functionalized with and without a palmitamide (C16) fatty acid group or fluorescein isothiocyanate (FITC) as fluorescent (FL) reporter to generate the bifunctional Au-templated siRNA particles targeting the GRP75 oncogene (**Figure 3.1**). This is in contrast to the commonly used alkylthio modifiers on DNA and RNA for Au surface immobilization studies.[47,48] Comparatively, this novel method involves the alkylamino linkers which are anticipated to provide the dual advantage of functionalization with a biological probe on the S1 strand and using the A1 strand for assembly onto the Au surface to generate the purported bifunctional Au-RNA particles (**Figure 3.1B**). The sequence composition of the dsRNAs encompassed the target sequences for the siRNAs

silencing GRP75 expression in PCa (PC-3) cells (**Figure 3.1A**).[44-46] The formulation will then be characterized by a combination of UV-Vis and fluorescence spectroscopy which will provide insights into the photophysical properties, specifically related to the fluorescence excitation/emission profiles for Au (λ_{exc}: 350 nm, λ_{em}: 650 nm) and FITC (λ_{exc}: 494 nm, λ_{em}: 522 nm). In collaboration with Drs. Uri Samuni and Jorge Ramos at Queen's College, City University of New York, the relative sizes, shapes, uniformities, and charge distributions of the Au-siRNA particles will be determined by a combination of dynamic light scattering (DLS) and transmission electron microscopy (TEM). Small particles, uniform, and of neutral charge are anticipated to be amenable to cell biology applications. In collaboration with Drs. Christopher Cultrara and Jenny Zilberberg at the Center for Discovery and Innovation, Hackensack-Meridian Health, the cell-uptake, GRP75 KD, and cell death effects in PC-3 prostate cancer cells will be evaluated. This thesis chapter thus describes our published collaborative work, highlighting the formulation, characterization, and biological evaluation of GRP75 silencing Au-siRNA formulations for anti-cancer applications.[49]

Texts and figures described in this thesis chapter have been adapted with permission from our publication Shah, S.S.; Cultrara, C.N.; Ramos, J.A.; Samuni, U.; Zilberberg, J.; Sabatino, D. *J Mater Chem B*. **2020,** *8(10),* 2169-2176.[49]

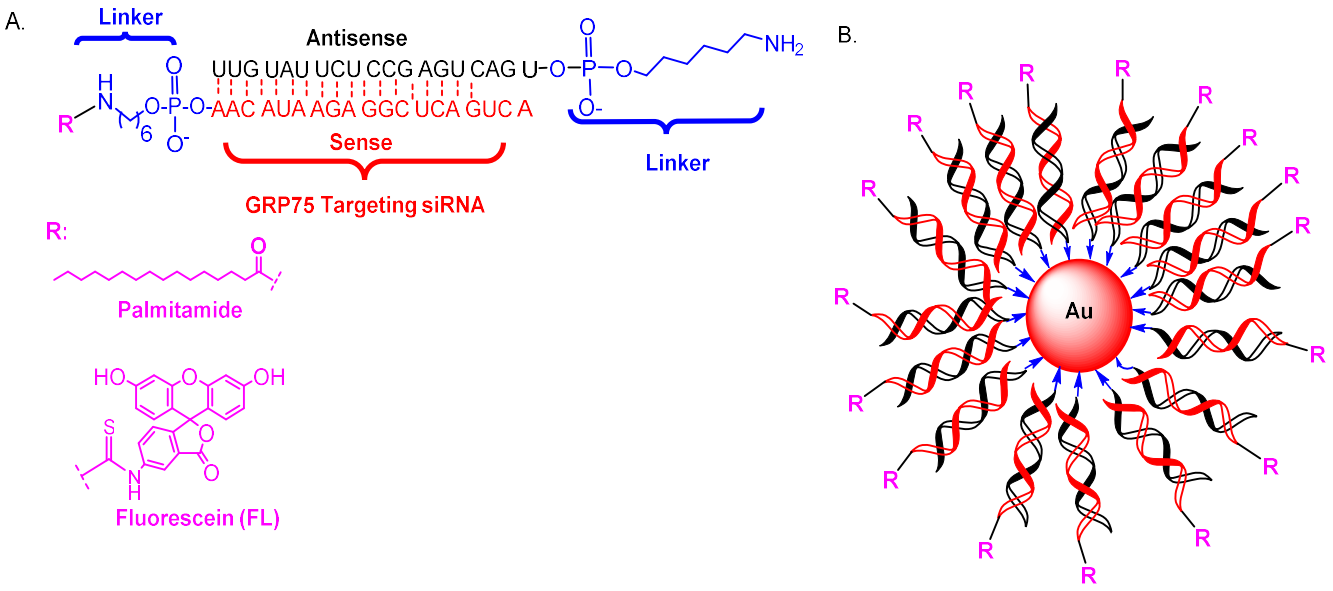

Figure 3.1. Rational design of (A) GRP75 targeting siRNA bioconjugates and (B) bifunctional Au-templated RNA particles. Figure reproduced with the permission from: Shah, S.S.; Cultrara, C.N.; Ramos, J.A.; Samuni, U.; Zilberberg, J.; Sabatino, D. *J Mater Chem B*. **2020,** *8(10),* 2169-217.[49]

3.4 Results and Discussion

3.4.1. Synthesis of Bifunctional Au-templated RNA particles

The rational design and synthesis of self-assembled Au-RNA nanoparticles were based on templating linear RNA sequences functionalized with a reactive hexamethylene amino linker at the 5'-termini of the antisense (A1) or sense (S1) single strands onto the Au surface under reducing conditions. This was followed by self-assembly with the complementary strands to generate the GRP75 targeting siRNA-Au particle formulation. Furthermore, adopting our previously reported bioconjugation strategies,[45,46] the S1 strands were conjugated with either

palmitic acid (C16) or fluorescein isothiocyanate (FITC). The biological probes were used respectively for facilitating cell uptake and tracking biological activity in cells. Following synthesis of the functionalized RNA strands, the samples were cleaved, deprotected from the solid support, and purified by RP IP HPLC with purities >90% for the generation of the bifunctional Au-RNA particles.

The formulation strategy for the bifunctional Au-RNA particles is based on a newly developed bottom-up approach, in which the 5'amino-functionalized A1 RNA single strands were expected to facilitate in-situ nucleation and growth of Au-RNA nanoparticles using mild reducing conditions (citric acid) in RNA annealing buffer (10 mM Tris, 50 mM NaCl, 1 mM EDTA, pH: 7.1). More specifically, this novel formulation approach required reduction of gold salts (hydrogen tetrachloroaurate (III) trihydrate, $HAuCl_4.3H_2O$, 0.01 M), with a mild reducing agent (trisodium citrate trihydrate, $Na_3C_6H_5O_7.3H_2O$, 0.1%) along with hybridization of equimolar concentrations (1.25 μM) of the complementary RNA strands (A1+S1) in RNA annealing buffer. This multi-component one-pot reaction was heated at 95 °C for 5 minutes followed by slow cooling to room temperature (22 °C) and overnight storage in the fridge (4 °C) before sample analysis (**Scheme 3.1**). In this manner, the Au-RNA formulation was anticipated to consist of a core of metallic (Au) nanoparticles decorated with surface functionalized GRP75-targeting siRNAs bearing a palmitamide or FITC group for cell biology.

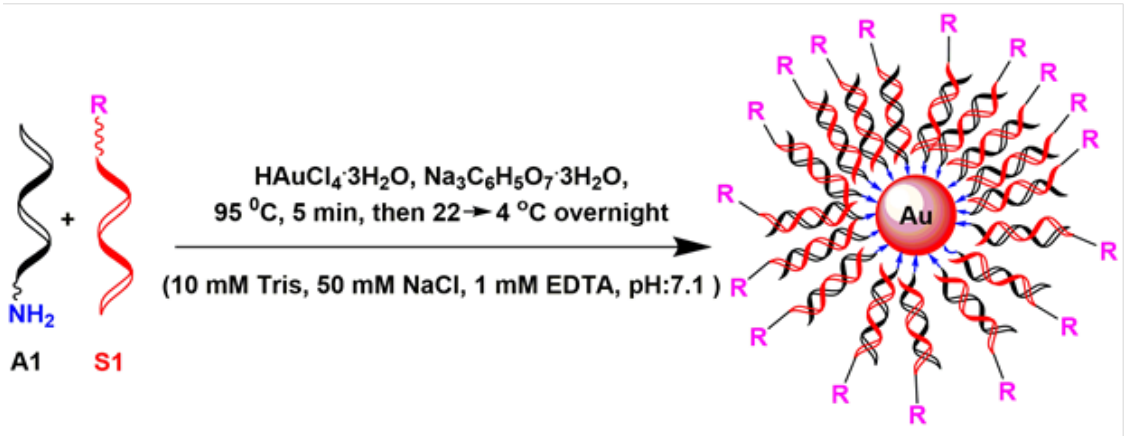

Scheme 3.1. Formulation strategy for the generation of bifunctional Au-RNA particles. Scheme reproduced with the permission from: Shah, S.S.; Cultrara, C.N.; Ramos, J.A.; Samuni, U.; Zilberberg, J.; Sabatino, D. *J Mater Chem B*. **2020,** *8(10),* 2169-217.[49]

3.4.2. Characterization of bifunctional Au-RNA particles

The physicochemical properties of the bifunctional Au-RNA particles were assessed by UV-Vis spectroscopy, to determine the characteristic absorption profiles of the RNA (λ_{max}: ~260 nm) and metallic (Au) (λ_{max}: ~530 nm) components (**Figure 3.2A**). A characteristic color change from a clear, transparent solution to a deep red color was initially observed and attributed to the reduction of the Au salts (HAuCl4; λ_{max}: ~302 nm) and the appearance of the characteristic surface plasmon absorption band of Au nanoparticles (λ_{max}: ~530 nm).[47] These characteristic absorption bands provide supportive evidence for the formation of stable Au-RNA particles, without any observable sample precipitation for weeks at 4 °C. However, further characterization using UV-Vis spectroscopy and DLS will be required to confirm sample stability. Interestingly, conjugated dsRNA bearing palmitamide (C16) or FL (FITC) labels on the S1 strands produced stable bifunctional Au-RNA particles, validating the reactivity of the free 5'-alkylamino termini from the complementary A1 strands for nucleation and growth of the Au-RNA particles, while

the complementary S1 strands provide further functionalization with bio-active probes. This is in contrast to the commonly used alkylthio modifiers on DNA and RNA for Au surface functionalization, which is prone to cross-linking under oxidative conditions due to its highly reactive nature, and may thus restrict the extent of functionalization of bio-active probes on the Au surface.[48] Alternatively, our new method of using the alkylamino linkers on the A1 or S1 strands offers the dual advantage of conjugation with a biological probe on the S1 strand and functionalizing the A1 strand onto the Au surface to generate the putative bifunctional Au-RNA particles.

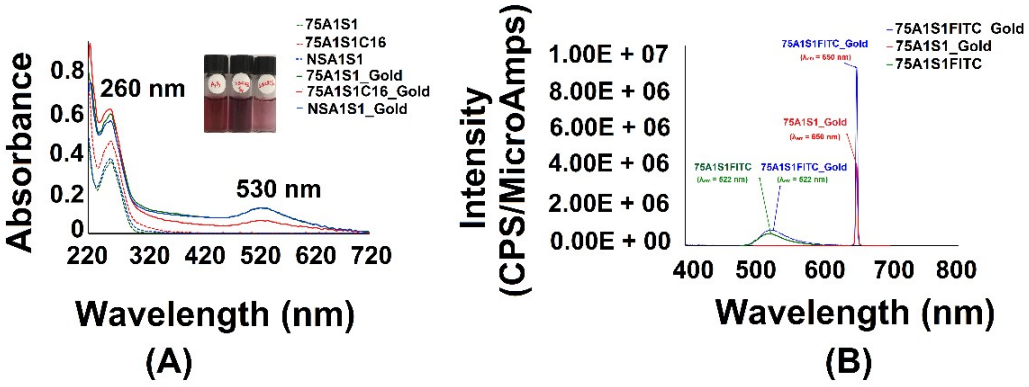

Figure 3.2. A) UV-Vis and B) Fluorescence spectra of Au-RNA particle formulations along with their dsRNA hybrid controls (75A1S1, NSA1S1). The inset provides a depiction of sample color changes (clear-to-deep red) without noticeable precipitation which is indicative of stable Au-RNA particles. C16 refers to palmitamide conjugation, 75 refers to GRP75 silencing siRNA, A1, S1 refers to the antisense, and sense dsRNA strands, NS refers to the non-specific dsRNA control. FITC (FL) or C16 (palmitamide) conjugation of the sense (S1) strand. Figure reproduced with the permission from: Shah, S.S.; Cultrara, C.N.; Ramos, J.A.; Samuni, U.; Zilberberg, J.; Sabatino, D. *J Mater Chem B*. **2020,** *8(10),* 2169-217.[49]

Fluorescence emission spectroscopy was also performed to evaluate the fluorescence emission intensities of the Au-RNA particles (**Figure 3.2B**). The fluorescence emission properties of the Au-RNA particles were determined with and without the fluorescein (FITC)

probe. Au-RNA particles required UV excitation (λ_{ex}: ~350 nm) in order to provide an emission (λ_{em}: ~650 nm) in the red region of the visible spectrum. Meanwhile, the FITC-labeled Au-RNA particles displayed characteristic excitation (λ_{ex}: ~495 nm) and emission (λ_{em}: 522 nm) bands for the (FITC) fluorophore, which were observed well into the visible region of the electromagnetic spectrum. The latter is a desirable property for cell biology studies which avoids the use of UV lasers that may be detrimental to cell viability. Therefore, the bifunctional FITC-labeled Au-RNA particles were selected to determine cell uptake within PC-3 prostate cancer (PCa) cells.

Prior to biological studies, DLS and TEM were used to determine the sizes, shapes and surface charge densities (zeta-potential) of the Au-RNA particles. Previous studies have shown that large, polyanionic aggregates of RNA particles abrogated their cell uptake and biological activity.[28,50] Therefore, DLS and TEM were conducted in order to determine whether the Au-RNA particles formed small, discrete, and neutrally charged nanoparticles that may facilitate cell uptake for biological activity in the absence of a transfection reagent. According to the DLS data, the linear RNA hybrid controls (75A1S1, NSA1S1, and 75A1S1C16) were prone to aggregation, producing particles of hydrodynamic diameters ranging from ~480-1200 nm (**Figure 3.3**, D-F and **Table 3.1**). These samples showed only slightly negative zeta potential values (-0.6 to -2.5 mV) which suggests a strong tendency to aggregate as confirmed by the observed size distribution data (**Table 3.1**). In general, the larger the value of the absolute magnitude of the zeta potential (regardless of if positive or negative), the more stable the particles in the solution. These samples also showed modest polydispersity indices (0.5-0.6) suggesting a large distribution of sizes, typical of particles that tend to aggregate (**Table 3.1**). In comparison, the Au-RNA particles showed a primary population of small size hydrodynamic diameters, ~24-30 nm (**Figure 3.3**, A-C, and Table 3.1). The Au-RNA particles also showed negative zeta

potentials of larger absolute values (-12 to -17 mV) and lower polydispersity indices (0.37-0.51) when compared to the RNA controls (**Table 3.1**). These results respectively suggest particles with higher stability in solution and narrow size distributions that may render them applicable to cell biology applications.

Table 3.1. DLS data for RNA hybrids with and without gold nanoparticles.[a]

Samples	Effective Particle Size (nm)	Polydispersity Index	Zeta Potential
75A1S1	674 ± 146	0.55 ± 0.11	-1.1 ± 0.58
NSA1S1	1186 ± 77	0.58 ± 0.03	-0.6 ± 0.58
75A1S1C16	484 ± 50	0.63 ± 0.10	-2.5 ± 1.40
75A1S1_Gold	24 ± 2	0.37 ± 0.09	-17.6 ± 1.7
NSA1S1_Gold	19 ± 2	0.51 ± 0.06	-12.6 ± 1.2
75A1S1C16_Gold	102 ± 66	0.41 ± 0.07	-17.1± 1.65

[a]Table reproduced with the permission from: Shah, S.S.; Cultrara, C.N.; Ramos, J.A.; Samuni, U.; Zilberberg, J.; Sabatino, D. *J Mater Chem B*. **2020,** *8(10),* 2169-217.[49]

The TEM images were consistent with the DLS data and provided further insight into particle sizes, morphology, and extent of aggregation for the linear RNA hybrid controls (75A1S1, NSA1S1, and 75A1S1C16) and the corresponding Au-RNA (75A1S1_Gold, NSA1S1_Gold, and 75A1SC16_Gold) particles. Most notably, the Au-RNA samples were found to be 10-20-fold smaller when compared to the RNA hybrid controls. For example, the Au-RNA (**Figure 3.3**, A-C) samples formed small, spherical nanoparticles (~15-44 nm) whereas the linear RNA hybrid controls (**Figure 3.3**, D-F) produced larger, non-uniform, polydisperse aggregates (~1-2 μm). Interestingly, incorporation of the palmitamide (C16) group resulted in larger

particles in the control RNA hybrid (**Figure 3.3**, F) when compared to the Au-RNA particles (**Figure 3.**3, C). It can be rationalized that in the absence of the Au nanoparticles, palmitamide provided an increase in RNA amphiphilicity which enhanced sample sizes (~124-1861 nm) and the potential for aggregation in aqueous media.[46] However, the Au-RNA nanoparticle formulation effectively served to restrict size, shape, while maintaining high surface zeta potentials which minimizes aggregation, making the nanoparticles applicable to cell uptake and downstream cell biology studies.

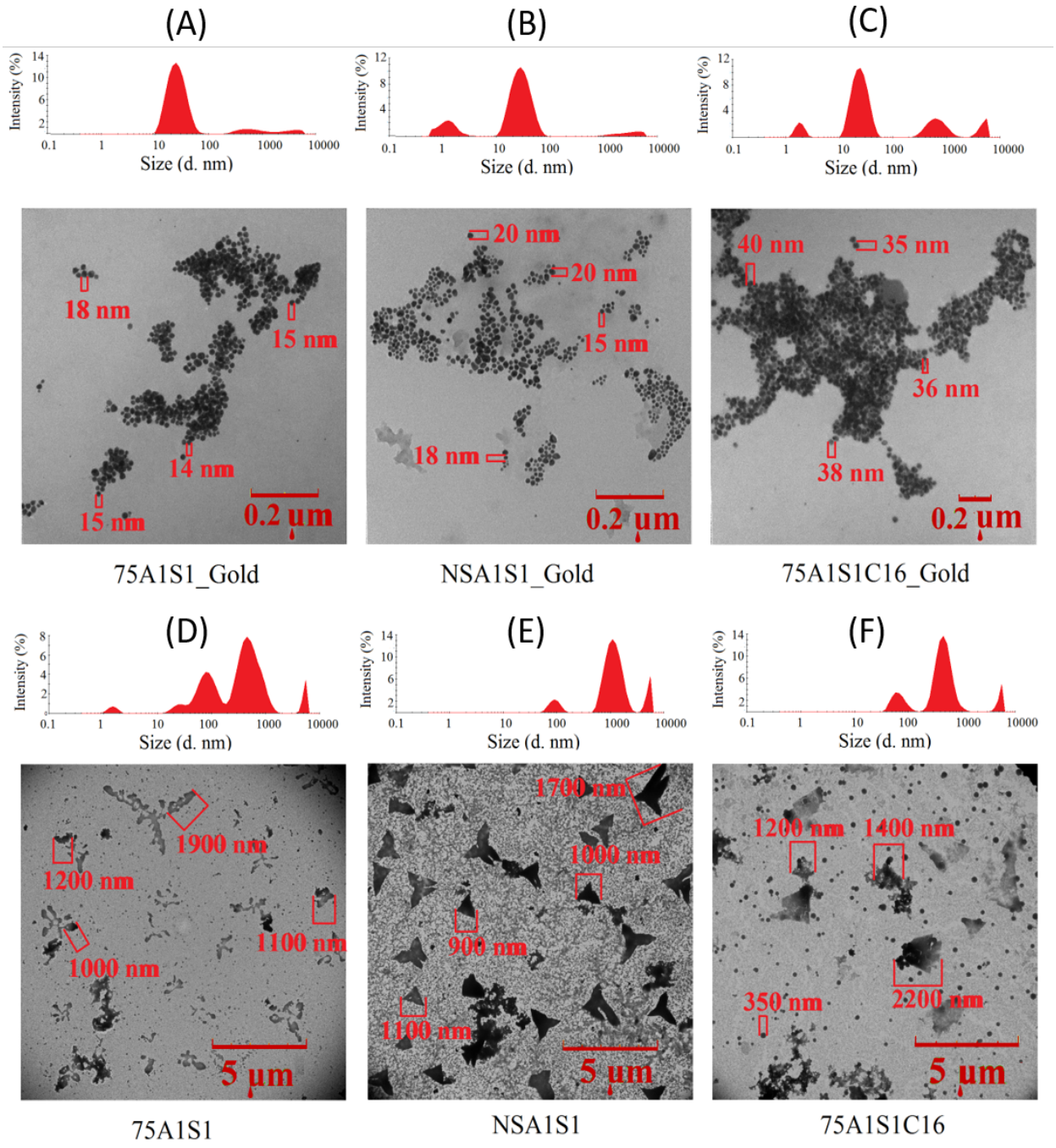

Figure 3.3. Representative TEM images (grayscale pictures) and corresponding DLS derived size distributions (red histograms) of Au-RNA hybrids (A) 75A1S1_Gold, (B) NSA1S1_Gold and (C) 75A1S1C16_Gold, and corresponding RNA hybrid controls (D-F) respectively. Figure reproduced with the permission from: Shah, S.S.; Cultrara, C.N.; Ramos, J.A.; Samuni, U.; Zilberberg, J.; Sabatino, D. *J Mater Chem B*. **2020,** *8(10),* 2169-217.[49]

3.4.3. Biological Activity of Au-RNA Nanoparticles

Following evaluation of chemical and physical properties, the biological activity of the Au-RNA nanoparticles was evaluated in a metastatic prostate (PC-3) cancer cell line. Initially, cell uptake experiments were conducted to establish the cell delivery potential of the Au-RNA nanoparticles with and without the commercial Trans-IT X2® dynamic delivery system functioning as a suitable RNA transfection reagent in suspension and adherent cancer cell lines.[51] Cell Insight CX5 high content screening microscopy (Thermo Fisher Scientific) was used to compare and visualize the time-dependent (2-30 h) cell uptake of the bifunctional FITC-labeled Au-RNA nanoparticle formulation in the absence of a transfection reagent (**Figure 3.4,** A). Significantly, an increase in fluorescence (FITC) signaling was observed as a function of time, which exceeded the signal detected by the control non-functionalized gold nanoparticles and the FITC-labeled RNA transfected with the commercial Trans-IT X2® dynamic delivery system (**Figure 3.5**). Thus, the FITC-labeled Au-RNA nanoparticle formulation was found to be amenable to direct PC-3 cell transfection, in the absence of an additional delivery system. Cell uptake was also detected in the absence of the C16 (palmitamide) group, which according to a previous study was incapable of achieving efficient RNA cell uptake for biological activity, presumably due to the large aggregated structures observed.[46] Moreover, it was also hypothesized that the enhanced fluorescence emission observed from the direct transfection of the FITC-labeled Au-RNA nanoparticles may be attributed to the intracellular separation and release of the FITC-labeled S1 strand from the Au-RNA nanoparticle formulation.

In order to provide supporting evidence into the increase in fluorescence emission signal from the bifunctional FITC-labeled Au-RNA nanoparticles, time-dependent FITC absorption and fluorescence emission assays were performed on a SPARK multimode microplate reader at 37

°C for 24 h (Figure 3.4, B). Increases in sample absorption (λabs: 495 and 530 nm) and fluorescence emission (λem: ~525 nm) as a function of time (2-24 h) were detected under physiological conditions (10 mM Tris, pH 7.5-8.0, 50 mM NaCl, 1 mM EDTA, pH 7.1) which served to mimic sample conditions for the cell uptake experiments. The two observable absorption bands once again served to support the presence of the bifunctional FITC-labeled Au-RNA formulation, with characteristic absorption bands for FITC (λabs: 495 nm) and the surface plasmon band (λabs: 530 nm) for the metallic (Au) component. Comparatively, the FITC-labeled RNA samples absent of the Au component also produced strong increases in fluorophore absorption and emission into the visible (green) region. Taken together, the bifunctional FITC-labeled Au-RNA nanoparticles effectively serve as time-dependent molecular beacons, emitting enhanced signal detection with time under physiological conditions that are applicable to cell biology. This phenomenon is critically important to enhanced sample detection in cancer cells that may lead to early-stage diagnosis and/or preventative treatment regimens.

The RNAi activity of Au-siRNA nanoparticles (75A1S1_Gold, NSA1S1_Gold, and 75A1S1C16_Gold) along with the unfunctionalized siRNA controls (75A1S1, NSA1S1, and 75A1S1C16) targeting GRP75 was next evaluated in the PC-3 cells. The siRNA controls were transfected with the Trans-IT X2® dynamic delivery system while the Au-siRNA nanoparticles were transfected directly and without the use of any transfection reagent. The knockdown efficiency was monitored by western blot at 72 h post-transfection. Downregulation of GRP75 protein expression levels (**Figure 3.4**, C) was observed to a comparable extent for the control siRNA sample (75A1S1_TX2) as well as the Au-siRNA nanoparticle formulation (75A1S1_Gold), validating its utility in downstream biological assays. Moreover, a serum stability assay (10 % FBS) proved the Au-siRNA formulation to be stable in serum for at least 24

h (**Figure 3.4**, D), whereas the control, naked siRNAs, even with the C16 palmitamide group proved to be much more susceptible to nuclease degradation, even after a much shorter incubation period (2 h).

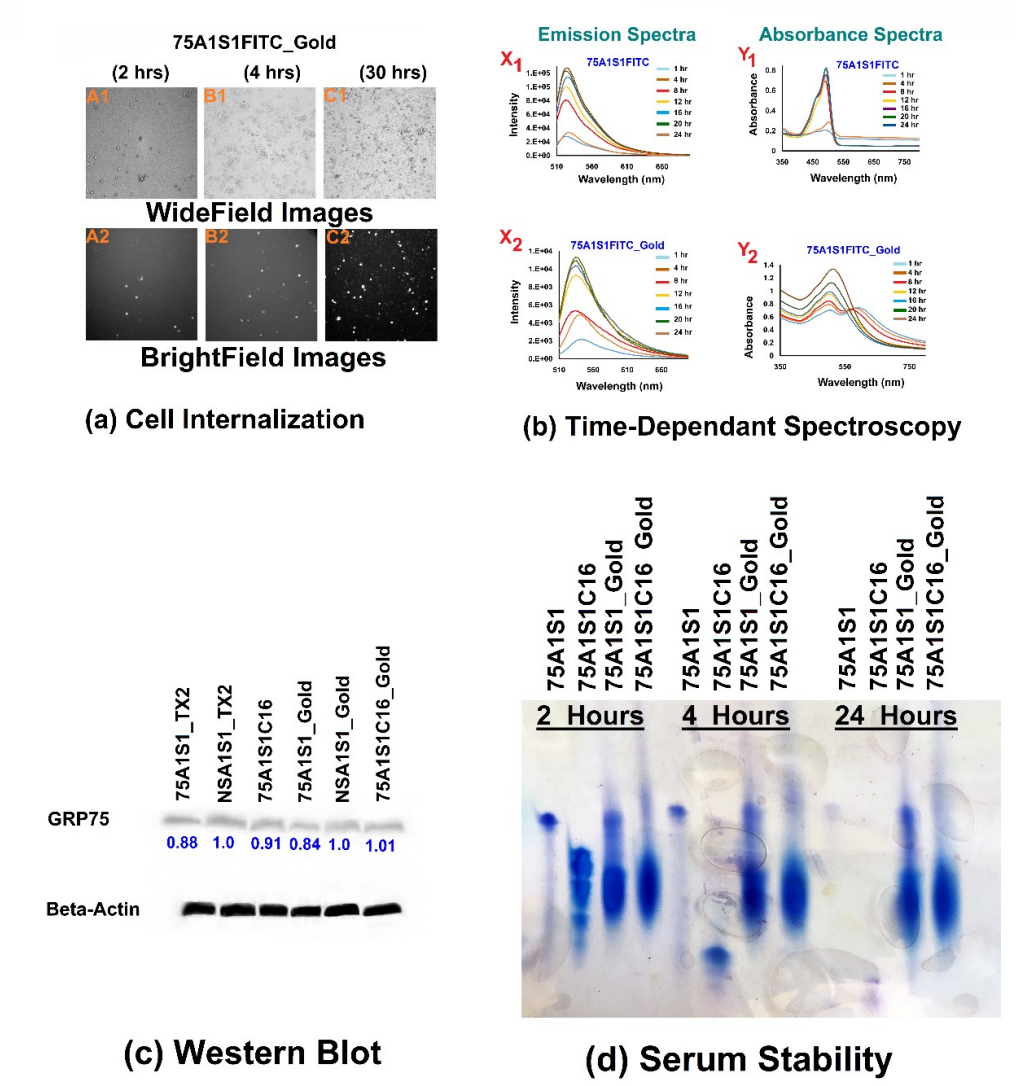

Figure 3.4. Biological activity of Au-siRNA nanoparticles. (a) Time-dependent (2-30 h) direct PC-3 cell uptake detection of bifunctional FITC-labeled Au-siRNA nanoparticles. Images were captured at 10X magnification. (b). Time-dependent (1-24 h) FITC (FL) fluorescence emission detection (λ_{max}: 522 nm) of (X1) FITC-labeled siRNA; (X2) FITC-labeled Au-siRNA and Time-dependent (1-24 h) FITC absorption detection (λ_{max}: 495-500 nm) of (Y1) FITC-labeled siRNA; and Au absorption detection (λ_{max}: 530 nm) (Y2) FITC-labeled Au-siRNA at 37 °C, (c). Western blot of GRP75 knockdown in PC-3 cells, and (d). Serum stability (10% FBS) of linear, control siRNA (75A1S1), C16 palmitamide conjugated siRNA (75A1S1C16), Au-siRNA (75A1S1_Gold), and palmitamide conjugated Au-siRNA (75A1S1C16_Gold) nanoparticles.

C16 refers to palmitamide conjugation, 75 refers to GRP75 silencing siRNA, A1, S1 refers to the antisense, and sense dsRNA strands, NS refers to the non-specific dsRNA control. FITC (FL) or C16 (palmitamide) conjugation of the sense (S1) strand. Figure reproduced with the permission from: Shah, S.S.; Cultrara, C.N.; Ramos, J.A.; Samuni, U.; Zilberberg, J.; Sabatino, D. *J Mater Chem B*. **2020,** *8(10),* 2169-217.[49]

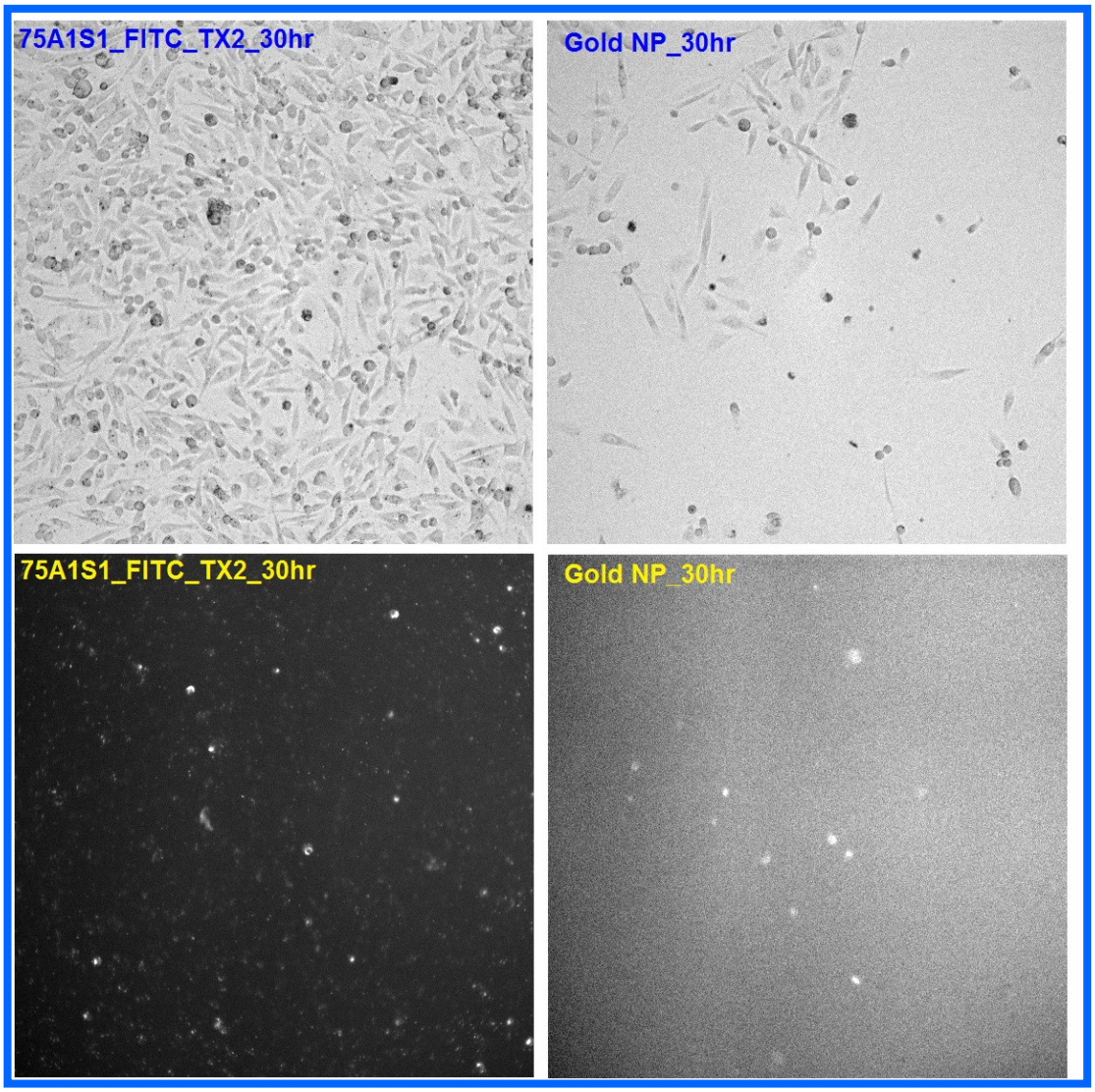

Figure 3.5. High content screen microscopy images for PC-3 cell uptake by FITC-tagged RNA hybrids and citrate-stabilized gold nanoparticles at 30 h with the Trans-IT X2® dynamic delivery system. Figure reproduced with the permission from: Shah, S.S.; Cultrara, C.N.; Ramos, J.A.; Samuni, U.; Zilberberg, J.; Sabatino, D. *J Mater Chem B*. **2020,** *8(10),* 2169-217.[49]

A cell viability stain using Annexin/PI confirmed the toxicity of the Au-siRNA formulation, providing a significant increase (40-50%) in early and late-stage apoptosis relative to the control conditions (30-35%), in which siRNA was transfected with the commercial Trans-IT X2 dynamic delivery system (**Figure 3.6**). Thus, this novel Au-siRNA formulation may enable a theranostic approach in the early detection and treatment in PCa and related solid tumors.

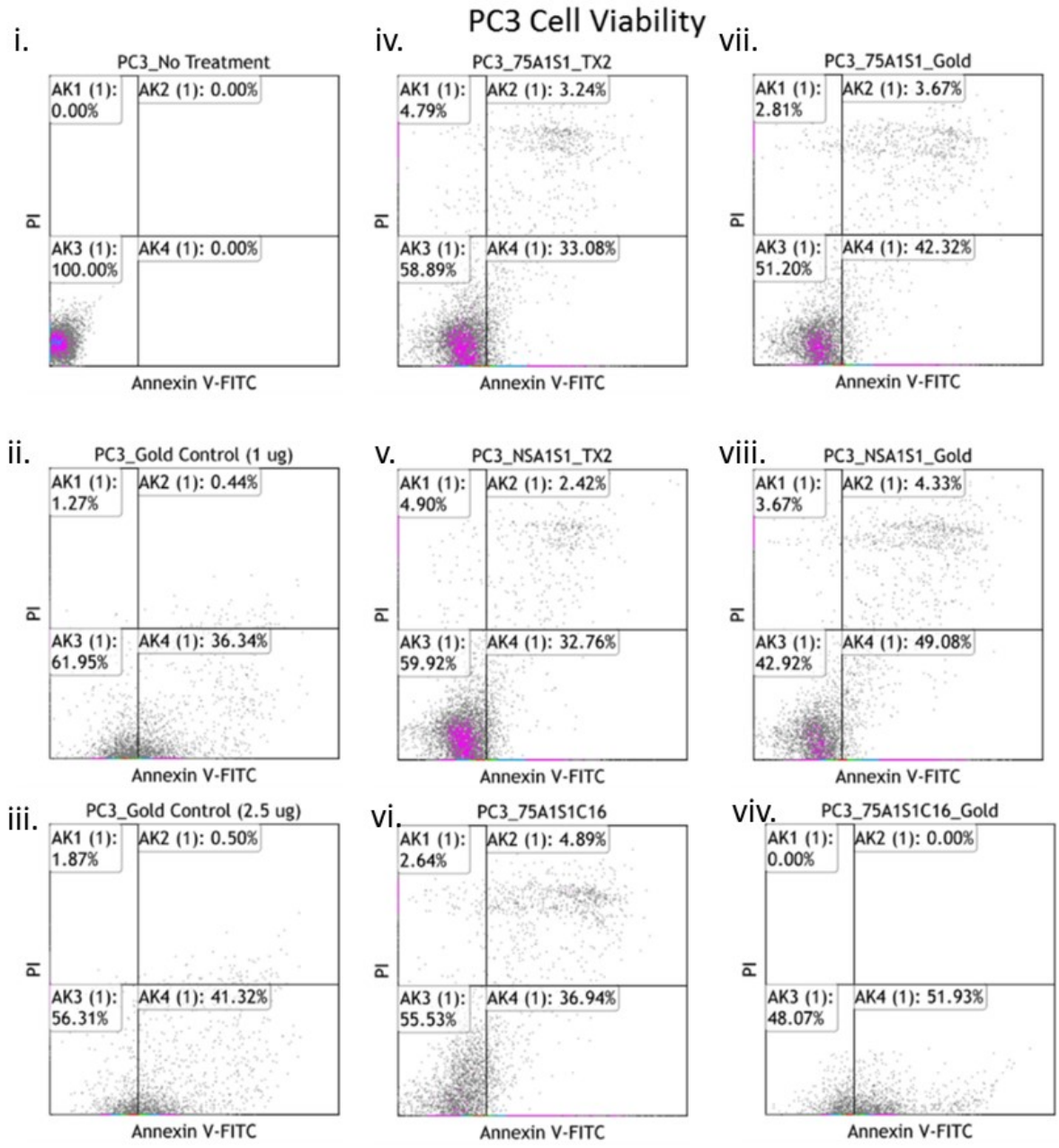

Figure 3.6. Flow cytometry data for PC-3 cell viability using Annexin V-PI stain. Detection of live cells (Annexin V^-, $7AAD^-$), early (Annexin V^+, $7AAD^-$) and late (Annexin V^+, $7AAD^+$) stage apoptosis, and necrosis (Annexin V^-, $7AAD^+$). Quadrants indicate cell viability as the following: AK3 (1) healthy cells; AK1 (1) cells undergoing early apoptosis; AK2 (1) cells undergoing late apoptosis and AK4 (1) necrotic cells. PC-3 cells treated with i. no treatment, Au nanoparticles at 1 µg (ii.) and 2.5 µg (iii.) iv. GRP75 siRNA + Trans-IT X2 dynamic delivery system, v. non-specific siRNA control + Trans-IT X2 dynamic delivery, vi. GRP75 C16-siRNA, vii. GRP75 siRNA-Au, viii., non-specific siRNA-Au, and viv. GRP75 C16-siRNA-Au nanoparticles. Figure reproduced with the permission from: Shah, S.S.; Cultrara, C.N.; Ramos, J.A.; Samuni, U.; Zilberberg, J.; Sabatino, D. *J Mater Chem B*. **2020,** *8(10),* 2169-217.[49]

3.5 Conclusions

This thesis chapter describes the synthesis, characterization, and biological evaluation of a new class of bifunctional Au-RNA nanoparticles. A newly developed, simple, bottom-up approach using alkylamino modified RNAs produced stable and small Au-RNA nanoparticle formulations bearing either a fluorescent reporter or a fatty acid group to track cell uptake in PC-3 PCa cells. Significantly, the bifunctional FL-labelled Au-siRNA nanoparticles absent of a C16 palmitamide delivery vector or an external commercial transfection reagent enabled direct cell uptake in PC-3 cells, which led to concomitant GRP75 knockdown and cell death. Consequently, this novel Au-RNA theranostic approach may significantly enable early detection and treatment in PCa and related solid tumors. Our on-going and future work are aimed at incorporating cell-targeting ligands within the Au-siRNA nanoparticle formulation to effect specific cancer detection and treatment in cell cultures and within tumor-bearing mice models.

3.6 Experimental Section

3.6.1. Materials and Method

Chemical synthesis reagents and solvents were obtained from ChemGenes, Aldrich, and VWR and used as received. Solid-phase RNA synthesis reagents were obtained from ChemGenes or Glen Research Inc. and used without further purification. Citrate stabilized Au nanoparticles (~20 nm) used as controls were obtained as a gift sample from BBI Solutions, Cardiff, UK. Materials for cell biology were obtained from Thermo Fisher Scientific, Cell Signaling, Bio-legend, Mirus, and Invitrogen Life Technologies and used as received according to the manufacturer's protocols.

3.6.2 Solid phase RNA Synthesis

Synthesis of alkyl (C6) amino linker GRP75 antisense RNA (5'-UUG UAU UCU CCG AGU CAG U-3'), sense RNA (5'-ACU GAC UCG GAG AAU ACU A-3'), and alkylamino linked nonspecific antisense RNA (5'-AGU UCA ACG AGU AUC AGA A-3') and sense RNA (5'- UGC UGA UAC UCG UUG AAC U-3') were performed on a 2000 Å UnyLinker controlled pore glass (CPG) support (ChemGenes) using a 1.0 μmol scale automated synthesis cycle on an ABI 3400 DNA synthesizer. All phosphoramidites were dissolved in anhydrous MeCN yielding 0.15 M solutions. The coupling times were 300 s using 0.25 M 5-ethylthiotetrazole (ETT) in MeCN as an activator. The detritylation times were set to 120 s using a solution of 3% dichloroacetic acid in CH_2Cl_2 (DCM). Capping and oxidation steps were performed using a mixture of acetic anhydride/*N*-methyl imidazole in MeCN and a solution of 0.01 M iodine in Pyr/THF/H_2O respectively. Following synthesis, oligonucleotides were cleaved from the CPG and deprotected with NH_4OH: EtOH (3:1 v/v) for 12-16 h. at 55 °C. The crude oligonucleotides were evaporated to dryness and re-suspended in a mixture of 1:1.5 v/v DMSO: triethylamine trihydrofluoride (100 μL:150 μL, 250 μL) to complete the 2'-desilylation reaction at 65 °C for 120 min. The crude RNA was precipitated from the reaction mixture with 3.0 M NaOAc (25 μL, pH = 5.2) in n-BuOH (500 μL). Precipitation was completed in -80 °C freezer 30 min prior to centrifugation (12,000 rpm, 5 min) leaving the crude oligonucleotides as a solid white pellet. Crude oligonucleotides were evaporated to dryness and resuspended in autoclaved water (1.0 mL) and the yields were determined by UV absorbance measurements at 260 nm. Crude RNA was purified by reverse-phase-ion pair HPLC on a Waters 2695 Alliance system equipped with a symmetry RP-C_{18} reverse-phase column (4.6 x 250 mm, 5 μm particle size) and gradient elution method 20−90% eluent B (20% acetonitrile in 0.1 M triethylammonium acetate, TEAA) in

eluent A (0.1 M TEAA). The HPLC flow rate was set at 1.0 mL/min, with run times of 27 min and with absorbance detection at 260 nm using a Waters 2489 UV/visible detector. Retention times (min) and peak areas (% area) were integrated with Empower II software (Waters) and used to confirm RNA purities. RNA-bioconjugation was conducted as described previously[45,46] for the generation of palmitamide and FITC-conjugated GRP75 RNA.

3.6.3. Synthesis of Au-siRNA particles

Equimolar concentrations (1.25 μM) of alkyl amino-linked antisense RNA and complementary sense RNA functionalized with or without palmitamide or FITC were combined in annealing buffer (10 mM Tris, pH 7.5-8.0, 50 mM NaCl, 1 mM EDTA, pH 7.5-8) in a 1.5 mL screw-cap Eppendorf tube in the absence and presence of hydrogen tetrachloroaurate (III) trihydrate ($HAuCl_4 \cdot 3H_2O$, 0.01 M). The sample was vortexed briefly and trisodium citrate was then added as a mild reducing agent to the mixture which was incubated on a standard heat block at 95 ± 1 °C for 5 min. The samples were then allowed to slowly cool to room temperature (22 °C) before cooling at 4 °C for 24 h prior to sample analysis. In-situ nucleation and growth of Au nanoparticles were clearly observed by the formation of a red color solution due to the unique optical properties of Au nanoparticles.

3.6.4. UV-Vis Spectroscopy

Optical absorption spectra were acquired with a CARY 3E UV-Vis spectrophotometer. Absorption measurements were recorded between 210-310 nm for RNA samples, which were quantified according to the Beer-Lambert law. Similarly, the optical absorption spectra of Au-

RNA nanoparticles were acquired between 220-750 nm with a CARY 3E/nanodrop UV-Vis spectrophotometer.

3.6.5. Reverse Phase Ion Pairing High-Performance Liquid Chromatography (RP IP HPLC)

The crude RNA samples were analyzed by Reverse Phase Ion Pairing High-Performance Liquid Chromatography (RP IP HPLC) to determine crude purities. Briefly, HPLC analyses (~0.1 OD) and purifications (1 OD) were performed on a Waters 2695 Alliance Separations Module. Crude RNA templates were dissolved in autoclaved water (1.0 mL) and injected into a Waters symmetry RP C_{18} reverse-phase column (4.6 x 250 mm, 5.0 μm particle size) heated at 60 °C. HPLC analyses and purifications for RNA controls were conducted using a gradient of 20−90% eluent B (20 % acetonitrile in 0.1 M triethylammonium acetate, TEAA) in eluent A (0.1 M TEAA) with a flow rate of 1 mL/min, run time of 30 min and with absorbance detection at 260 nm using a Waters 2489 UV/Visible detector. Similarly, RP IP HPLC for fatty acid conjugated RNAs were conducted using a gradient of 7-70% eluent C (100% acetonitrile) in eluent A (0.1 M triethylammonium acetate), with a run time 40 min and sample detection at 260 nm. Retention times (min) and peak areas (% area) were integrated with Empower II software and used to confirm RNA purities >90% following sample purifications.

3.6.6. Dynamic Light Scattering (DLS)

A Malvern Zetasizer, Nano-ZS (Malvern Instruments, UK) employing a 173° scattering angle and a 4-mW incident He-Ne laser (633 nm) was used to measure the particle sizes (hydrodynamic diameter), size distributions, and zeta potentials of the control siRNA hybrids along with the Au-siRNA nanoparticles. Samples were measured in triplicates at 25 °C. All

samples were loaded into folded capillary cells (DTS 1070) equipped with electrodes on both sides to allow measurement of their zeta potentials and by extension, the stability and degree of aggregation. Particle suspensions with highly positive or highly negative zeta potentials are considered stable because the electrical repulsion between the particles tends to counter the van der Waals forces that would otherwise result in aggregation and precipitation.

3.6.7. Transmission Electron Microscopy (TEM)

TEM analyses of the linear control siRNA hybrids along with the Au-siRNA nanoparticles were performed with a JEOL 1200EX Transmission Electron Microscope (JEOL Ltd, Japan) at an accelerating voltage of 80 kV. A mixture of 1:1 volume ratio 1.0 % uranyl acetate and sample suspension were prepared and 10 μL of this solution was placed on a TEM carbon-film-coated copper grid of 300 mesh (Electron Microscopy Sciences Inc., Hatfield, PA). Each sample was allowed to sit for five minutes on the grid before wicking the excess liquid followed by storage for 12-24 h to allow the samples to dry. Images were taken with an SIA-L3C CCD camera (Scientific Instruments and Applications, Inc.) using the software Maxim DL5 (Diffraction Limited, Ottawa, Canada).

3.6.8. Serum Stability Assay

siRNA samples were hybridized and formulated as previously described in annealing buffer (30 μM, 10 mM Tris, 50 mM NaCl, 1 mM EDTA, pH 7.1, 50 μL). An aliquot (50 μL, 30 μM) was added to a 10% FBS solution (50 μL in phosphate buffer, pH 7.4). The mixtures were incubated at 37 °C and periodically (0-24 h) sample aliquots (15 μL) were removed and frozen at -80 ºC prior to analyses. Samples were thawed to room temperature (22 °C) and diluted with 30

% sucrose loading buffer and analyzed on a 24% denaturing PAGE for 2.5 h. The gel was then visualized with a Stains-All (Sigma-Aldrich™) solution.

3.6.9. Time-Dependent Absorption and Emission Assays

FITC-labeled siRNA samples with and without gold nanoparticles were hybridized and formulated as previously described in annealing buffer (5 μM, 10 mM Tris, 50 mM NaCl, 1 mM EDTA, pH 7.5–8.0, 75 μL) and allowed to slowly cool to room temperature (22 °C) before cooling at 4 °C for 24 h prior to sample analysis. The Spark multimode microplate reader equipped with Spark Control™ Excel software was used to study the time-dependent absorption and emission spectra at 37 °C. The FITC-labeled siRNA controls and FITC-labeled Au-siRNA samples (75 μL, 5 μM) were placed in low volume microplate reader incubated at 37 °C. Time-dependent absorption (350-800 nm) and emission (490-700 nm) scans were programmed and collected for 24 h. analyses.

3.6.10. Cell Culture

Prostate cancer cell line PC-3 (ATCC® CRL-1435™) was purchased from ATCC and cultured in RPMI-1640 complete growth medium supplemented with 10% (v/v) fetal bovine serum (FBS), 2.5 mM of L-glutamine, and 1% (v/v) penicillin/streptomycin (P/S) under 5% CO_2 at 37 °C in a humidified tissue culture incubator. Lower passages (between 6-12) were used for all experiments.

3.6.11. siRNA transfections, cell uptake, and viability in PC-3 cells

PC-3 cells were grown in 24-well culture plates in RPM-1640 complete growth media until 60-70 % confluence as per the 3.6.10 protocol. Prior to transfections, the nonspecific and control siRNA hybrids (2.5 μL, 10 μM, in Opti-MEM, 137.5 μL) were mixed with the transfection reagent (TransIT-X2® Dynamic Delivery System, 9 μL, in Opti-MEM, 250 μL) and kept at 37 °C for 15 minutes according to the manufacturer's recommendation. Both the linear siRNAs and nonspecific siRNA hybrids complexed with the commercial Tran-IT X2 transfection reagent in Opti-MEM was added to the cells at final concertation of 25 nM. RNA bioconjugates templated to Au such as the palmitamide or FITC-siRNA-Au samples were transfected directly, in the absence of an external transfection reagent, at a final concentration of 25 nM. The mixtures were incubated (15 min, 22 °C) then added to the PC-3 cell culture and incubated at 37 °C with 5% CO_2 over a three-day (72 h) period. To determine time-dependent cell uptake, FITC-labeled siRNA samples with and without Au nanoparticles were transfected with and without the commercial transfection reagent along with their respective controls. Cell-uptake was determined using a Cell Insight CX5 High Content Screening (HCS) Platform (Thermo Fisher Scientific). Cells were visualized for 2, 4, and 30 h post-transfection. Images were analyzed using Thermo Scientific HCS Studio Cell Analysis software. Similarly, cell viability was performed in a 24-well plate with PC-3 cells cultured in RPMI-1640 complete growth media and incubated with samples for 24 h at 37 °C. Briefly, after 24 h the supernatant was collected, and the remaining cells were removed using trypsin. Cell samples were pelleted and resuspended in 1% bovine serum albumin in phosphate-buffered saline (1 mL) and stained using Annexin-PI according to the manufacturer's recommendation. Data was collected on an FC 500 flow cytometer (Beckman Coulter) and analyzed with Kaluza (Beckman Coulter) flow analysis software.

3.6.12. Western Blot

Total protein was isolated from the cell cultures following transfection (72 h). Protein lysates were prepared by lysing the cells in ice-cold RIPA buffer (G-Biosciences) supplemented with protease and phosphatase inhibitors (Millipore Sigma) which were diluted 1:10 v/v as per the manufacturer's recommendations. Cell debris was removed by centrifugation at 16,000g at 4 °C and protein concentrations were determined using a Pierce™ BCA kit (Thermo Fisher Scientific). A sample (20-35 mg) of the supernatant protein was mixed with LDS buffer and DTT, incubated at 70 °C for 10 min, and resolved on a 4-12% Bis-Tris PAGE gradient gel before being transferred to a PVDF membrane. Following the transfer, the membrane was blocked in 5% skim milk for 1 h, washed and incubated at 4 °C overnight with a rabbit 1° monoclonal antibody against human GRP75 and β-Actin (all purchased from Cell Signaling Technology) at a 1:1000 dilution. The membrane was subsequently washed and incubated with an anti-rabbit HRP-conjugated 2° Ab (Cell Signaling Technology) for 1 h at room temperature at 1:2000 dilution. The bands were visualized using a Signal Fire™ ECL reagent (Cell signaling Technology) on a Protein Simple Fluor Chem E imager.

3.7 References

1. Grabow, W.W.; Jaeger, L. RNA self-assembly and RNA nanotechnology. *Acc Chem Res*. **2014**, *47(6)*, 1871-1180.
2. Young, S.W.; Stenzel, M.; Yang, J.L. Nanoparticle-siRNA: A potential cancer therapy? *Crit Rev Oncol Hematol.* **2016,** *98,* 159-69.
3. Guo, P. The emerging field of RNA nanotechnology. *Nat. Nanotechnol*. **2010**, *5*, 833–842.
4. Shukla, C.; Haque, F.; Tor, Y.; Wilhelmsson, L.M.; Toulme, J.J.; Isambert, H.; Guo, P.; Rossi, J.J.; Tenenbaum, S.A.; Shapiro, B.A. A Boost for the Emerging Field of RNA Nanotechnology. *ACS Nano,* **2011**, *5*, 3405–3418.
5. Jiang, X.; Du, B.; Huang, Y.; Zheng, J. Ultrasmall noble metal nanoparticles: Breakthroughs and biomedical implications. *Nano Today*. **2018,** *21*, 106–125.

6. Luo, Z.; Zhang, K.; Xie, J. Engineering ultrasmall water-soluble gold and silver nanoclusters for biomedical applications. *Chem. Commun*. **2014,** *50(40)*, 5143–5155.
7. Goswami, N.; Zheng, K.; Xie, J. Bio-NCs-the marriage of ultrasmall metal nanoclusters with biomolecules. *Nanoscale*. **2014,** *6(22)*, 13328–13347.
8. Zheng, K.; Yuan, X.; Goswami, N.; Zhang, Q.; Xie, J. Recent advances in the synthesis, characterization, and biomedical applications of ultrasmall thiolated silver nanoclusters. *RSC Adv.* **2014,** *4*, 60581–60596.
9. Tao, Y.; Li, M.; Ren, J.; Qu, X. Metal nanoclusters: novel probes for diagnostic and therapeutic applications. *Chem. Soc. Rev*. **2015**, *44*, 8636–8663.
10. Song, X.R.; Goswami, N.; Yang, H.H.; Xie, J. Functionalization of metal nanoclusters for biomedical applications. *Analyst.* **2016,** *141(11)*, 3126–3140.
11. Shang, L.; Dong, S.; Nienhaus, G.U. Ultra-small fluorescent metal nanoclusters: Synthesis and biological applications. *Nano Today*. **2011,** *6(4)*, 401–418.
12. Jin, R.; Zeng, C.; Zhou, M.; Chen, Y. Atomically Precise Colloidal Metal Nanoclusters and Nanoparticles: Fundamentals and Opportunities. *Chem. Rev*. **2016**, *116(18)*, 10346–10413.
13. Kang, X.; Zhu, M. Tailoring the photoluminescence of atomically precise nanoclusters. *Chem. Soc. Rev*. **2019**, *48(8)*, 2422–2457.
14. Ding, Y.; Jiang, Z.; Saha, K.; Kim, C.S.; Kim, S.T.; Landis, R.F.; Rotello, V.M. Gold nanoparticles for nucleic acid delivery. *Mol. Ther.,* **2014**, *22(6)*, 1075–1083.
15. Medalia, O.; Heim, M.; Guckenberger, R.; Sperling, R.; Sperling, J. Gold-Tagged RNA—A Probe for Macromolecular Assemblies. *J. Struct. Biol.*, **1999,** *127(2)*, 113–119.
16. Tian, L.; Qian, K.; Qi, J.; Liu, Q.; Yao, C.; Song, W.; Wang, Y. Gold nanoparticles superlattices assembly for electrochemical biosensor detection of microRNA-21. *Biosens. Bioelectron.*, **2018**, *99*, 564–570.
17. Liang, R.Q.; Li, W.; Li, Y.; Tan, C.Y.; Li, J.X.; Jin, Y.X.; Ruan, K.C. An oligonucleotide microarray for microRNA expression analysis based on labeling RNA with quantum dot and nanogold probe. *Nucleic Acids Res*., **2005,** *33(2)*, e17.
18. Watanabe, K.; Ohtsuki, T. Photocontrolled Intracellular RNA Delivery Using Nanoparticles or Carrier-Photosensitizer Conjugates. *Prog. Mol. Biol. Transl. Sci.* **2016**, *139,* 101–119.
19. Matsushita-Ishiodori, Y.; Ohtsuki, T. Photoinduced RNA Interference. *Acc. Chem. Res.* **2012**, *45(7)*, 1039–1047.
20. Artiga, A.; Sevilla, I.S.; Matteis, L.D.; Mitchell, S.G.; DeLaFuente, J.M. Current status and future perspectives of gold nanoparticle vectors for siRNA delivery. *J. Mater. Chem. B,* **2019**, *7(6),* 876–896.
21. Guo, J.; O'Driscoll, C.M.; Holmes, J.D.; Rahme, K. Bioconjugated gold nanoparticles enhance cellular uptake: A proof of concept study for siRNA delivery in prostate cancer cells. *Int. J. Pharm.,* **2016**, *509(1-2)*, 16–27.
22. Rahme, K.; Guo, J.; Holmes, J.D. Bioconjugated Gold Nanoparticles Enhance siRNA Delivery in Prostate Cancer Cells. *Methods Mol. Biol*. **2019**, *1974*, 291–301.
23. Fitzgerald, K.A.; Rahme, K.; Guo, J.; Holmes, J.D.; O'Driscoll, C.M. Anisamide-targeted gold nanoparticles for siRNA delivery in prostate cancer – synthesis, physicochemical characterization and in vitro evaluation. *J. Mater. Chem. B,* **2016,** *4(13)*, 2242–2252.

24. Giljohann, D.A.; Seferos, D.D.; Prigodich, A.E.; Patel, P.C.; Mirkin, C.A. Gene Regulation with Polyvalent siRNA−Nanoparticle Conjugates. *J. Am. Chem. Soc.,* **2009**, *131*, 2072–2073.
25. Lee, S.H.; Bae, K.H.; Kim, S.H.; Lee, K.R.; Park, T.G. Amine-functionalized gold nanoparticles as non-cytotoxic and efficient intracellular siRNA delivery carriers. *Int. J. Pharm.,* **2008,** *364(1)*, 94–101.
26. Huschka, R.; Barhoumi, A.; Liu, Q.; Roth, J.A.; Ji, L.; Halas, N.J. Gene Silencing by Gold Nanoshell-Mediated Delivery and Laser-Triggered Release of Antisense Oligonucleotide and siRNA. *ACS Nano*, **2012**, *6(9)*, 7681–7691.
27. Jones, C.H.; Chen, C.K.; Ravikrishnan, A.; Rane, S.; Pfeifer, B.A. Overcoming Nonviral Gene Delivery Barriers: Perspective and Future. *Mol. Pharmaceutics*, **2013**, *10(11)*, 4082–4098.
28. Cultrara, C.N.; Shah, S.; Antuono, G.; Heller, C.J.; Ramos, J.A.; Samuni, U.; Zilberberg, J.; Sabatino, D. Size Matters: Arginine-Derived Peptides Targeting the PSMA Receptor Can Efficiently Complex but Not Transfect siRNA. *Mol. Ther. Nucleic Acids*. **2019**, *18*, 863–870.
29. Zhang, Y.; Satterlee, A.; Huang, L. In vivo gene delivery by nonviral vectors: overcoming hurdles? *Mol. Ther.* **2012**, *20(7)*, 1298–1304.
30. Lee, A.S. Glucose-regulated proteins in cancer: molecular mechanisms and therapeutic potential. *Nat. Rev. Cancer.*, **2014**, *14*, 263–276.
31. Mylonis, I.; Kourti, M.; Samiotaki, M.; Panayotou, G.; Simos, G. Mortalin-mediated and ERK-controlled targeting of HIF-1α to mitochondria confers resistance to apoptosis under hypoxia. *J. Cell Sci*., **2017**, *130(2),* 466–479.
32. Mazkereth, N.; Rocca, F.; Schubert, J.R.; Geisler, C.; Hillman, Y.; Enger, A.; Fishelson, Z. Complement triggers relocation of Mortalin/GRP75 from mitochondria to the plasma membrane. *Immunobiology*, **2016**, *221*, 1395–1406.
33. Kang, Q.; Zou, H.; Yang, X.; Cai, J.B.; Liu, L.X.; Xie, N.; Wang, L.M.; Li, Y.H.; Zhang, X.W. Characterization and prognostic significance of mortalin, Bcl-2 and Bax in intrahepatic cholangiocarcinoma. *Oncol. Lett***., 2018**, *15*, 2161–2168.
34. Cui, X.; Li, Z.; Piao, J.; Li, J.; Li, L.; Lin, Z.; Jin, A. Mortalin expression in pancreatic cancer and its clinical and prognostic significance. *Human Pathol***. 2017**, *64*, 171–178.
35. Sun, J.; Che, S.L.; Piao, J.J.; Xu, M.; Chen, L.Y.; Lin, Z.H. Mortalin overexpression predicts poor prognosis in early stage of non–small cell lung cancer. *Tumor Biol*. **2017**, *39(3)*, 1–9, 1010428317695918.
36. Yan, M.M.; Ni, J.D.; Song, D.; Dian, M.; Huang, J. Interplay between unfolded protein response and autophagy promotes tumor drug resistance. *Oncol. Lett.* **2015**, *10(4),* 1959-1969.
37. Wadhwa, R.; Takano, S.; Kaur, K.; Deocaris, C.C. Pereira-Smith, O.M.; Reddel, R.R. Kaul, S.C. Upregulation of mortalin/mthsp70/Grp75 contributes to human carcinogenesis. *Int. J. Cancer*, **2006**, *118(12)*, 2973–2980.
38. Starenki, D.; Hong, S.K.; Lioyd, R.C.; Park, J.I. Mortalin (GRP75/HSPA9) upregulation promotes survival and proliferation of medullary thyroid carcinoma cells. *Oncogene.* **2015**, *34(35),*4624-34.
39. Li, Q.; Li, Y.; Wang, Y.; Cui, Z.; Gong, L.; Qu, Z.; Zhong, Y.; Zhou, J.; Zhou, Y.; Gao, Y.; Li, Y. Quantitative proteomic study of human prostate cancer cells with different metastatic potentials. *Int. J. Oncol*., **2016**, *48(4)*, 1437-1446.

40. Wadhwa, R.; Sugihara, T.; Yoshida, A.; Nomura, H.; Reddel, R.R.; Simpson, R.; Maruta, H.; Kaul, S.C. Selective Toxicity of MKT-077 to Cancer Cells Is Mediated by Its Binding to the hsp70 Family Protein mot-2 and Reactivation of p53 Function. *Cancer Res*. **2000**, *60(24)*, 6818–6821.
41. Utomo, D.H.; Widodo, N.; Rifa'I, M. Identifications small molecules inhibitor of p53-mortalin complex for cancer drug using virtual screening. *Bioinformation*, **2012**, *8(9)*, 426-429.
42. Szabadkai, G.; Bianchi, K.; Varnai, P.; De Stefani, D.; Wieckowski, M.R.; Cavagna, D.; Nagy, A.I.; Balla, T.; Rizzuto, R. Chaperone-mediated coupling of endoplasmic reticulum and mitochondrial Ca^{2+} channels. *J. Cell Biol.,* **2006**, *175(6)*, 901–911.
43. Maina, A.; Blackman, B.A.; Parronchi, C.J.; Morozko, E.; Bender, M.E.; Blake, A.D.; Sabatino, D. Solid-phase synthesis, characterization and RNAi activity of branch and hyperbranch siRNAs. Bioorg Med Chem Lett**. 2013,** *23(19*), 5270-5274.
44. Patel, M.R.; Kozuch, S.D.; Cultrara, C.N.; Yadav, R.; Huang, S.; Samuni, U.; Koren, J., Chiosis, G.; Sabatino, D. RNAi Screening of the Glucose-Regulated Chaperones in Cancer with Self-Assembled siRNA Nanostructures. *Nano Lett.* **2016,** *16(10)*, 6099–6108
45. Kozuch, S.D.; Cultrara, C.N.; Beck, A.E.; Heller, C.J.; Shah, S.S.; Patel, M.R.; Zilberberg, J.; Sabatino, D. Enhanced Cancer Theranostic with Self-Assembled, Multilabeled siRNAs. *ACS Omega,* **2018,** *3,* 12975–12984.
46. Shah, S.S.; Cultrara, C.N.; Kozuch, S.D.; Patel, M.R.; Ramos, J.A.; Samuni, U.; Zilberberg, J.; Sabatino, D. Direct Transfection of Fatty Acid Conjugated siRNAs and Knockdown of the Glucose-Regulated Chaperones in Prostate Cancer Cells. *Bioconjugate Chem.,* **2018,** *29*, 3638–3648.
47. Haiss, W.; Thanh, N.T.K.; Aveyard, J.; Fernig, D.G. Determination of size and concentration of gold nanoparticles from UV-vis spectra. *Anal. Chem.,* **2007**, *79(11)*, 4215–4221.
48. Braun, G.B.; Pallaoro, A.; Wu, G.; Missirlis, D.; Zasadzinski, J.A.; Tirrell, M.; Reich, N.O. Laser-Activated Gene Silencing via Gold Nanoshell−siRNA Conjugates. *ACS Nano*, **2009**, *3(7)*, 2007-2015.
49. Shah, S.S.; Cultrara, C.N.; Ramos, J.A.; Samuni, U.; Zilberberg, J.; Sabatino, D. Bifunctional Au-templated RNA nanoparticles enable direct cell uptake detection and GRP75 knockdown in prostate cancer. *J. Mater.Chem. B,* **2020,** *8*, 2169-2176.
50. Zhang, S.; Li, J.; Lykotrafitis, G.; Bao, G.; Suresh, S. Size-Dependent Endocytosis of Nanoparticles. *Adv. Mater*., **2009**, *21(4)*, 419–424.
51. Cultrara, C.N.; Kozuch, S.D.; Ramasundaram, P.; Heller, C.J.; Shah, S.S.; Beck, A.E.; Zilberberg, J.; Sabatino, D. GRP78 modulates cell adhesion markers in prostate cancer and multiple myeloma cell lines. *BMC Cancer,* **2018**, *18*, 1–14.

Chapter 4: Conclusions, Contributions to Knowledge, and Future Work

4.1 Conclusions and Contributions to Knowledge Made in this Thesis

4.1.1 Investigating the role of siRNA bioconjugates and their nanoparticle formulations for improved biological activity

siRNA-based therapeutics have been developed over the course of the last two decades in precision medicine applications of difficult-to-treat diseases, including those that are genetically driven. The advancement of novel synthetic techniques has provided a diverse class of modified siRNAs with improved pharmacological properties resulting in more potent RNAi applications. However, their limited cell uptake has restricted their widespread therapeutic utility. To address these limitations, gene delivery systems have been engineered and optimized for siRNA delivery *in vitro* and *in vivo*. Among the more appealing are the non-viral based delivery methods that implicate bioconjugation strategies for the ligation of cell targeting/delivery vectors, polycationic/amphiphilic synthetic and biological polymers as well as biocompatible inorganic materials which enable siRNA functionalization or encapsulation for delivery applications.

In our contributions for improving the structure-function properties of siRNAs, the design and development of higher-ordered RNA templates that can self-assemble into multifunctional siRNA nanostructures have served to expand the scope of bioactive siRNA candidates while enhancing their therapeutic potential in cancer gene therapy applications. This is because the self-assembled siRNA nanostructures may be used to effectively screen and silence multiple oncogenes leading to a synergistic knockdown and therapeutic effects. In this manner, the higher-order siRNA nanostructures served as important tools in the knockdown of oncogenic Glucose Regulated Proteins (GRPs), in various cancerous cells leading to potent anti-cancer responses. Building upon this research work, the main research objectives of this thesis revolve

around improving the utility of synthetic siRNAs in cancer gene therapy by either bioconjugation and/or formulation into multifunctional nanoparticles applicable for direct transfection and RNAi activity. In this manner, the novel siRNA constructs disclosed in this thesis are based on higher-order siRNA bioconjugates bearing either fatty acids or fluorescein labels used for tracking cell uptake efficacy for RNAi activity in prostate cancer cells. Our contributions towards the development of a novel platform for functionalizing siRNAs onto Au surfaces were used for the generation of multifunctional Au-siRNA nanoparticles for theranostic (therapy+diagnostic) activity in prostate cancer cells. These contributions led to target-specific silencing of the GRPs, which impacted key roles in the development, progression, and spread of cancer. Thus, novel methods for the generation of higher-order siRNA motifs and their bioconjugation with functional probes may serve to improve cellular uptake for more potent RNAi activity in cancer gene therapy applications (**Figure 4.1**).

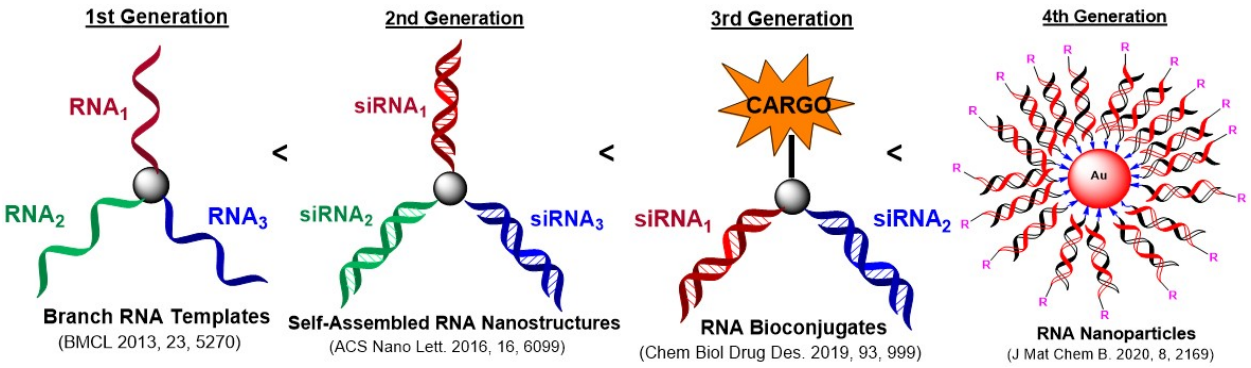

Figure 4.1. Next-generation siRNA motifs for cancer gene therapy applications. Figure Drawn using Chemdraw version 19.1 software.

4.1.2 Development of Higher Order siRNA Hybrids and their Bioconjugates for RNAi Activity in Cancer

Chapter 2 discussed our specific efforts on the development of an effective technique for the cellular delivery of our higher-order siRNA structures, including those adopting V-, and Y-shape siRNA for knockdown of GPRs, upregulated in various cancers. More specifically, in this chapter, a bioconjugation approach was developed for the incorporation of a series of saturated and unsaturated fatty acids within linear, V- and Y-shape siRNAs to improve cellular uptake and knockdown efficacy of the oncogenic GRPs in a model prostate cancer (PC-3) cell line **(Figure 4.2)**. These fatty-acid conjugated siRNA motifs provided valuable insights into the requisite amphiphilicity for cell uptake activity. The solid-phase RNA bio-conjugation approach reported in this study provided an important entry point for the incorporation of various hydrophobic and amphiphilic functional groups onto higher-order, multifunctional siRNA constructs, A small set of linear saturated and unsaturated fatty acids (C12 to C18 carbon chain lengths) was successfully conjugated to the RNA templates with both antisense and sense sequences. The amphiphilic siRNA-fatty acid motifs incorporating a fluorescent (FITC) label for tracking cell uptake indicated initial (6 h) transfection with little observed cellular siRNA left following 24 h incubation. The modest cell uptake effects translated into a moderate GRP knockdown (~30-40%) within PC-3 cells, albeit without the use of a commercial transfection reagent (**Figure 2.7**). To better understand the observed moderate cell uptake and GRP knockdown effects of the fatty acid labeled siRNAs, structural characterization by DLS and TEM revealed very large, aggregated particles (**Figure 2.6 and Table 2.3**), which in-turn likely contributed to the moderate RNAi effects in the PC-3 cell line. Taken together, these results confirm the ability to modulate siRNA structure-function properties via conjugation of bio-active probes (e.g. fatty acids and fluorophores). However, effective siRNA activity is dependent on a variety of factors requiring optimization of siRNA sequence, and structure composition as well as the delivery

method for generating suitable formulations capable of effective siRNA delivery and release for silencing of important oncogene targets in cancer gene therapy applications.

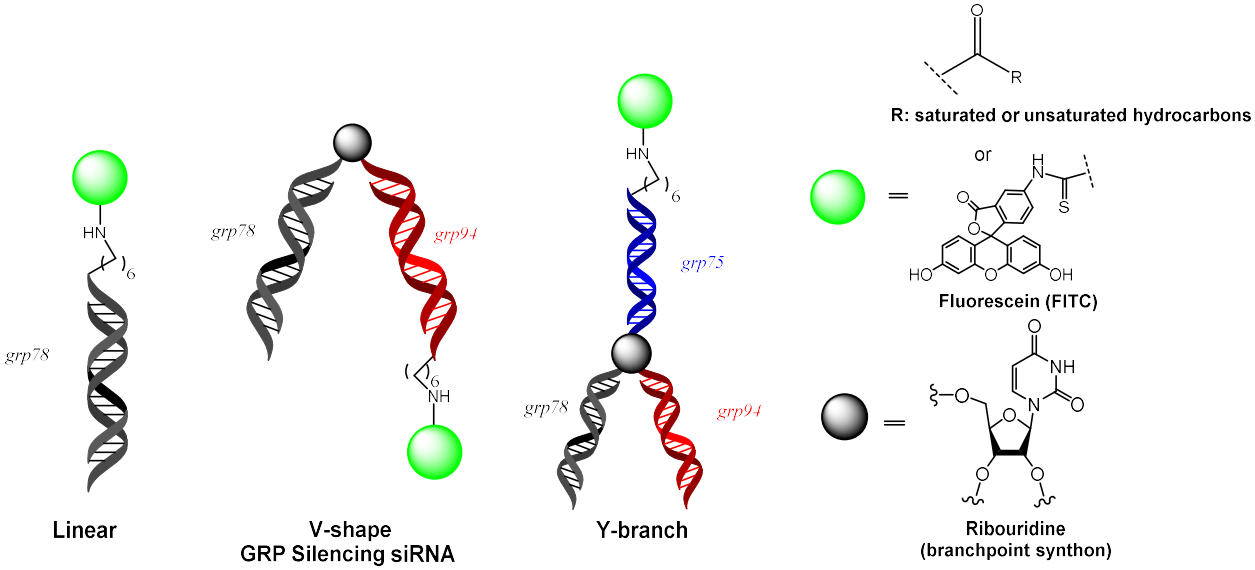

Figure 4.2. Fatty acid conjugated siRNAs with a fluorescence probe (fluorescein) for tracking cell uptake efficiency in PC-3 prostate cancer cells. Figure drawn using Chemdraw version 19.1 software.

4.1.3 Development of Bifunctional Au-templated RNA nanoparticle formulation for siRNA activity in PCa Cells

A major limitation of the self-assembled siRNA structures and the bioconjugates described in chapter 2, was based on their limited cell uptake for silencing activity in PC-3 cells. Structural studies by DLS and TEM revealed that large, charged aggregates likely contributed to poor cell uptake which diminished RNAi activity. Thus, modification strategies for fine-tuning the structure-function properties of siRNAs must optimize the requisite size and surface charge density of particles that may be applicable to cell uptake for RNAi potency. Chapter 3 of this thesis focused on the design and development of bifunctional RNA nanoparticles based on a Au formulation, which was selected to improve siRNA structure-function properties for enhanced

cell-uptake and RNAi activity in PC-3 cells. In this application (**Figure 4.3**), a simple method for templating amino-functionalized RNA onto Au surfaces and their self-assembly into small, discrete siRNA nanoparticles was established and also extended to our bioconjugation approaches for the incorporation of palmitamide and fluorescein. In this newly developed synthetic method (**Scheme 3.1**), a novel bottom-up approach for nucleating synthetic double-stranded (ds) RNA in which the antisense (A1) strand bearing a reactive alkylamino linker was used to template RNA onto the surface of reduced Au particles. The complementary sense (S1) strand was functionalized with and without a palmitamide (C16) fatty acid group or fluorescein isothiocyanate (FITC) as fluorescent (FL) reporter to generate the bifunctional Au-templated siRNA particles. It was observed that the Au-functionalized RNA particles with and without the fatty acid or fluorophore appendages were found to be stable under reducing conditions according to UV-Vis spectroscopy (**Figure 3.4**). These samples also produced primarily small (~10-40 nm), well-defined spherical shaped self-assembled nanoparticles (**Figure 3.5**), which were expected to be amenable to cell biology. The introduction of FITC within the Au-functionalized RNA particles produced a bifunctional probe, in which FITC fluorescence emission (λ_{exc}: 494 nm, λ_{em}: 522 nm) facilitated cell uptake detection, in a time-dependent manner **(Figure 3.6**, A and B). Moreover, western blot data showed knockdown of GRP75, which led to detectable levels of cell death in PC-3 cells treated with the Au-siRNA formulation in the absence of a transfection vector. Thus, the methodology shows the formulation of stable, small, and discrete Au-functionalized RNA nanoparticles, which may prove to be valuable bifunctional probes in the theranostic study of cancer cells.

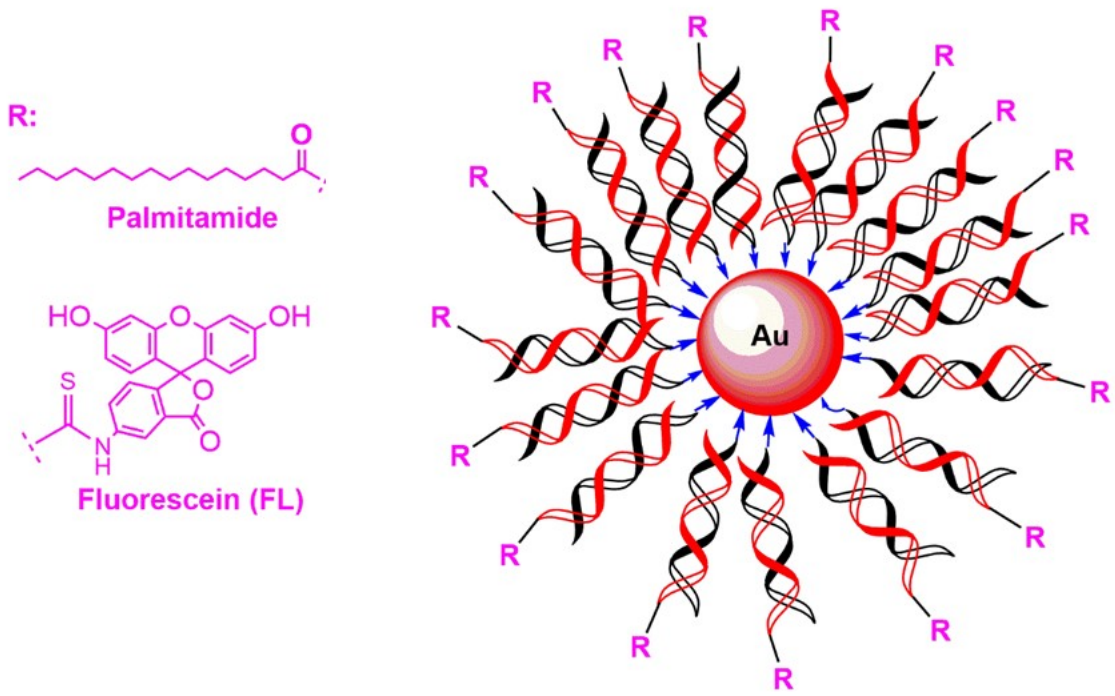

Figure 4.3. Structural representation of the multifunctional Au-siRNA nanoparticles bearing either a palmitamide or fluorescein group for cell biology in PC-3 prostate cancer cells. Figure drawn using Chemdraw version 19.1 software.

4.2. Ongoing and Future Work

While the results in this thesis highlight important accomplishments in the design and development of higher-order siRNA bioconjugates and their nanoparticle formulations for enhancing cell uptake and silencing of GRP expression for anti-cancer activity in prostate cancer cells, there is still the need for further refinement and optimization. Among the areas that remain underexplored and underdeveloped in our research work, are the cell-targeting ligands, that provide specificity and targetability, for minimizing off-target gene silencing effects while improving the efficacy of our cancer-targeted gene therapy approach. The ongoing and future work is aimed at the incorporation of polyarginine derived cell-targeting peptides that own the ability to bind and release siRNAs selectively within targeted cell lines. Our previous work indicated that the peptides were able to condense and release siRNAs, however, with limited cell

uptake efficacy due to the large, aggregated particles observed. In order to address this limitation, we are working on developing Au-siRNA formulations that contain cell-targeting peptides that own the ability to bind selectively onto the PSMA receptor localized on the surface of prostate cancer cells (**Figure 4.4**). In this manner, we anticipate that the Au-RNA formulation functionalized with the PSMA specific peptide may further improve the targetability, stability, and potency of the formulation for the requisite RNAi response in prostate cancer cells that may ultimately lead to the desired cancer-targeted gene therapy applications.

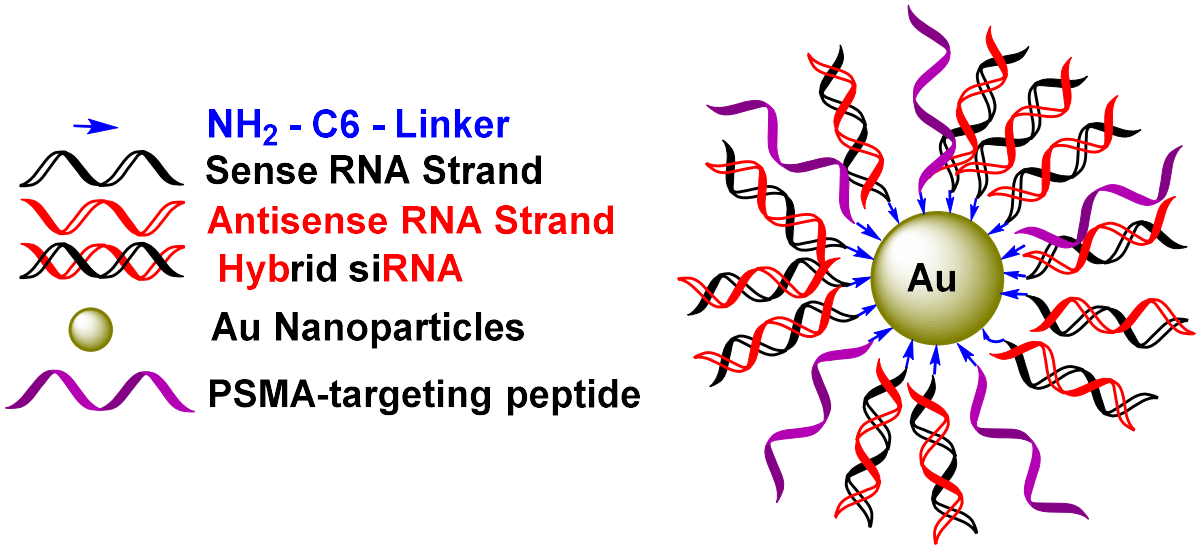

Figure 4.4. Proposed PSMA-targeting Au-siRNA formulation for targeted gene therapy in prostate cancer cells. Figure drawn using Chemdraw version 19.1 software.

4.3 Publications, Awards, Invention Disclosures, and Conference Presentations

4.3.1 Publications

1. Shah, S.; Casanova, N.; Antuono, G.; Sabatino, D. Polyamide Backbone Modified Cell Targeting and Penetrating Peptides in Cancer Detection and Treatment. *Front. Chem*. **2020**, *31*, 218. https://doi.org/10.3389/fchem.2020.00218
2. Shah, S.S.; Cultrara, C.N.; Ramos, J.; Sumani, U.; Zilberberg, J.; Sabatino, D. Bifunctional Au-templated RNA nanoparticles enable direct cell uptake detection and GRP75 knockdown in prostate cancer. *J. Mater.Chem. B,* **2020,** *8*, 2169-2176. https://doi.org/10.1039/C9TB02438G
3. Cultrara, C.N.; Shah, S.; Antuono, G.; Heller, C.J.; Ramos, J.A.; Samuni, U.; Zilberberg, J.; Sabatino, D. Size Matters: Arginine-Derived Peptides Targeting the PSMA Receptor Can Efficiently Complex but Not Transfect siRNA. *Mol. Ther. Nucleic Acids,* **2019,** *18*, 863–870.https://doi.org/10.1016/j.omtn.2019.10.013
4. Cultrara, C.N.; Shah, S.S.; Kozuch, S.D.; Patel, M.R.; Sabatino, D. Solid phase synthesis and self-assembly of higher-order siRNAs and their bioconjugates. *Chem.Biol.Drug Des.* **2019,** *93*, 999-1010. https://doi.org/10.1111/cbdd.13448
5. Cultrara, C.N.; Kozuch, S.D.; Ramasundaram, P.; Heller, C.J.; Shah, S.S.; Beck, A.E.; Zilberberg, J.; Sabatino, D. GRP78 modulates cell adhesion markers in prostate Cancer and multiple myeloma cell lines. *BMC Cancer,* **2018**, *18*, 1–14. https://doi.org/10.1186/s12885-018-5178-8
6. Kozuch, S.D.; Cultrara, C.N.; Beck, A.E.; Heller, C.J.; Shah, S.S.; Patel, M.R.; Zilberberg, J.; Sabatino, D. Enhanced Cancer Theranostic with Self-Assembled, Multilabeled siRNAs. *ACS Omega,* **2018,** *3,* 12975–12984.https://doi.org/10.1021/acsomega.8b01999
7. Shah, S.S.; Cultrara, C.N.; Kozuch, S.D.; Patel, M.R.; Ramos, J.A.; Samuni, U.; Zilberberg, J.; Sabatino, D. Direct Transfection of Fatty Acid Conjugated siRNAs and Knockdown of the Glucose-Regulated Chaperones in Prostate Cancer Cells. *Bioconjugate Chem.,* **2018,** *29*, 3638–3648. https://doi.org/10.1021/acs.bioconjchem.8b00580

4.3.2 Awards

1. Dr. Robert DeSimone Graduate Fellowship, Seton Hall University USA- 2018-2019.
2. Best Teaching Assistant Award, Seton Hall University, USA-2017
3. Honorable Mention in Basic Medical Sciences, Hackensack Meridian Health & SHU, USA-2017.

4.3.3 Poster Presentations

1. Shah, S.; Cultrara, C. N.; Kozuch, S. D.; Ramos, J.; Samuni, U.; Zilberberg, J.; Sabatino, D. **Higher-Order, Self-Assembled, Multi-labeled siRNAs for Silencing the Glucose Regulated Chaperones in Cancer.** *RNA-2020.* (**Poster Presentation**)

2. Shah, S.; Antuono, G.L.; Mateen, A.I; Colmenares, V.E.; Beck, A.E.; Ramos, J.; Samuni, U.; Zilberberg, J.; Sabatino, D. **Higher-Order siRNAs and their Bioconjugates for Silencing the Glucose Regulated Chaperones in Cancer.** *New York Academy of Sciences Meeting*, New York, NY. May 2020. (**Poster Presentation**)

3. Shah, S.; Antuono, G.L.; Mateen, A.I; Colmenares, V.E.; Beck, A.E.; Ramos, J.; Samuni, U.; Zilberberg, J.; Sabatino, D. **Self-assembly of higher-order siRNAs and their Bioconjugates for Silencing the Glucose Regulated Chaperones in Cancer.** *Petersheim Academic Exposition*, Seton Hall University, April 2020. (**Poster Presentation**).

4. Kozuch, SD; Cultrara, CN; Shah, S; Beck, AE; Heller, CJ; Zilberberg, J; Sabatino, D. **Cancer Gene Therapy using siRNA Nanotechnology and Bioconjugation.** *New York Academy of Sciences Meeting*, New York, NY. May 2018. (**Poster Presentation**)

5. Kozuch, SD; Cultrara, C.N.; Shah, S; Beck, AE; Heller, CJ; Zilberberg, J; Sabatino, D. **Cancer Gene Therapy using siRNA Nanotechnology and Bioconjugation.** *Petersheim Academic Exposition*, Seton Hall University, April 2018. (**Poster Presentation**)

6. Kozuch, SD; Cultrara, C.N.; Shah, S; Zilberberg, J; Sabatino, D. **Cancer Gene Therapy using siRNA Nanotechnology and Bioconjugation.** *New York Academy of Sciences Meeting*, New York, NY. May 2017. (**Poster Presentation**)

7. Kozuch, SD; Cultrara, C.N.; Shah, S; Zilberberg, J; Sabatino, D. **Cancer Gene Therapy using siRNA Nanotechnology and Bioconjugation.** *Petersheim Academic Exposition*, Seton Hall University, April 2017. (**Poster Presentation**).

APPENDIX

TABLE OF CONTENTS

A. SUPPLEMENTAL RP-IP-HPLC CHROMATOGRAMS

Figure A1 HPLC chromatogram of amino-functionalized GRP75 A1 RNA

Empower 2 software

Default Individual Report

SAMPLE INFORMATION

Sample Name:	75A1NH2	Acquired By:	System
Sample Type:	Unknown	Sample Set Name:	PURITY
Vial:	5	Acq. Method Set:	DS_RNA analysis_4_9_19_MS
Injection #:	1	Processing Method:	Default
Injection Volume:	25.00 ul	Channel Name:	2487Channel 1
Run Time:	25.0 Minutes	Proc. Chnl. Descr.:	
Date Acquired:	5/30/2019 2:42:05 PM EDT		
Date Processed:	6/6/2019 11:57:43 AM EDT		

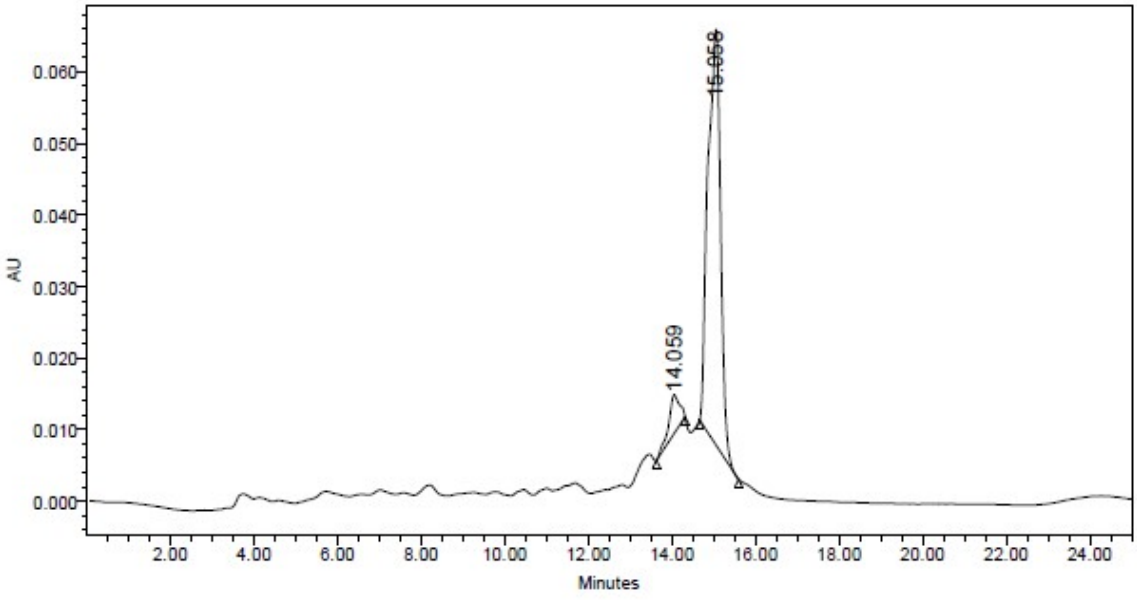

	RT	Area	% Area	Height
1	14.059	95143	7.30	5351
2	15.058	1208269	92.70	58261

Figure A2 HPLC chromatogram of amino-functionalized GRP75 S1 RNA

Empower 2 software

Default Individual Report

SAMPLE INFORMATION

Sample Name:	75S1	Acquired By:	System
Sample Type:	Unknown	Sample Set Name:	PURITY
Vial:	6	Acq. Method Set:	DS_RNA analysis_4_9_19_MS
Injection #:	1	Processing Method:	Default
Injection Volume:	25.00 ul	Channel Name:	2487Channel 1
Run Time:	25.0 Minutes	Proc. Chnl. Descr.:	
Date Acquired:	5/30/2019 3:08:08 PM EDT		
Date Processed:	6/6/2019 11:58:24 AM EDT		

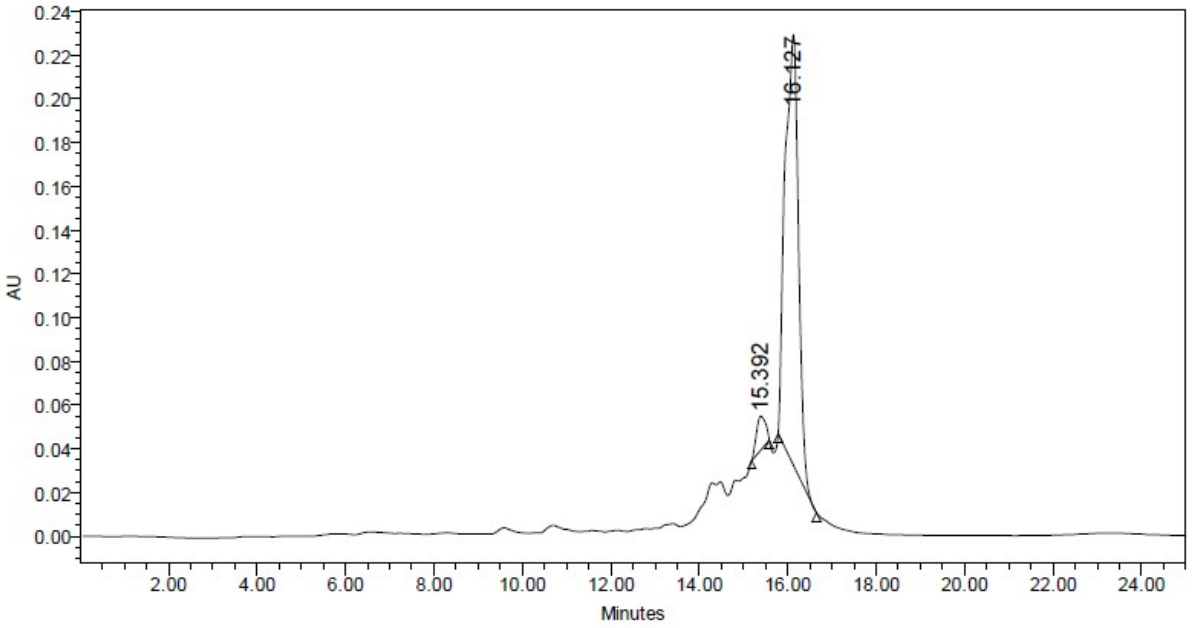

	RT	Area	% Area	Height
1	15.392	222437	5.15	15626
2	16.127	4094945	94.85	197157

Figure A3 HPLC chromatogram of amino-functionalized NS A1 RNA

Empower 2 software

Default Individual Report

SAMPLE INFORMATION

Sample Name:	NSA1NH2	Acquired By:	System
Sample Type:	Unknown	Sample Set Name:	PURITY
Vial:	8	Acq. Method Set:	DS_RNA analysis_4_9_19_MS
Injection #:	1	Processing Method:	Default
Injection Volume:	25.00 ul	Channel Name:	2487Channel 1
Run Time:	25.0 Minutes	Proc. Chnl. Descr.:	
Date Acquired:	5/30/2019 4:00:12 PM EDT		
Date Processed:	6/6/2019 12:00:28 PM EDT		

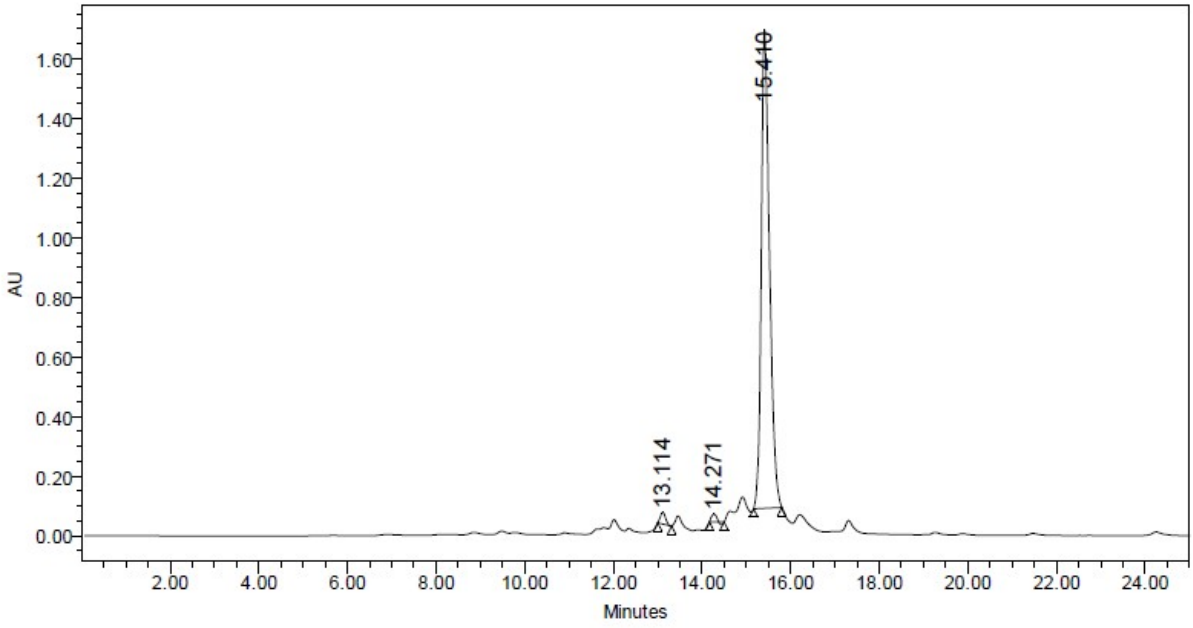

	RT	Area	% Area	Height
1	13.114	326964	1.54	39693
2	14.271	255222	1.20	26559
3	15.410	20617738	97.25	1617291

Figure A4 HPLC chromatogram of amino-functionalized NS S1 RNA

Empower 2 software

Default Individual Report

SAMPLE INFORMATION

Sample Name:	NSS1	Acquired By:	System
Sample Type:	Unknown	Sample Set Name:	PURITY
Vial:	7	Acq. Method Set:	DS_RNA analysis_4_9_19_MS
Injection #:	1	Processing Method:	Default
Injection Volume:	25.00 ul	Channel Name:	2487Channel 1
Run Time:	25.0 Minutes	Proc. Chnl. Descr.:	
Date Acquired:	5/30/2019 3:34:09 PM EDT		
Date Processed:	6/6/2019 11:59:44 AM EDT		

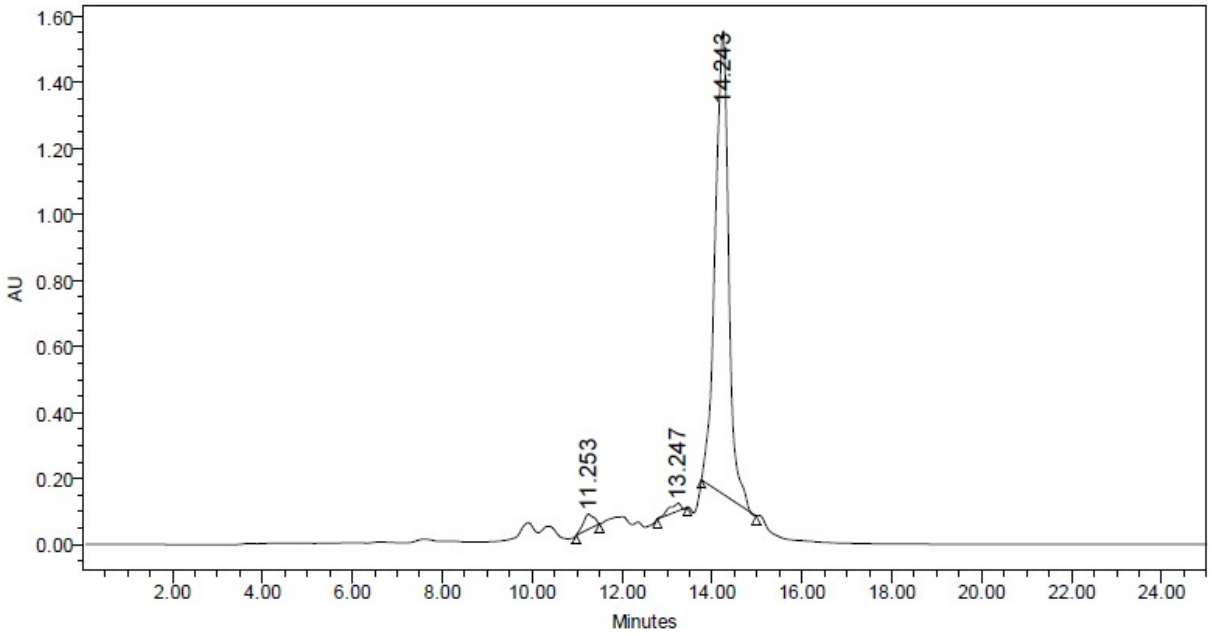

	RT	Area	% Area	Height
1	11.253	745077	2.44	45139
2	13.247	476309	1.56	22939
3	14.243	29312050	96.00	1404741

Figure A5 HPLC chromatogram of C16 conjugated GRP75 S1 RNA

Empower 2 software

Default Individual Report

SAMPLE INFORMATION

Sample Name:	c16-2	Acquired By:	System
Sample Type:	Unknown	Sample Set Name:	test
Vial:	4	Acq. Method Set:	SS_RNA BIO analysis_4_23_19_MS
Injection #:	1	Processing Method:	Default
Injection Volume:	25.00 ul	Channel Name:	2487Channel 1
Run Time:	40.0 Minutes	Proc. Chnl. Descr.:	
Date Acquired:	5/30/2019 12:17:05 PM EDT		
Date Processed:	6/6/2019 11:55:44 AM EDT		

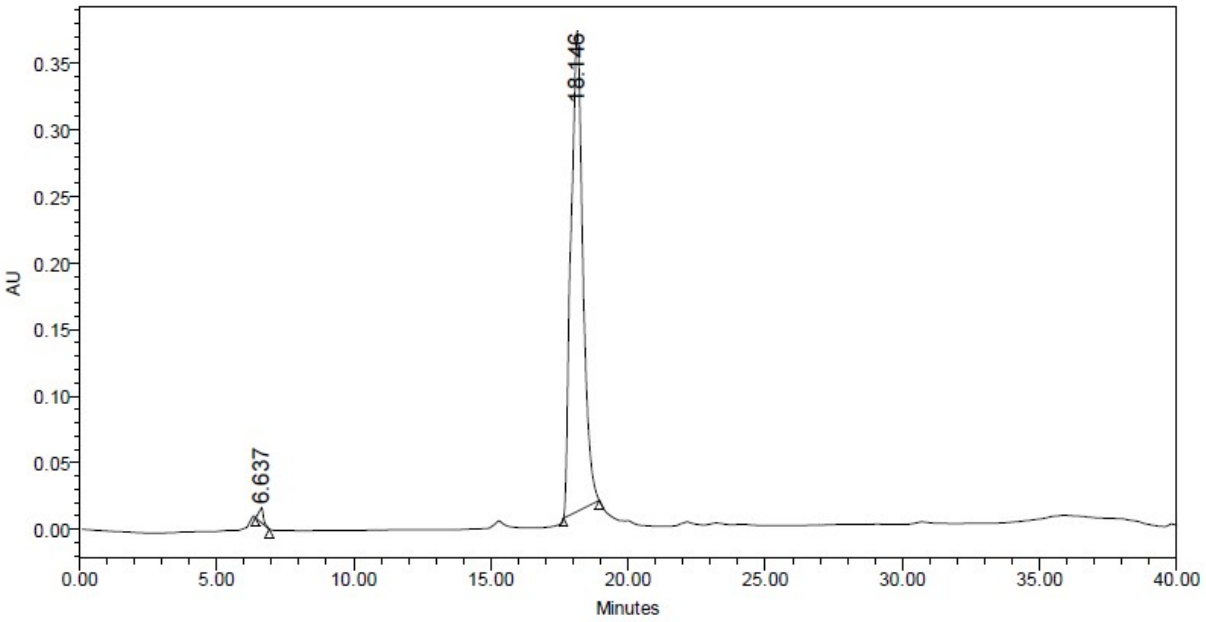

	RT	Area	% Area	Height
1	6.637	127004	1.16	11052
2	18.146	10843518	98.84	360505